2020
~ December ~
No. 4

HIDRAULICA

HYDRAULICS-PNEUMATICS-TRIBOLOGY-ECOLOGY-SENSORICS-MECHATRONICS

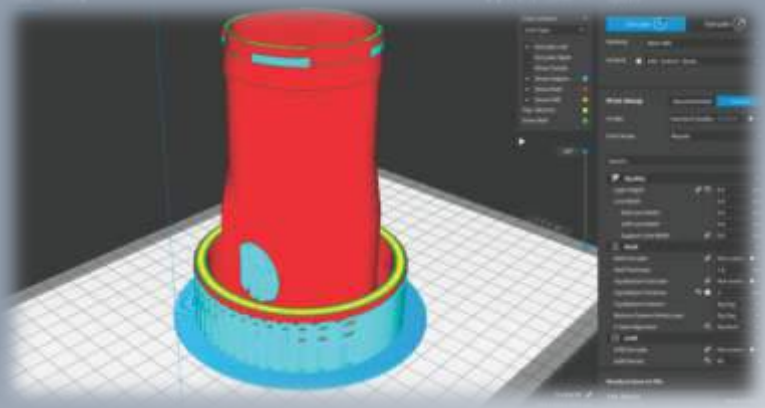

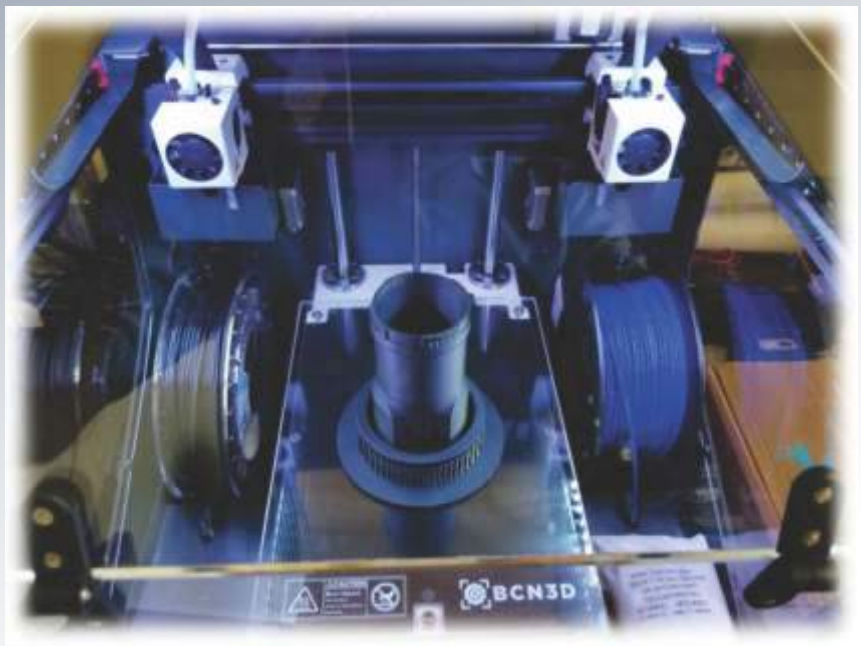

ISSN 1453-7303
ISSN-L 1453-7303

Available online at
hidraulica.fluidas.ro

CONTENTS

BOARD

Published by:
Hydraulics and Pneumatics Research Institute, Bucharest-Romania
Address: 14 Cuţitul de Argint, district 4, Bucharest, 040558, Romania
Phone: +40 21 336 39 91; Fax: +40 21 337 30 40; e-Mail: ihp@fluidas.ro; Web: www.ihp.ro
with support from:
National Professional Association of Hydraulics and Pneumatics in Romania - FLUIDAS
e-Mail: fluidas@fluidas.ro; Web: www.fluidas.ro

HIDRAULICA Magazine is indexed by international databases

ISSN 1453 – 7303; ISSN – L 1453 – 7303

EDITORIAL

Hidraulica și pandemia

Dr. Ing. Petrin DRUMEA
DIRECTOR PUBLICAȚIE

Zilnic aflăm prin diferite mijloace despre efectele catastrofale ale pandemiei asupra diverselor domenii economico-sociale. Întrebarea care se pune este dacă domeniile tehnice, iar în cazul nostru - dacă domeniul hidraulicii este afectat și dacă se poate face ceva util, rapid, pentru îmbunătățirea situației.

Dacă împărțim activitățile din domeniu în trei mari grupe, și anume: de producție efectivă, de utilizare a produselor în alte domenii industriale și serviciile de tot felul necesare desfășurării unei activități tehnico-economice normale, constatăm că, de fapt, nu avem posibilitatea lucrului de la distanță decât sporadic, nesemnificativ și neproductiv.

Despre producție și despre utilizarea produselor în sisteme și utilaje complexe s-a văzut că nu suntem pregătiți la modul industrial și că poate după dezvoltarea și depășirea celei de a 4-a revoluții industriale să putem discuta la modul serios despre teleproducție și alte metodologii care să nu implice prezența operatorului în hala de fabricație.

Inițial, se părea că serviciile de tip cercetare, proiectare, marketing, vânzare, mentenanță etc. ar putea să se desfășoare fără prezența la locul de muncă, însă în timp s-a constatat de către conducători și de către specialiștii coordonatori că, deocamdată, trebuie ca periodic să existe întruniri și discuții pentru alegerea soluțiilor și metodologiilor și pentru definitivarea lor.

De fapt, s-a constatat că de la distanță se pot rezolva activitățile repetitive, cu nivel de concepție la îndemâna tuturor specialistilor, și deocamdată activitățile cu înalt grad de specializare și de cercetare nu pot fi făcute decât de echipe bine structurate și care dispun de laboratoare și ateliere de lucru specializate și cu dotare imposibil de avut acasă. Acest lucru era ușor de dedus dacă s-ar fi analizat serios care este nivelul atins de proiectarea asistată de calculator și cum s-a redefinit în timp. Poate viitorul ne va aduce mari transformări, dar deocamdată noutățile cu șanse de introducere în economia reală sunt încă într-o fază de tatonare.

În realitate, astăzi constatăm că producția, inclusiv cea de hidraulică, s-a redus, că noutățile și-au redus ritmul de dezvoltare și că lucrătorii din industrie trebuie sa meargă la locul de muncă în majoritatea timpului de lucru. Poate că va fi o parte a soluției și modernizarea locurilor de muncă prin crearea unor spații de lucru adecvate, prin retehnologizarea lor, prin reorganizarea serviciilor și prin trecerea în practică a tuturor ideilor privind fabrica inteligentă, privind standurile inteligente și mai ales privind implicarea oamenilor inteligenți.

Multă sănătate!

EDITORIAL

Hydraulics and the pandemic

Ph.D.Eng. Petrin DRUMEA
MANAGING EDITOR

Every day we learn through various means about the devastating effects of the pandemic on various economic and social fields. The question that arises is whether the technical fields, and in our case - whether the field of hydraulics is affected, and whether something useful can be done, quickly, to improve the situation.

If we divide the activities in the field into three main groups, namely: production itself; use of products in other industrial fields; and services of all kinds necessary to conduct a normal technical and economic activity, we find that, in fact, we have the possibility of working remotely only sporadically, insignificantly and ineffectively.

As to the production and the use of products in complex systems and equipment, one could see that we are not prepared in an industrial way, and maybe only after developing and transcending the 4th industrial revolution we can seriously discuss teleproduction and other methodologies that do not involve the presence of the operator in the manufacturing hall.

Initially, it seemed that services such as research, design, marketing, sales, maintenance, etc. could take place without requiring physical presence at the workplace, but over time it has been found by the leaders and the coordinating specialists that, for the time being, there must be regular meetings and discussions in order to choose and finalize solutions and methodologies.

Actually, it has been found that only repetitive activities, with a level of contriving available to all specialists, can be solved remotely, and for the time being the activities with a high degree of specialization and research can only be carried out by well-structured teams which, in addition, have specialized laboratories and shop floors that are impossible for someone to have at home. This was easy to imagine if one seriously considered the level of computer-aided design and how it was redefined over time. Maybe the future will bring us great transformations, but for now the novelties with chances to be introduced in the real economy are still in a testing phase.

In fact, today we find that production, including hydraulics, has declined, that novelties have slowed down, and industry workers have to go to their workplace most of the time. Maybe workplace modernization by creating adequate work spaces, by re-engineering them, by reorganizing services and putting into practice all the ideas on smart factory, on smart stands, and especially on the involvement of smart people, will be part of the solution, as well.

I wish you all good health.

Mathematics for Real-Time S-Curve Profile Generator

PhD Eng. **Marian BLEJAN[1*],** student **Robert BLEJAN[2]**

[1] Hydraulics and Pneumatics Research Institute INOE 2000-IHP

[2] University POLITEHNICA of Bucharest, Faculty of Electrical Engineering

* blejan.ihp@fluidas.ro, robertblejan@yahoo.com

Abstract: *Position control is usually achieved using a position controller and a profile generator. The motion profile generator establishes the trajectory based on reference position and imposed motion constrains, and the position controller forces the actual position to trace the generated position trajectory. The S-curves motion profile generator allows control for the maximum values of speed, acceleration and jerk. When profile position value reaches the value of final point position, the generator sends a signal to the set-point generator to move on to next desired point of motion profile, and so on. This motion profile generator will be implemented as a software sequence which is executed in real-time. The software of motion profile generator will be validated by comparison with the simulation in MATLAB for S-curve motion.*

Keywords: *S-curve motion, profile generator, real-time software, mathematics*

1. Introduction

In many mechatronic and robotic applications, it is necessary to perform the movement from one point to another, a point-to-point movement profile of the third order is used [1]. This paper provides analytical formulas to calculate the fastest movement between two points, based on the given maximum levels of speed, acceleration, jerk and jump value.
In the chapter two we study the three-order movement profiles possible for the movement between two points. Based on the general equations of motion for position, velocity, acceleration and shock, the six phases of motion identified by the time values *0, t1 .. t6, t7* were determined. The general equations are customized for each phase of the motion, resulting in six sets of equations that describe the motion [2].
The next chapter is intended to choose the optimal movement profile and determine the durations of the movement phases. The profile selection criterion is the minimum duration of the movement in the conditions of performing the desired jump with the limitations of speed, acceleration and shock. The parameters v_a, s_a si s_v are defined and calculated, which in correlation with the desired jump value and with the values of the speed, acceleration and shock limits allow the choice of the optimal movement profile. Thus, six possible movement profiles are identified. The equations of motion and the durations of the phases of motion are determined for each possible motion profile.
Chapter four is dedicated to the description of the original algorithm for generating the motion profile in real time. The motion algorithm is a software sequence that is called by the main program every time the input of the motion profile generator changes, for example it can be called at each reference sampling. Thus, the algorithm is developed according to the real-time programming paradigm "Time-driven programming" [3], at each change of the input the generator calculates the motion profile at the current time which is the set of values for position, speed, acceleration and shock.
Chapter five evaluates the S-curve motion profile generation algorithm by comparing the motion profiles generated by the proposed algorithm and a completely built simulation model in MATLAB. The chosen assessment criterion was the value of the position error for the final position of the generated and simulated motion profiles. A full assessment was performed for all six cases of possible movement profiles.
Finally, the results obtained are analysed and the directions to be followed for further research are proposed.

2. Definition of terms and mathematical description of the movement profile

The general equations of motion are:

$$j(t); can\ be\ J, -J\ or\ 0 \quad (1)$$

$$a(t) = a_0 + j(t) * t \quad (2)$$

$$v(t) = v_0 + a_0 * t + j(t) * \frac{t^2}{2} \quad (3)$$

$$p(t) = p_0 + v_0 * t + a_0 * \frac{t^2}{2} + j(t) * \frac{t^3}{6} \quad (4)$$

Note: it is enough to calculate the trajectory up to half the movement time $t_{miscare}$ and the position is $\frac{s}{2}$, the rest of the trajectory is symmetrical horizontally, with respect to the y-axis $y(t) = \frac{t_{miscare}}{2}$ and vertically with respect to the y-axis $y(t) = \frac{s}{2}$. The jump, the amplitude of the movement, is denoted by *s*.

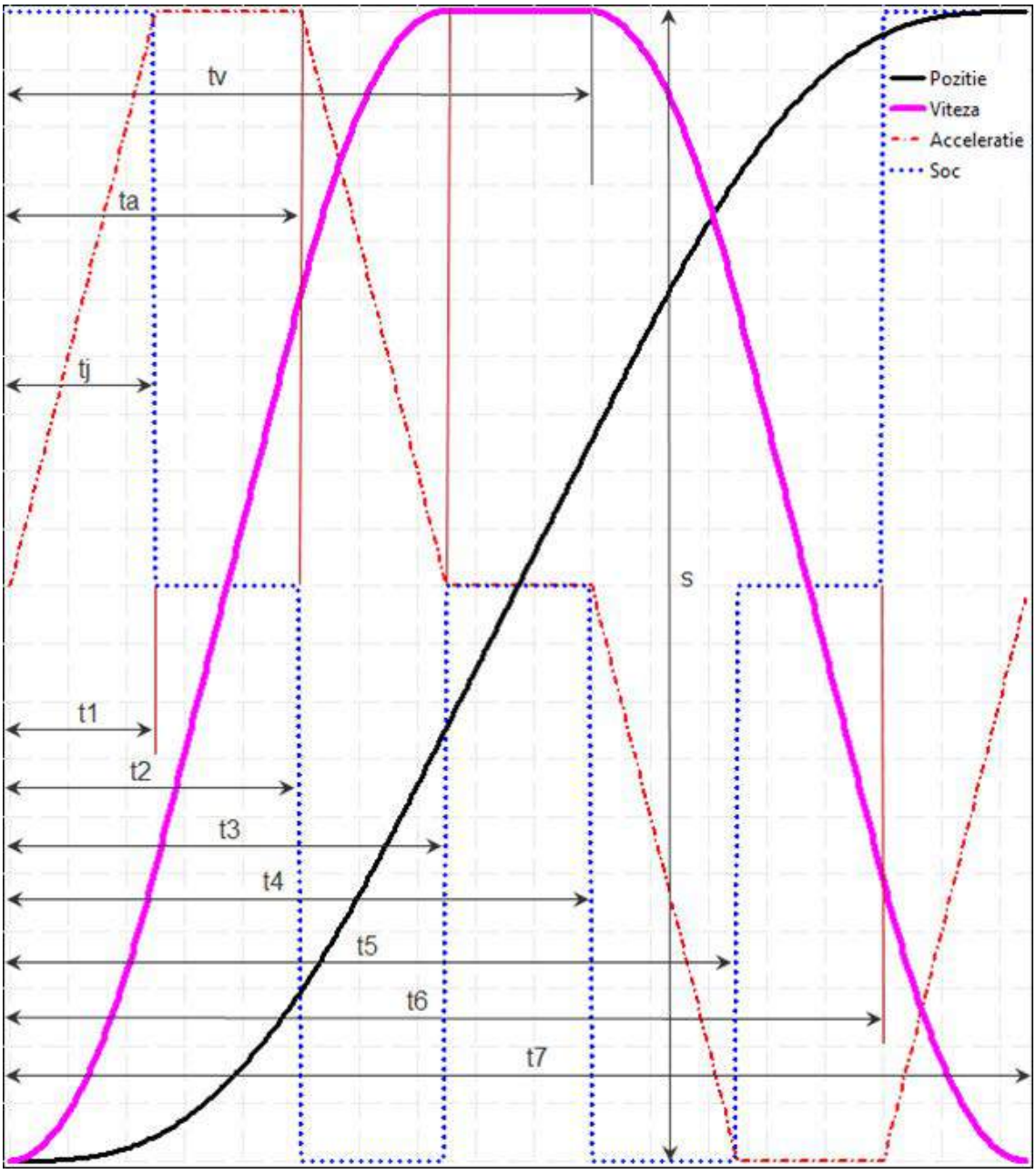

Fig. 1. Defining times t_j, t_a, t_v, $t_{1..7}$ and the amplitude of the jump *s*

Equations of motion as a function of time, see fig. 1, are:

$[0, t_1) \Rightarrow$

$$j(t) = J \quad (5)$$

$$a(t) = J * t;\ a_1 = J * t_1 \quad (6)$$

$$v(t) = J * \frac{t^2}{2};\ v_1 = J * \frac{{t_1}^2}{2} \quad (7)$$

$$p(t) = J * \frac{t^3}{6};\ p_1 = J * \frac{{t_1}^3}{6} \quad (8)$$

$[t_1, t_2) \Rightarrow$

$$j(t - t_1) = 0 \quad (9)$$

$$a(t - t_1) = a_1;\ a_2 = a_1 \quad (10)$$

$$v(t - t_1) = v_1 + a_1 * (t - t_1);\ v_2 = v_1 + a_1 * (t_2 - t_1) \quad (11)$$

$$p(t - t_1) = p_1 + v_1 * (t - t_1) + a_1 * \frac{(t - t_1)^2}{2};\ p_2 = p_1 + v_1 * (t_2 - t_1) + a_1 * \frac{(t_2 - t_1)^2}{2} \quad (12)$$

$[t_2, t_3) \Rightarrow$

$$j(t - t_2) = -J \quad (13)$$

$$a(t - t_2) = a_2 - J * (t - t_2);\ a_3 = a_2 - J * (t_3 - t_2) = 0 \quad (14)$$

$$v(t - t_2) = v_2 + a_2 * (t - t_2) - J * \frac{(t - t_2)^2}{2};\ v_3 = v_2 + a_2 * (t_3 - t_2) - J * \frac{(t_3 - t_2)^2}{2} \quad (15)$$

$$p(t - t_2) = p_2 + v_2 * (t - t_2) + a_2 * \frac{(t - t_2)^2}{2} - J * \frac{(t - t_2)^3}{6};$$

$$p_3 = p_2 + v_2 * (t_3 - t_2) + a_2 * \frac{(t_3 - t_2)^2}{2} - J * \frac{(t_3 - t_2)^3}{6} \quad (16)$$

$[t_3, t_4) \Rightarrow$

$$j(t - t_3) = 0 \quad (17)$$

$$a(t - t_3) = 0;\ a_4 = 0 \quad (18)$$

$$v(t - t_3) = v_3;\ v_4 = v_3 \quad (19)$$

$$p(t - t_3) = p_3 + v_3 * (t - t_3);\ p_4 = p_3 + v_3 * (t_4 - t_3) \quad (20)$$

$[t_4, t_5) \Rightarrow$

$$j(t - t_4) = -J \quad (21)$$

$$a(t - t_4) = -J * (t - t_4);\ a_5 = -J * (t_5 - t_4) = -a_1 \quad (22)$$

$$v(t - t_4) = v_4 - J * \frac{(t - t_4)^2}{2};\ v_5 = v_4 - J * \frac{(t_5 - t_4)^2}{2} \quad (23)$$

$$p(t - t_4) = p_4 + v_4 * (t - t_4) - J * \frac{(t - t_4)^3}{6};$$

$$p_5 = p_4 + v_4 * (t_5 - t_4) - J * \frac{(t_5 - t_4)^3}{6} \quad (24)$$

$[t_5, t_6) \Rightarrow$

$$j(t - t_5) = 0 \quad (25)$$

$$a(t - t_5) = a_5;\ a_6 = a_5 = -a_1 \quad (26)$$

$$v(t - t_5) = v_5 - a_{max} * (t - t_5);\ v_6 = v_5 - a_{max} * (t_6 - t_5) \quad (27)$$

$$p(t - t_5) = p_5 + v_5 * (t - t_5) + a_5 \frac{(t - t_5)^2}{2};\ p_6 = p_5 + v_5 * (t_6 - t_5) + a_5 \frac{(t_6 - t_5)^2}{2} \quad (28)$$

$[t_6, t_7) \Rightarrow$

$$j(t - t_6) = J \quad (29)$$

$$a(t - t_6) = a_6 + J * (t - t_6);\ a_7 = a_6 + J * (t_7 - t_6) = 0 \quad (30)$$

$$v(t - t_6) = v_6 + a_6 * (t - t_6) + J * \frac{(t - t_6)^2}{2};\ v_7 = v_7 + a_6 * (t_7 - t_6) - J * \frac{(t_7 - t_6)^2}{2} = 0 \quad (31)$$

$$p(t-t_6) = p_6 + v_6 * (t-t_6) + a_6 * \frac{(t-t_6)^2}{2} + J * \frac{(t-t_6)^3}{6};$$

$$p_7 = s = p_6 + v_6 * (t_7-t_6) + a_6 * \frac{(t_7-t_6)^2}{2} + J * \frac{(t_7-t_6)^3}{6} \quad (32)$$

The values of the times corresponding to the phases of the movement are:

$$t_1 = t_j \quad (33)$$
$$t_2 = t_a \quad (34)$$
$$t_3 = t_j + t_a \quad (35)$$
$$t_4 = t_v \quad (36)$$
$$t_5 = t_j + t_v \quad (37)$$
$$t_6 = t_v + t_a \quad (38)$$
$$t_7 = t_v + t_a + t_j \quad (39)$$

3. Determining the optimal movement profile and duration of movement phases

Fig. 2 shows the motion curves in the situation where the maximum values for acceleration and speed are not maintained; this implies, see fig. 1,

$$t_1 = t_2, t_3 = t_4 = \frac{t_7}{2}, t_5 = t_6 \quad (40)$$

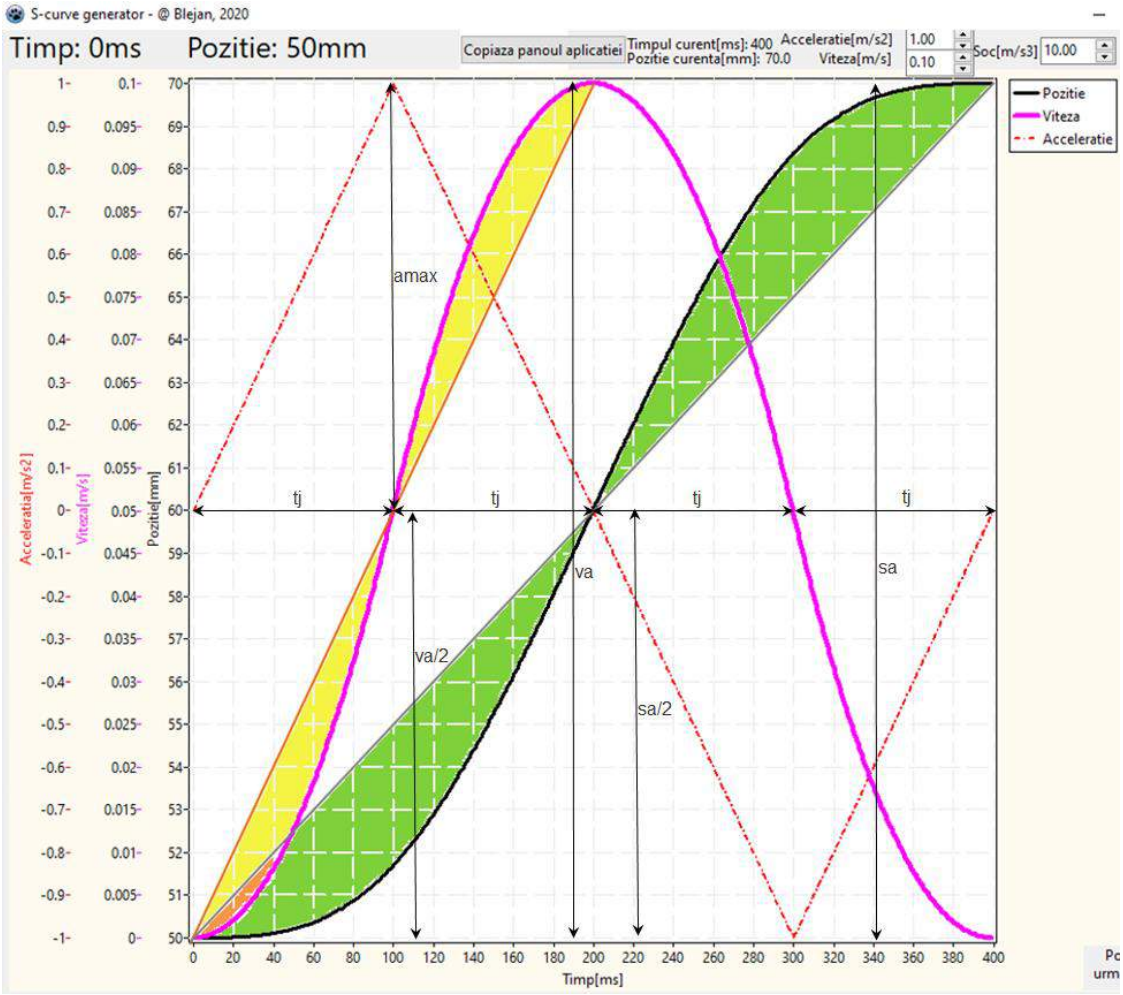

Fig. 2. Movement without acceleration and constant speed

It is observed on the graph that the convex part and the concave part of the velocity and position graphs cancel each other out if you want to calculate the integrals of these quantities.

Thus, the integral of the velocity, at half the duration of the motion, is equal to the area below the graph, which means, according to the previous observation, that the yellow area on the concave side is equal to the yellow area on the convex side of the graph (half stroke) multiplying the value of the movement time and the amplitude of the speed, respectively

$$Integral\ of\ the\ speed = \frac{t_7}{2} * (v_{max} - 0) * \frac{1}{2} = v_{max} * \frac{t_7}{4} \quad (41)$$

Applying a similar reasoning to the position graph, it results

$$Integral\ of\ the\ position = \frac{t_7}{2} * s \quad (42)$$

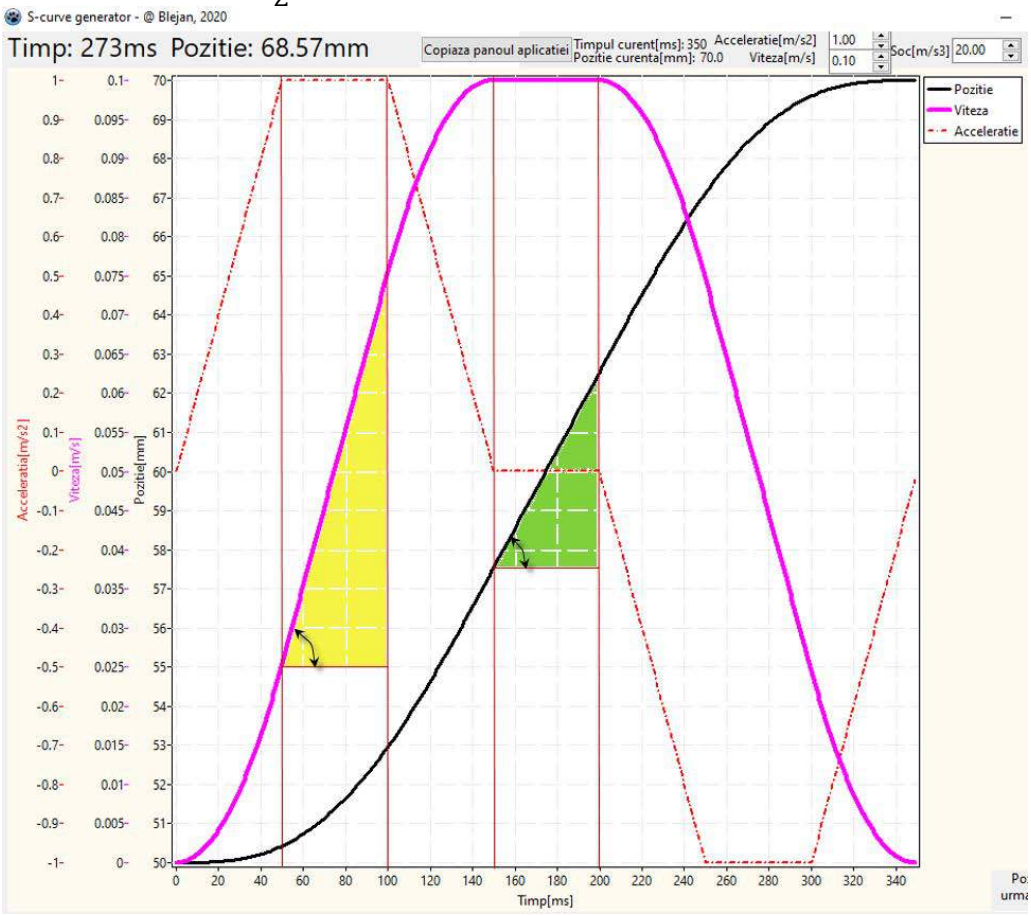

Fig. 3. Motion with acceleration and constant speed

Fig. 3 shows the motion curves in the situation where the maximum values for acceleration and speed are reached and the motion occurs by keeping these values at the maximum limit, the interval $[t_1, t_2]$ in which the motion is performed with the acceleration a_{max}, and in the interval $[t_3, t_4]$ the movement is performed with the speed v_{max}. The corresponding integrals of velocity and position on the mentioned intervals are the areas of the colored triangles, see fig. 3, with yellow for full speed and green for full position, respectively

$$Integral\ of\ the\ speed = \frac{a_{max}}{2} * (t_2 - t_1)^2 \quad (43)$$

$$Integral\ of\ the\ position = \frac{v_{max}}{2} * (t_4 - t_3)^2 \quad (44)$$

because the tangent of the angle marked in the yellow triangle is a_{max}, respectively v_{max} for the angle marked in the green triangle.

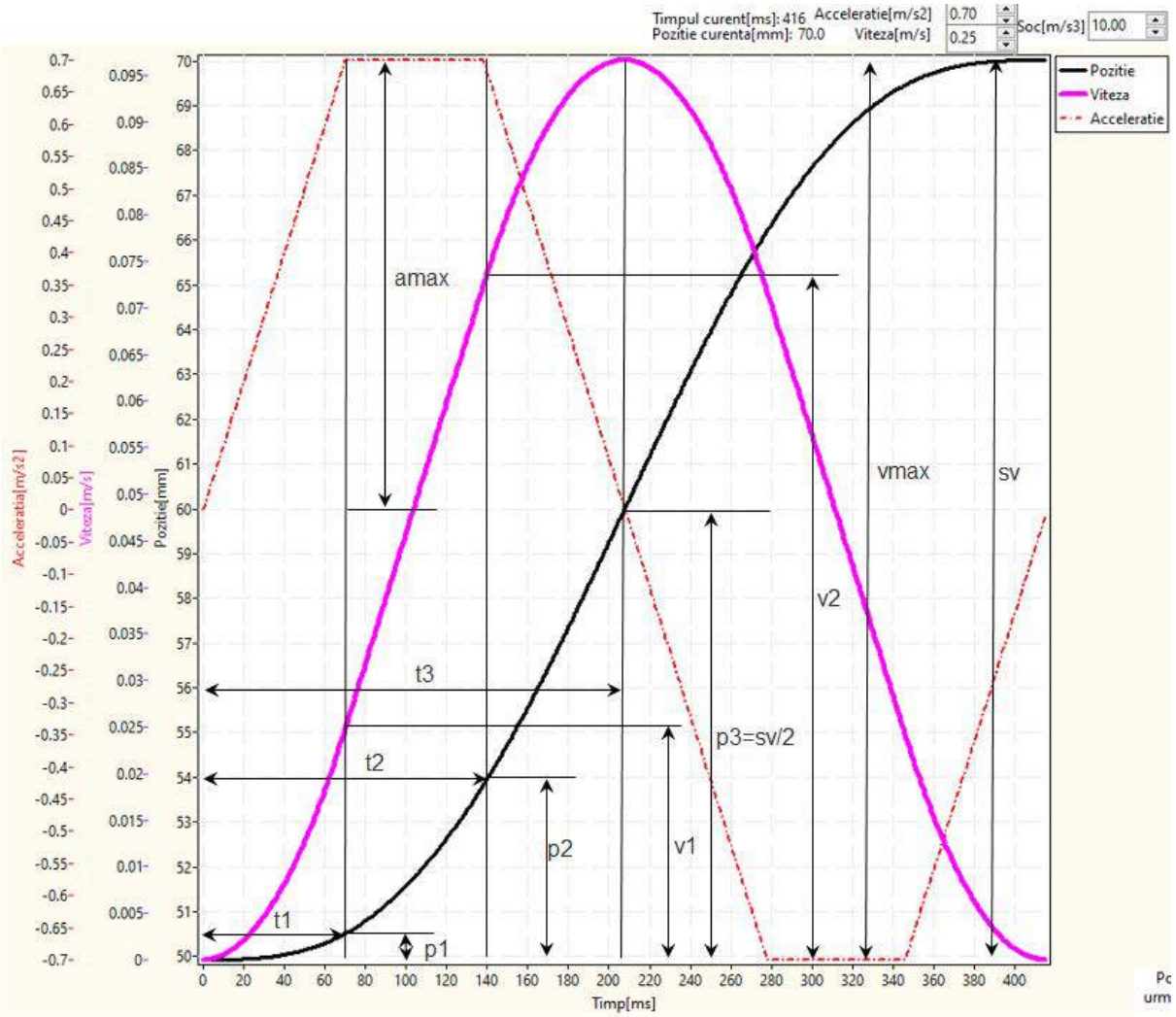

Fig. 4. Motion with constant acceleration

3.1 The definition and calculation of v_a, s_a and s_v

The parameters v_a, s_a and s_v are limit values for speed and space being defined and calculated below.

Considering realization of the movement having as limitation only the maximum value of the acceleration, see fig. 2, will be defined v_a as the maximum value of the speed reached during the movement, and s_a as the value of the stroke at the end of the movement. Reaching the maximum value of the acceleration is followed by stopping the movement as quickly as possible.

To calculate the motion parameters at time t_j, we apply formulas (5), (6), (7) and (8)

$$a_{max} = J * t_j \Rightarrow t_j = \frac{a_{max}}{J} \tag{45}$$

$$\frac{v_a}{2} = J * \frac{t_j^2}{2} \Rightarrow v_a = \frac{a_{max}^2}{J} \tag{46}$$

$$p_{12} = J * \frac{t_j^3}{6} = \frac{a_{max}^3}{6 * J^2} \tag{47}$$

To calculate s_a apply formula (16) to moment $2*t_j$, with the value of t_j given by (45)

$$\frac{s_a}{2} = p(2 * t_j - t_j) = \frac{a_{max}^3}{6 * J^2} + \frac{a_{max}^2}{2 * J} * t_j + a_{max} * \frac{t_j^2}{2} - J * \frac{t_j^3}{6} = \frac{a_{max}^3}{J^2} \Rightarrow s_a = \frac{2 * a_{max}^3}{J^2} \quad (48)$$

Similarly, considering the limitation of the maximum value of the speed, not taking into account the limitation of the value of the position (jump), reaching the maximum value of the speed being followed by stopping the movement as fast as possible, results s_v as the value of the stroke at the end of the movement. We distinguish two cases:

Case 1, a trajectory with the shape of fig. 2, in which the acceleration has a triangular shape ($t_2 = t_1$ and $t_5 = t_6$) and the positive ramp is connected with the negative acceleration ramp

Case 2, a trajectory with the shape of fig. 4, in which the acceleration has a trapezoidal shape and the positive ramp is connected with the negative acceleration ramp ($t_3 = t_4$) and reaching the maximum speed is immediately followed by the decrease of its value in order to stop the movement as fast as possible.

The detection between the two presented cases is made according to the value of the acceleration at time t_2, in the sense it does not reach the maximum imposed value, case 1 or reaches the maximum imposed value and maintains it, case 2. According to formula (46) the choice of case 1 is made if

$$v_{max} * J < a_{max}^2 \Rightarrow Case\ 1, fig.2 \quad (49)$$

, respectively

$$v_{max} * J \geq a_{max}^2 \Rightarrow Case\ 2, fig.4\ with\ positive\ and\ negative\ ramp\ of\ acceleration\ connected \quad (50)$$

We determine the value s_v in case 1, for the beginning we apply the formula (7) with $v_1 = v_{max} / 2$, it results

$$t_j = \sqrt{\frac{v_{max}}{J}} \quad (51)$$

It follows from (6) and (51)

$$a_1 = J * \sqrt{\frac{v_{max}}{J}} \quad (52)$$

, and from (8) and (51) we have

$$p_1 = v_{max} * \sqrt{\frac{v_{max}}{J}} \quad (53)$$

Taking into account that $p_3 = s_v / 2$ and replacing in (16) the values calculated in (51), (52) and (53) results

$$s_v = 2 * v_{max} * \sqrt{\frac{v_{max}}{J}}, pentru\ \ v_{max} * J < a_{max}^2 \quad (54)$$

To determine the value s_v in case 2, apply (6) with $a_1 = a_{max}$ obtaining

$$t_1 = \frac{a_{max}}{J} \quad (55)$$

, and then from (7) and (55) we have

$$v_1 = \frac{a_{max}^2}{2 * J} \quad (56)$$

And from (8), (55) it results

$$p_1 = \frac{a_{max}^3}{6 * J^2} \quad (57)$$

Similarly, for the interval t_1 .. t_2, we have

$$t_2 = \frac{v_{max}}{a_{max}} \quad (58)$$

$$v_2 = v_{max} - \frac{a_{max}^2}{2 * J} \quad (59)$$

$$p_2 = \frac{v_{max}^2}{2 * a_{max}} + \frac{a_{max}^3}{6 * J^2} - \frac{a_{max} * v_{max}}{J} \quad (60)$$

For the interval t_2 .. t_3, taking into account that $p_3 = s_v / 2$, it also results

$$s_v = v_{max} * \left(\frac{v_{max}}{a_{max}} + \frac{a_{max}}{J}\right), pentru \;\; v_{max} * J \geq a_{max}^2 \quad (61)$$

3.2 Possible movement profiles

The values of the parameters v_a and s_a represent the maximum limits of the speed and the jump of the position that can be reached, on an S-curve trajectory, without the need for motion with constant acceleration or, in other words, the shape of the acceleration curve to be triangular, see fig. 2.

The value of the parameter s_v represents the maximum limit of the position jump that can be reached without the need for constant speed movement, ie its speed characteristic has a saturation portion, see fig. 4.

Thus, depending on the values of the independent parameters, imposed by the user J, a_{max}, v_{max}, s and the values of the limit parameters of the motion v_a, s_a and s_v we distinguish the following scenarios and below motion scenarios:

A. $v_{max} < v_a; s > s_a$ → the acceleration curve is triangular, the velocity curve is limited so the positive and negative parts of the acceleration are not continuous, fig. 5.A. The final position can be reached if a portion of the trajectory is traveled with constant speed v_{max}.

B. $v_{max} > v_a; s < s_a$ → the acceleration curve is triangular, the velocity curve is not limited so the positive and negative parts of the acceleration are continuous, fig. 5.B

C. $v_{max} < v_a; s < s_a$ → the acceleration curve is triangular, and if $s > s_v$ the maximum speed is reached in case the positive and negative parts of the acceleration are not continuous, fig. 5.C.1, while if $s < s_v$ the positive and negative parts of the acceleration are continuous, fig. 5.C.2. In this case the speed curve is saturated at the value v_{max}, and if the final position $s < s_v$ is not reached, it is necessary to introduce a constant walking portion with the maximum speed.

D. $v_{max} > v_a; s > s_a$ → the acceleration curve is trapezoidal, and if $s > s_v$ the maximum speed is reached in case the positive and negative parts of the acceleration are not continuous, fig. 5.D.1, while if $s < s_v$ the positive and negative parts of the acceleration are continuous, fig. 5.D.2. In this situation, the final position cannot be reached unless a continuously accelerated driving section with the maximum value is entered; the walking portion with constant speed is given by the value of the parameter s_v.

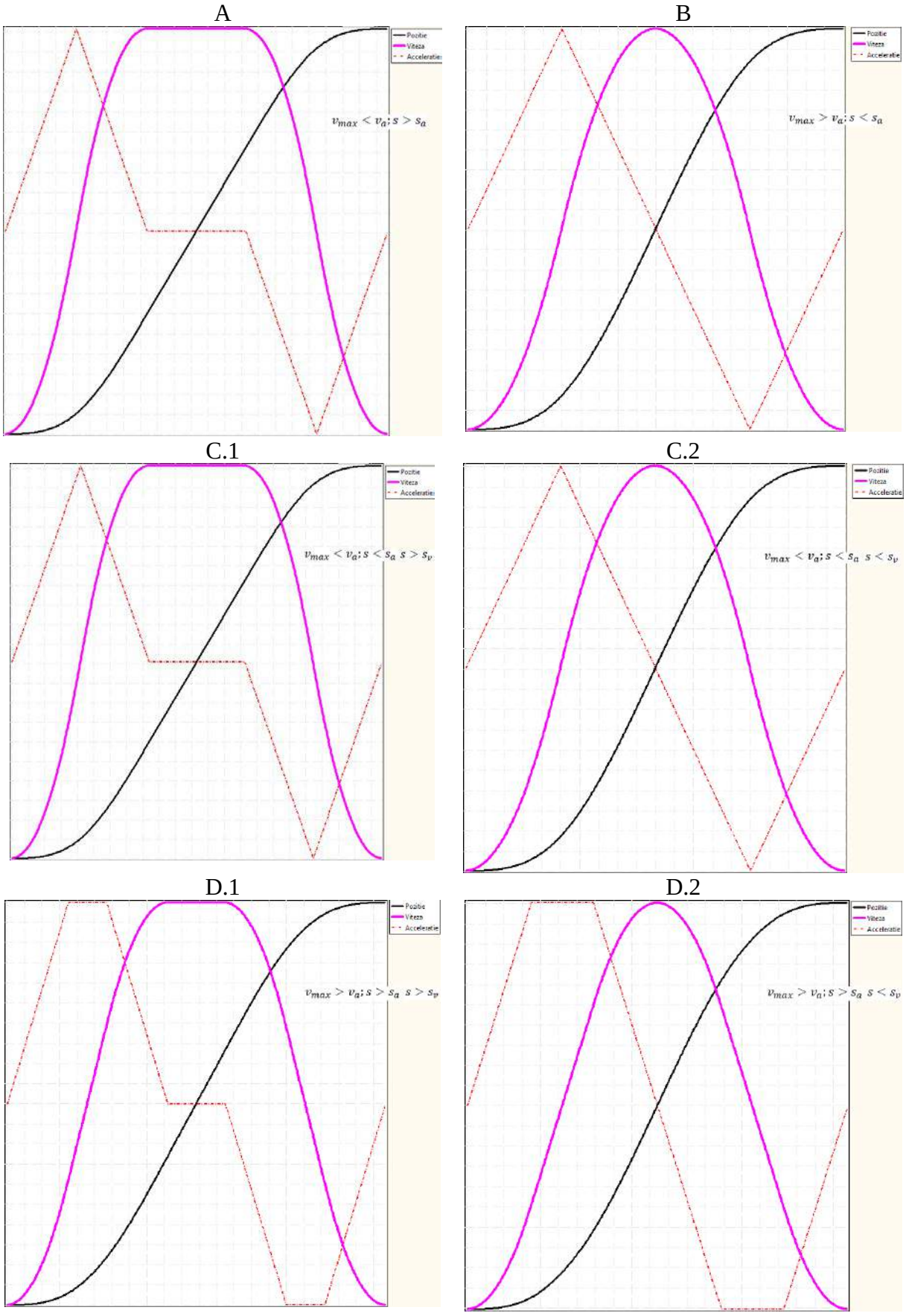

Fig. 5. Possible motion profiles

3.3 Calculation of times corresponding to the phases of movement

To generate the motion profiles, it is necessary to know the values t_1 … t_7. According to formulas (33)… (39), these values can be calculated if the values t_v, t_a, t_j, defined in fig. 1. The calculation of these times will be performed separately for the six possible profiles presented in fig. 5.

It is observed that at profiles B and C.2 the values of maximum speed and acceleration are not reached. Applying (6), (7), (8) and considering that $t_1 = t_j$, we obtain

$$a(t) = J * t \Rightarrow a(t_j) = J * t_j \quad (62)$$

$$v(t) = J * \frac{t^2}{2} \Rightarrow v(t_j) = J * \frac{{t_j}^2}{2} \quad (63)$$

$$p(t) = J * \frac{t^3}{6} \Rightarrow p(t_j) = J * \frac{{t_j}^3}{6} \quad (64)$$

Since $t_1 = t_2 = t_j$ and $t_3 = 2 * t_j$, replacing in (16) we have

$$p(t - t_j) = J * \frac{{t_j}^3}{6} + J * \frac{{t_j}^2}{2} * (t - t_j) + J * t_j * \frac{(t - t_j)^2}{2} - J * \frac{(t - t_j)^3}{6}$$

$$\Rightarrow p(2 * t_j - t_j) = \frac{s}{2} = J * {t_j}^3 \quad (65)$$

so

$$t_j = \sqrt[3]{\frac{s}{2 * J}} \quad (66)$$

The values t_v, t_a, see fig. 1, fig. 5.B and fig. 5.C.2, are

$$t_a = t_j \quad (67)$$

$$t_v = 2 * t_j \quad (68)$$

Trajectories A and C.1 reach the value of the maximum speed. The equations of motion will be applied at intervals.

Interval $0 .. t_j$: apply (6), (7) and (8) for the calculation of the initial values on the next interval.

Interval $t_j .. 2 * t_j$:

$$a(t - t_j) = J * t_j - J * (t - t_j) \quad (69)$$

$$v(t - t_j) = J * \frac{t_j^2}{2} + J * t_j * (t - t_j) - J * \frac{(t - t_j)^2}{2} \quad (70)$$

$$p(t - t_j) = J * \frac{t_j^3}{6} + J * \frac{t_j^2}{2} * (t - t_j) + J * t_j * \frac{(t - t_j)^2}{2} - J * \frac{(t - t_j)^3}{6} \quad (71)$$

Substituting in (70) $t = 2 * t_j$ and taking into account that $v(2 * t_j) = v_{max}$ at the moment $2 * t_j$

$$\Rightarrow t_j = \sqrt{\frac{v_{max}}{J}} \quad (72)$$

, and from (71) and (72) with $t = 2 * t_j$, also at the moment $2 * t_j$

$$\Rightarrow p_{2tj} = v_{max} * \sqrt{\frac{v_{max}}{J}} \quad (73)$$

The interval $2 * t_j .. 2 * t_j + \frac{t_v - 2 * t_j}{2}$, ie half of the total duration of the movement, when the distance $\frac{s}{2}$ has been covered:

replacing in (4), with the initial values calculated in (69), (70) and (71), we obtain

$$p(t - 2 * t_j) = v_{max} * \sqrt{\frac{v_{max}}{J}} + v_{max} * (t - 2 * t_j) \quad (74)$$

, and from (74) at the moment $t = 2 * t_j + \frac{t_v - 2*t_j}{2}$ the space travelled is $\frac{s}{2}$

$$\Rightarrow t_v = \frac{s}{v_{max}} \tag{75}$$

Because the acceleration trajectory is triangular, we have

$$t_a = t_j \tag{76}$$

In the case of trajectory D.1, the values of maximum speed and acceleration are reached. Taking into account the explanations regarding fig. 2 and fig. 3 and relations (41), (42), (43) and (44), we have

- The value of the shock integral on the interval *0 .. t_1* is the value of the acceleration at the moment $t_1 = t_j$, which has the value a_{max}. It is thus obtained

$$t_j = \frac{a_{max}}{J} \tag{77}$$

- The value of the acceleration integral on the interval *0 .. t_3* is the value of the speed at time t_3, ie v_{max}. So

$$t_a = \frac{v_{max}}{a_{max}} \tag{78}$$

Similarly, the value of the velocity integral over the interval *0 .. t_7* is the value of the position at time *t*, i.e. *s*. So

$$t_v = \frac{s}{v_{max}} \tag{79}$$

Trajectory D.2, see fig. 6, reaches and maintains the value of the maximum acceleration, and the value of the maximum speed is not reached.

Interval *0 .. t_j* : apply (6), (7) and (8) for the calculation of the initial values on the next interval.

Because $a(t_j) = a_{max}$ and taking into account (5) we have

$$t_j = \frac{a_{max}}{J} \tag{80}$$

Interval t_j .. t_a :

$$a(t - t_j) = a_{max} \tag{81}$$

$$v(t - t_j) = J * \frac{{t_j}^2}{2} + a_{max} * (t - t_j) \tag{82}$$

$$p(t - t_j) = J * \frac{{t_j}^3}{6} + J * \frac{{t_j}^2}{2} * (t - t_j) + a_{max} * \frac{(t - t_j)^2}{2} \tag{83}$$

Substituting in (82) $t = t_j + \frac{t_a - t_j}{2}$, when the speed reaches half of the maximum value

$$\frac{v_{tv}}{2} = J * \frac{{t_j}^2}{2} + a_{max} * \frac{t_a - t_j}{2} \tag{84}$$

Substituting t_j from (80) into (84) results

$$v_{tv} = a_{max} * t_a \tag{85}$$

Taking into account that *Space = Integral of velocity*, considering the moment $t_v = t_a + t_j$ and taking into account fig. 2 and fig. 3 in which it is shown that the part of the areas of the convex and concave part of the graph is cancelled, see fig.6 where the integral is marked in yellow, we have

$$\frac{s}{2} = \frac{t_v}{2} * 2 * v_{tv} \tag{86}$$

Substituting $t_v = t_a + t_j$ and (85) in relation (86) we obtain

$$s = 2 * a_{max} * t_a * \left(t_a + \frac{a_{max}}{J}\right) \tag{87}$$

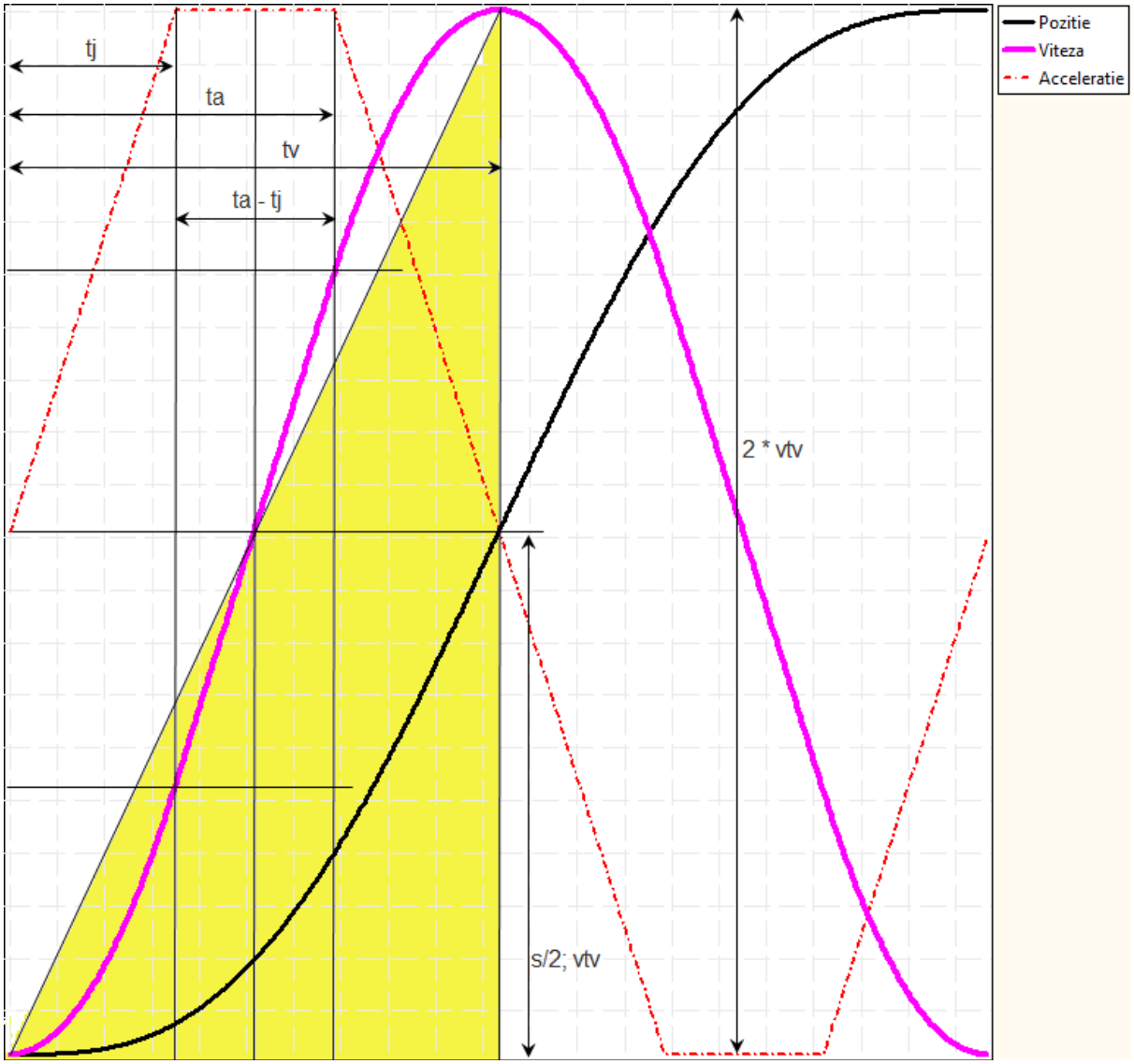

Fig. 6. Case D.2 - the value of the maximum acceleration is reached, the value of the maximum speed is not reached

Solving the equation of degree 2 (87) and taking the positive solution, we have

$$t_a = \frac{1}{2} * \left(\sqrt{\frac{4 * s * J^2 + a_{max}^3}{a_{max} * J^2}} - \frac{a_{max}}{J} \right) \tag{88}$$

and

$$t_v = t_a + t_j \tag{89}$$

4. Real-time motion profile generation algorithm

The generation of S-curve motion profiles for position, speed, acceleration and shock is triggered when a significant jump occurs at the generator input followed by the calculation of the current values of position, speed, acceleration and shock, values that are delivered at the output of the S-curve generator in real time. At each change of the current time, it is necessary to call the calculation of the new values of position, speed, acceleration and shock corresponding to the current value of time; the generation of the profiles is completed when the final position is reached, the value of which is the algebraic sum between the value of the initial position and the value of the position jump.

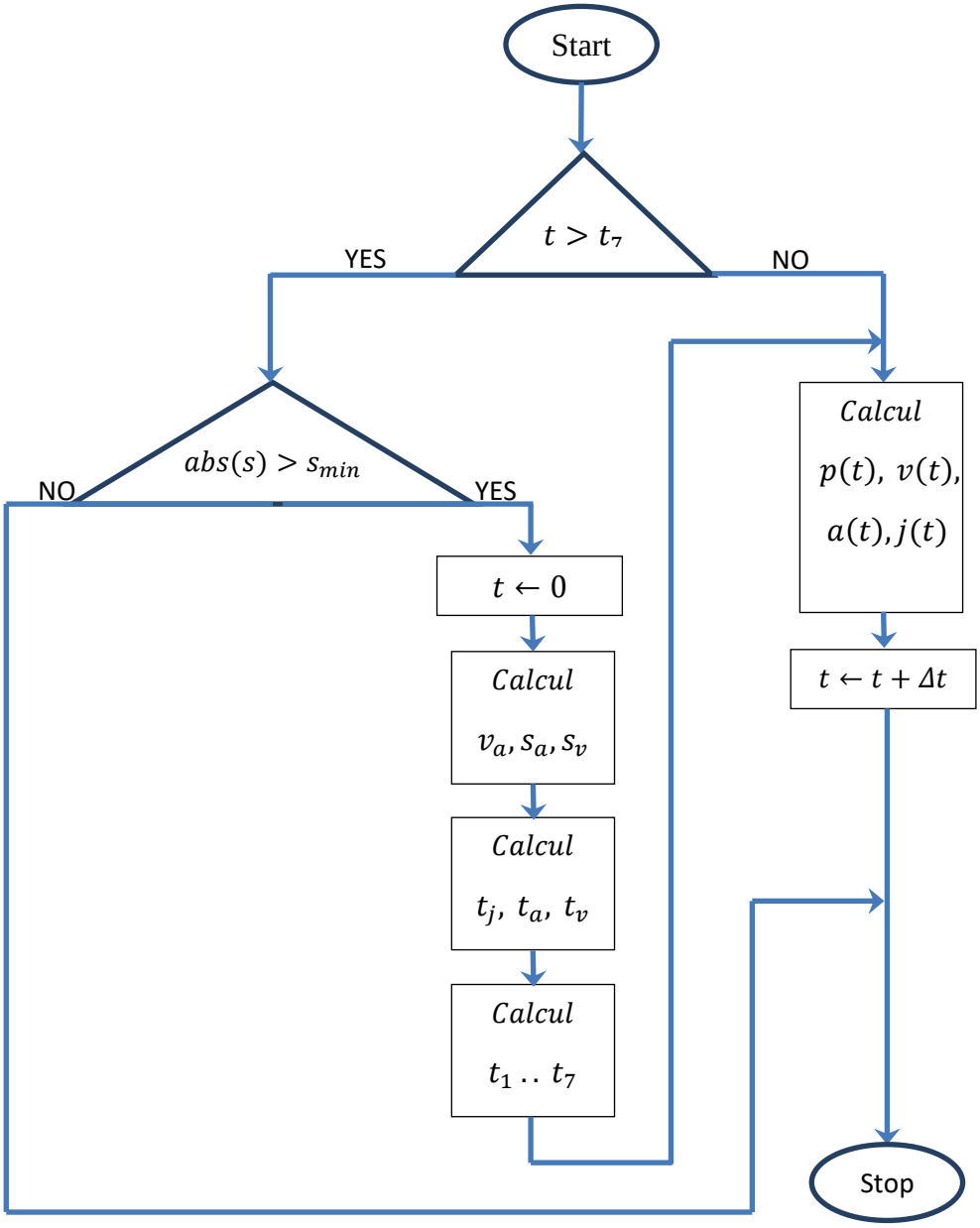

Fig. 7. Real-time S-curve generation algorithm

Fig. 7 presents the S-curve generation algorithm in real time, and further the calculation steps will be presented, in correlation with the previously presented formulas.
Thus *Calcul* v_a, s_a, s_v is performed according to (46), (48) for v_a, s_a respectively (54) or (61) for s_v, depending on where we fit. The calculated values allow us to establish one of the motion trajectories shown in fig. 5, which allows us to calculate the values t_j, t_a, t_v thus
- For trajectories B and C.2 apply (66), (67) and (68)

- For trajectories A and C.1 (72), (75) and (76) apply

- For trajectory D.1 apply (77), (78) and (79)

- For trajectory D.2 apply (80), (88) and (89)

The calculation of the values t_1 .. t_7 is presented in the relations (33) .. (39) and uses the values t_j, t_a, t_v calculated previously.

Finally, the values *p(t), v(t0), a(t)* and *j(t)* are calculated using the relations (1), (2), (3) and (4) in which the initial values p_0, v_0 and a_0 are zero at the first calculation step (*t = 0*), and then are the values *p(t), v(t0), a(t)* and *j(t)* at the previous calculation step. The values of *J* are those corresponding to the current time, on the current trajectory, see fig. 5; that is, one of the values *J, -J* or *0*.

The value of the parameter *Δt* is the time interval between two successive calls of the algorithm shown in fig. 7, in other words the integration step used to calculate the values of *p(t), v(t0)* and *a(t)*.

5. Confirmation of the proposed algorithm by simulation

The units of measurement for time and space used in the simulation will be *ms* and *mm*, and we need to use the units of measurement that use the following conversion ratios:

$$1\ m = 1000\ mm \tag{90}$$

$$1\ \frac{m}{s} = 1\ \frac{mm}{ms} \tag{91}$$

$$1\ \frac{m}{s^2} = 10^{-3}\ \frac{mm}{ms^2} \tag{92}$$

$$1\ \frac{m}{s^3} = 10^{-6}\ \frac{mm}{ms^3} \tag{93}$$

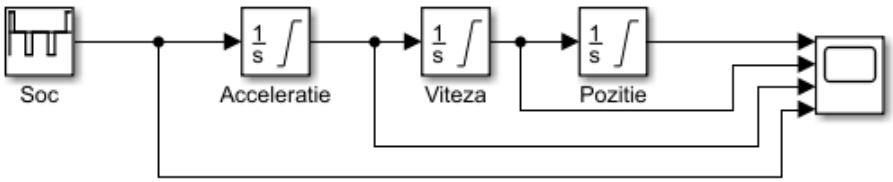

Fig. 8. Simulation model used

The simulation model used, see fig. 8, contains three "Integrator" blocks (*Acceleration, Speed* and *Position*) with saturation, the saturation limits being $\pm a_{max}, \pm v_{max}$ and *[0 .. 100 mm]*. The jerk is generated with the "Repeating Sequence Stair" block, and the output signals are viewed with the "Scope" block.

The S-curve generator was implemented according to the algorithm shown in fig. 7, in the Lazarus application development environment (www.lazarus-ide.org) under Windows. 32-bit arithmetic was used, in floating point with 24-bit mantissa and 8-bit exponent, respectively single type variables, see https://wiki.freepascal.org/IEEE_754_formats.

The evaluation of the developed algorithm was performed by programming the jerk generator from the simulation model, fig. 8, with the jerk route data from the S-curve generator, respectively the jerk values correlated with the movement times. The data were packaged for simulation as a vector with a time resolution of *1 ms*. Because of this it was necessary to convert the units of measurement according to relations (90), (91), (92) and (93).

The assessment criterion was the value of the position error, calculated as the difference between the values of the final positions of the S-curve generator and of the simulation on the model in fig. 8.

The simulation was performed in MATLAB & Simulink, variant R2019b.

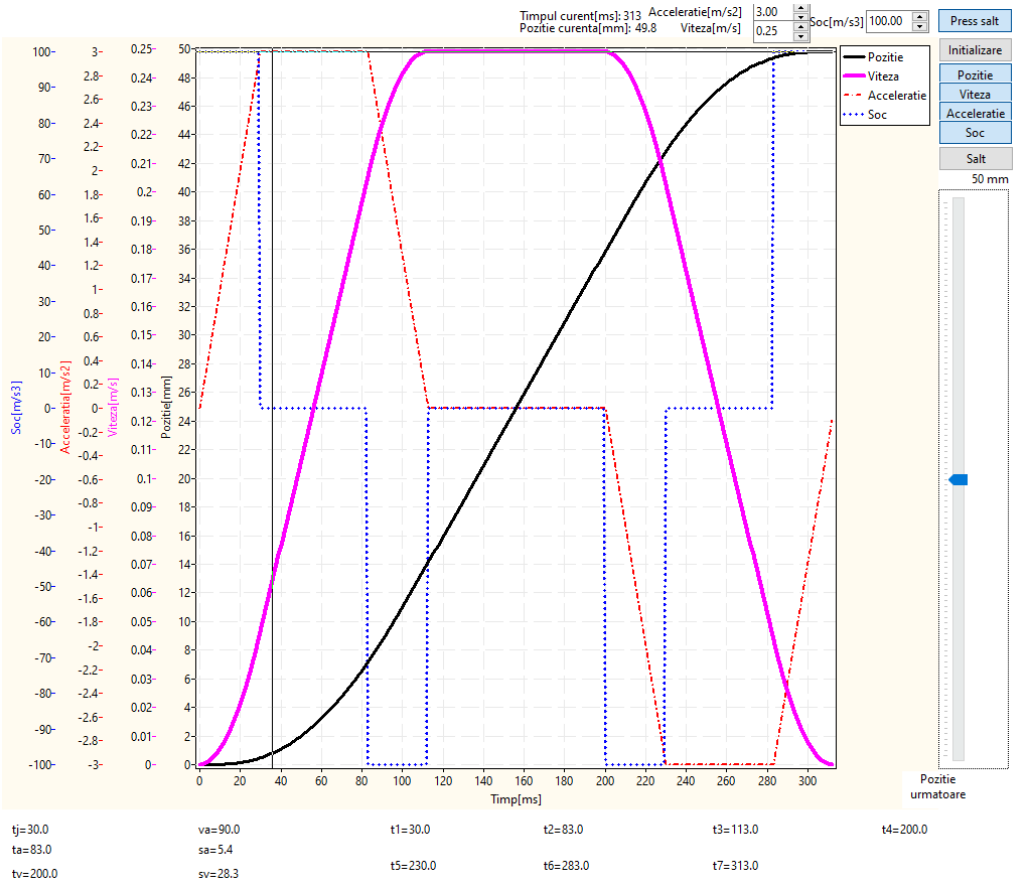

Fig. 9. Movement profile D.1

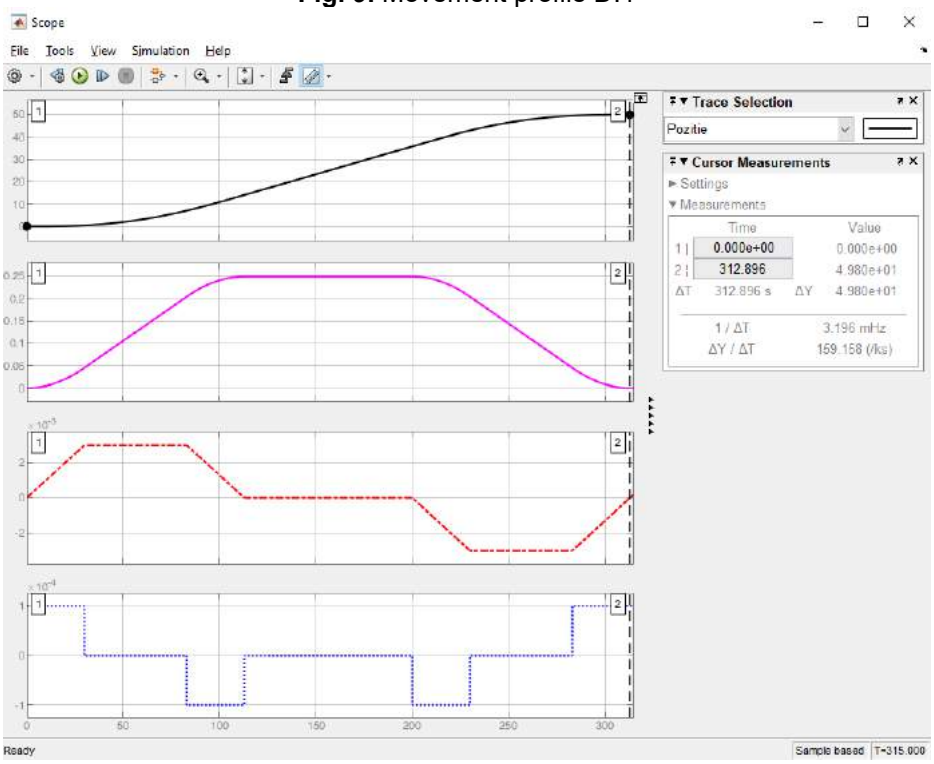

Fig. 10. Simulation results for case D.1

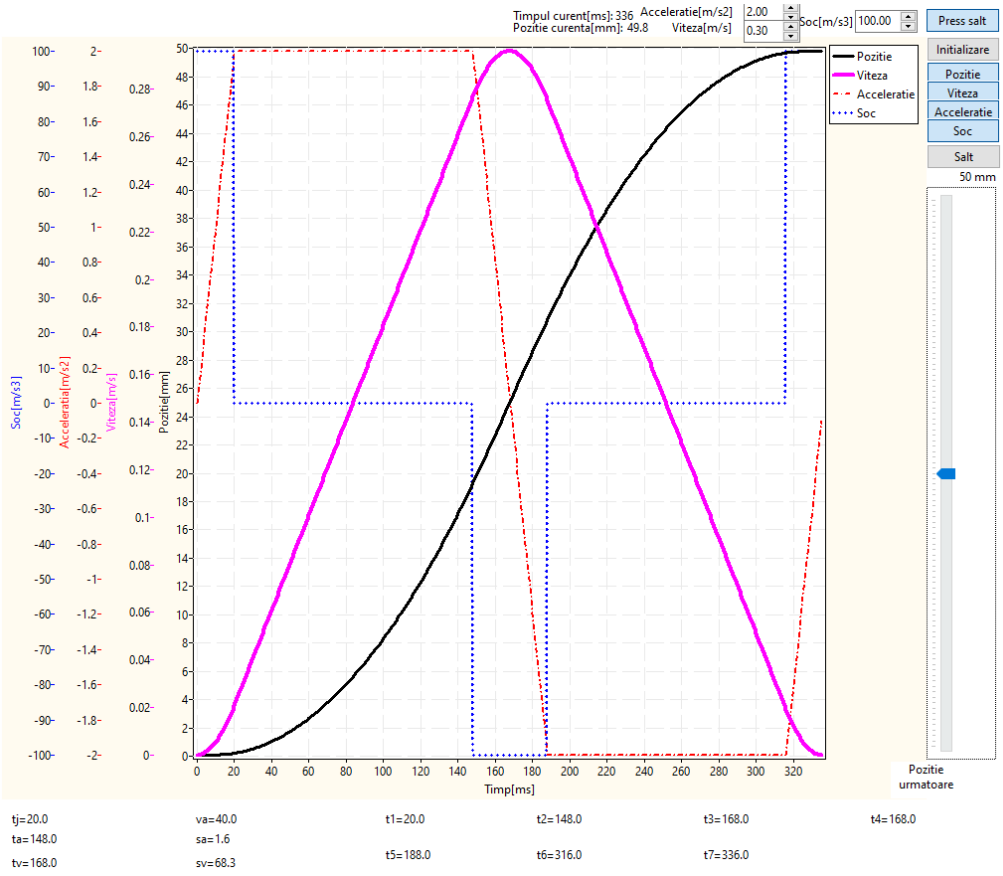

Fig. 11. Movement profile D.2

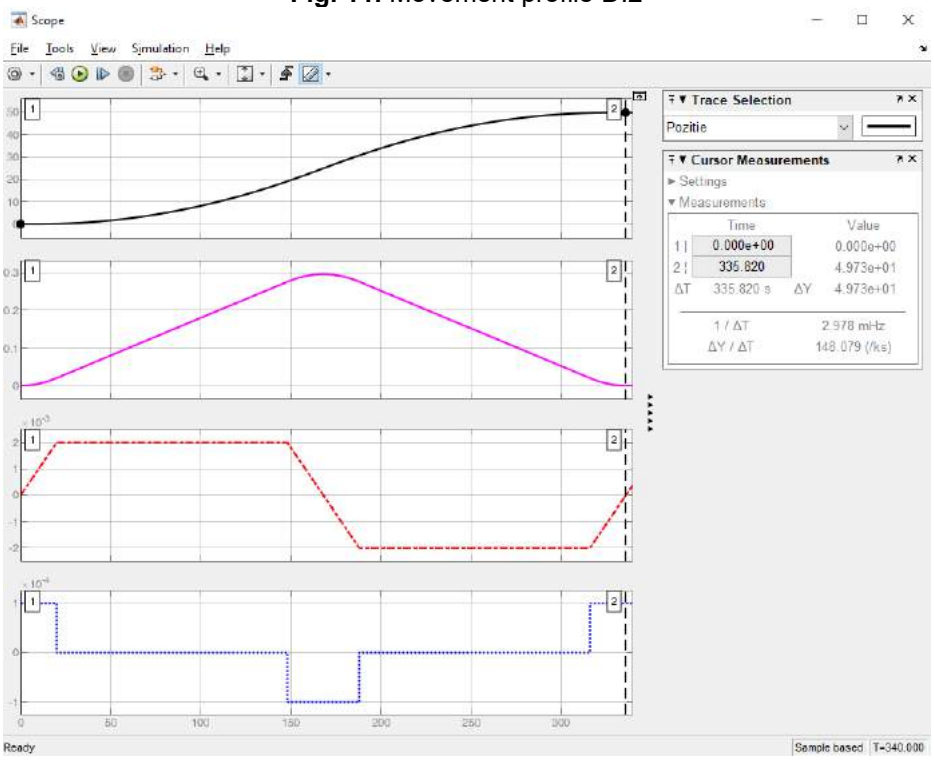

Fig. 12. Simulation results for case D.2

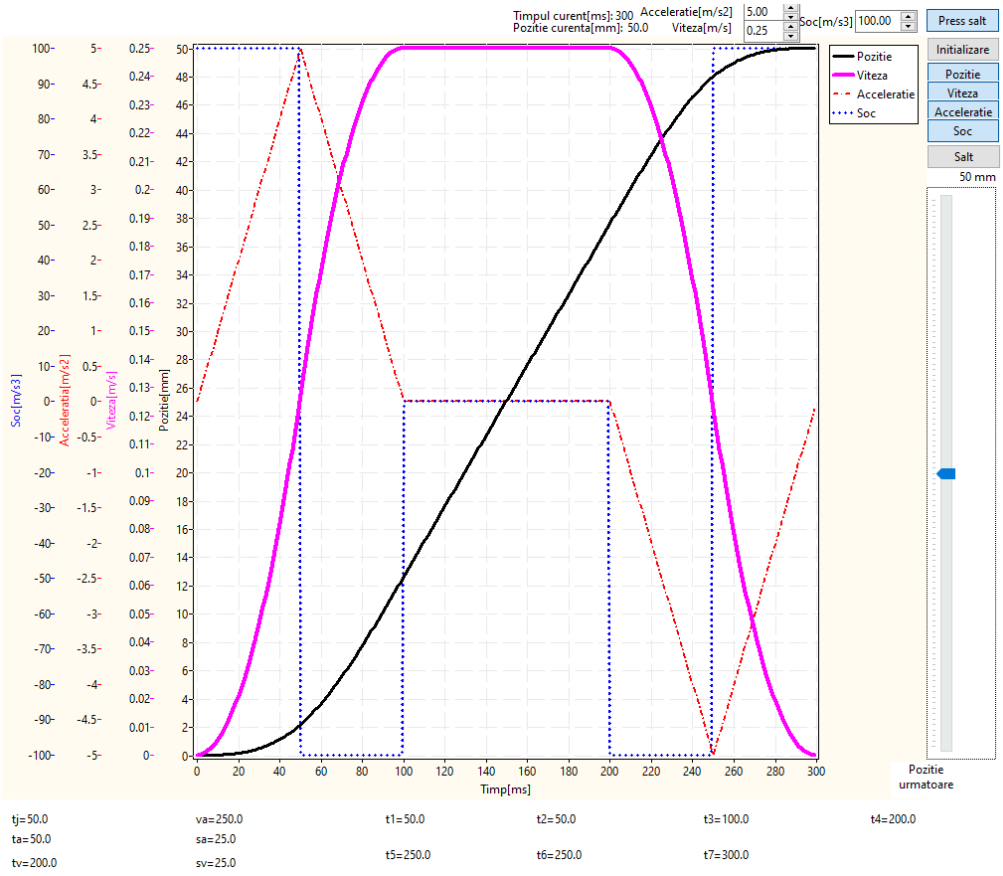

Fig. 13. Movement profiles A and C.1

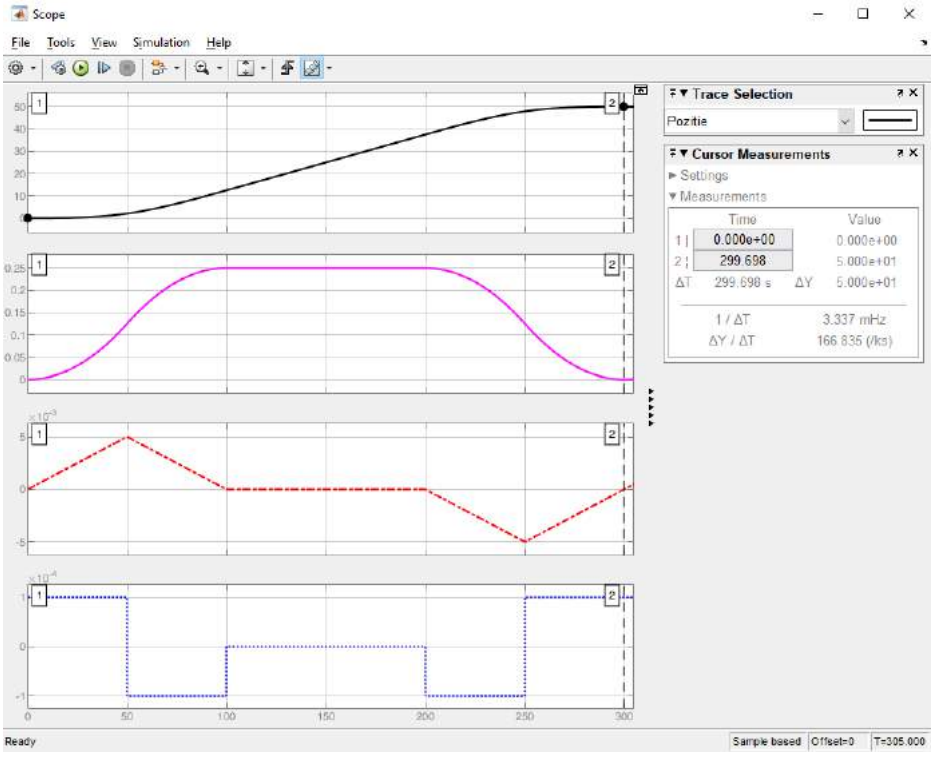

Fig. 14. Simulation results for cases A and C.1

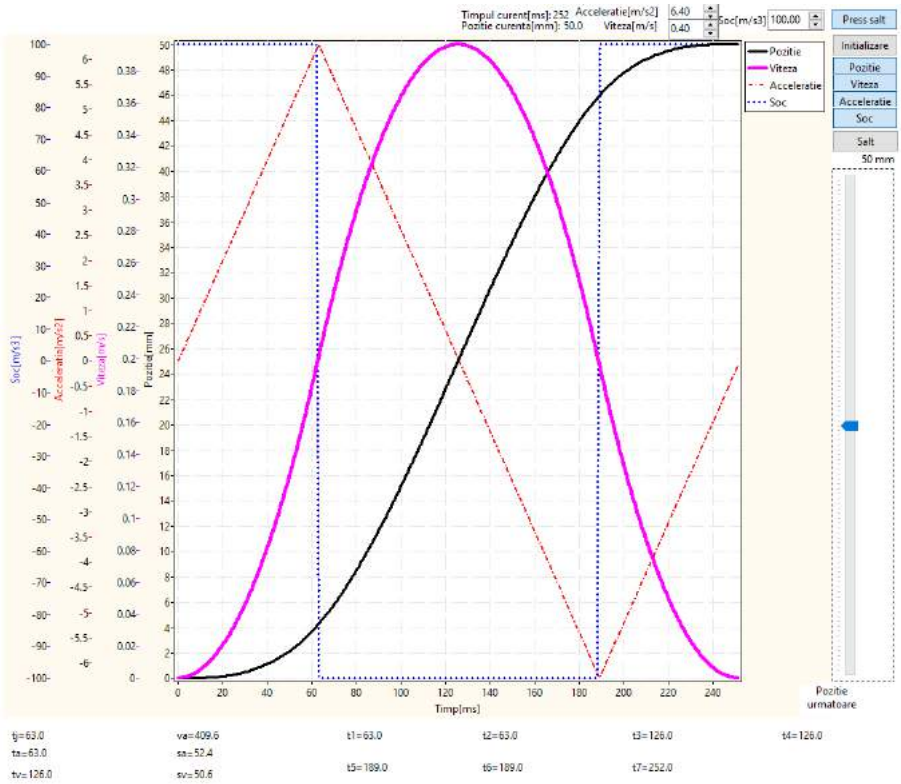

Fig. 15. Movement profiles B and C.2

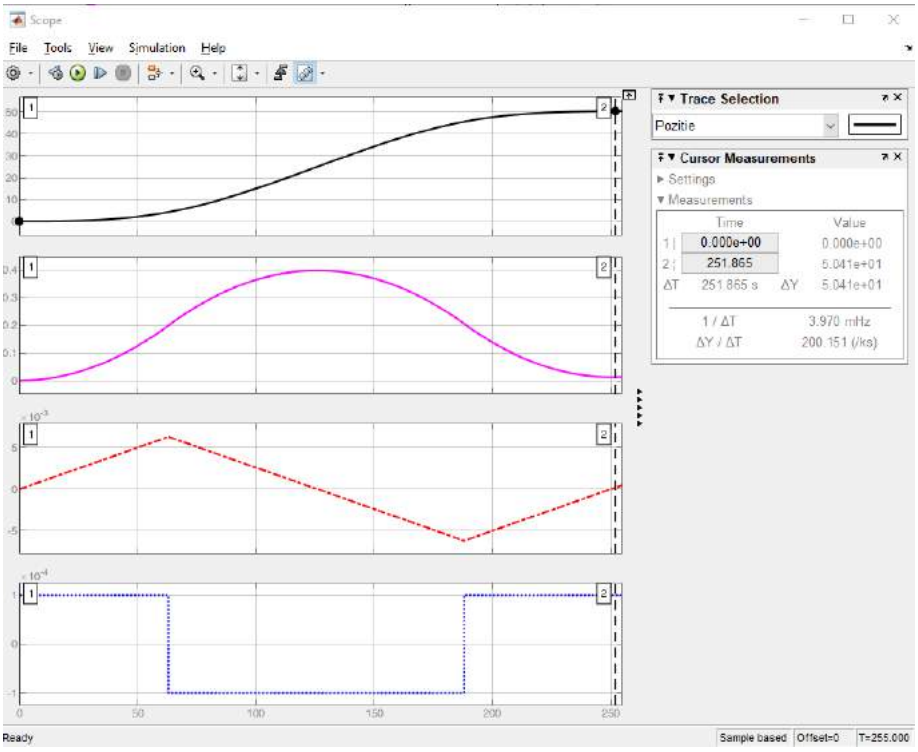

Fig. 16. Simulation results for cases B and C.2

Fig. 9 shows the motion profiles generated for a *50mm* jump, with limitations

$$J = 100\frac{m}{s^3} = 10^{-4}\frac{mm}{ms^3}\ ; a_{max} = 3\frac{m}{s^2} = 3 * 10^{-3}\frac{mm}{ms^2}\ ;\ v_{max} = 0.25\frac{m}{s} = 0.25\frac{mm}{ms}$$

, and the signal for the simulated jerk, see fig. 10, is the vector

[1e-4+zeros(1,30) zeros(1,53) -1e-4+zeros(1,30) zeros(1,87) -1e-4+zeros(1,30) zeros(1,53) 1e-4+zeros(1,30)].
In simulation the final value of the position is *49.8mm*, resulting in a position error that has the value of *0.2mm*, or in percent $\frac{0.2}{50} * 100 = 0.4\%$.
Fig. 11 shows the motion profiles generated for a *50mm* jump, with limitations

$$J = 100\frac{m}{s^3} = 10^{-4}\frac{mm}{ms^3}\ ; a_{max} = 2\frac{m}{s^2} = 2 * 10^{-3}\frac{mm}{ms^2}\ ;\ v_{max} = 0.3\frac{m}{s} = 0.3\frac{mm}{ms}$$

, and the signal for the simulated jerk, see fig. 12, is the vector
[1e-4+zeros(1,20) zeros(1,128) -1e-4+zeros(1,40) zeros(1,128) 1e-4+zeros(1,20)].
In simulation the final value of the position is *49.73mm*, resulting in a position error that has the value of *0.27mm*, or in percent $\frac{0.27}{50} * 100 = 0.54\%$.
Fig. 13 shows the motion profiles generated for a *50mm* jump, with limitations

$$J = 100\frac{m}{s^3} = 10^{-4}\frac{mm}{ms^3}\ ; a_{max} = 5\frac{m}{s^2} = 5 * 10^{-3}\frac{mm}{ms^2}\ ;\ v_{max} = 0.25\frac{m}{s} = 0.25\frac{mm}{ms}$$

, and the signal for the simulated jerk, see fig. 14, is the vector
[1e-4+zeros(1,50) -1e-4+zeros(1,50) zeros(1,100) -1e-4+zeros(1,50) 1e-4+zeros(1,50)].
In simulation the final value of the position is *50mm*, resulting in a position error that has the value of *0mm*, or in percent $\frac{0.27}{50} * 100 = 0\%$.
Fig. 15 shows the motion profiles generated for a *50mm* jump, with limitations

$$J = 100\frac{m}{s^3} = 10^{-4}\frac{mm}{ms^3}\ ; a_{max} = 6.4\frac{m}{s^2} = 6.4 * 10^{-3}\frac{mm}{ms^2}\ ;\ v_{max} = 0.4\frac{m}{s} = 0.4\frac{mm}{ms}$$

, and the signal for the simulated jerk, see fig. 16, is the vector
[1e-4+zeros(1,63) -1e-4+zeros(1,126) 1e-4+zeros(1,63)].
In simulation the final value of the position is *50.41mm*, resulting in a position error that has the value of *0.41mm*, or in percent $\frac{0.41}{50} * 100 = 0.82\%$.

6. Conclusions

After an exhaustive mathematical analysis of the movement between two points following a third order movement profile, a real-time algorithm is developed for the implementation of an online S-curve profile generator.
In order to confirm the correctness of the developed algorithm, a mathematical model of the third order motion is made using the MATLAB simulation environment. The motion profiles generated by the real-time algorithm and by the simulation model were compared in order to evaluate the performances of the S-curve generator. The parameter followed was an error in reaching the final position of the movement. The motion profile generator used 32-bit floating point arithmetic, with a 24-bit mantissa and an 8-bit exponent, as well as a calculation interval of *1ms*. The value of the error of reaching the final position, analysed in all possible cases of movement, turned out to be less than 1% of the value of the position jump.
In order to improve the value of the error, it is proposed to use the representation of numbers with a higher precision in the elaboration of the generator algorithm, for example the 64-bit floating point arithmetic, as well as a reduction of the calculation interval under *1ms*.

References

[1] Lewin, Chuck. "S-Curve Motion Profiles - Vital For Optimizing Machine Performance." https://www.pmdcorp.com/resources/type/articles/get/s-curve-profiles-deep-dive-article. Accessed November 26, 2020.
[2] Mu, Haihua, Yunfei Zhou, Sijie Yan, and Aiguo Han. "Third-order trajectory planning for high accuracy point-to-point motion." *Frontiers of Electrical and Electronic Engineering in China* 4, no.1 (March 2009): 83–87.
[3] ***. "Real-time computing", *Wikipedia*. https://en.wikipedia.org/wiki/Real-time_computing. Accessed November 26, 2020.

Automatic System for Handling Fragile Objects

Ph.D. Eng. **Ionel Laurențiu ALBOTEANU**[1]

[1] University of Craiova, Faculty of Electrical Engineering, lalboteanu@em.ucv.ro

Abstract: *The paper presents an automatic handling system made on a small scale. The entire structure is integrated in an electro-pneumatic drive. The handling of fragile objects is done using vacuum technology. The system is controlled by a PLC in accordance with the required operating protocol.*

Keywords: *Handling, automatic system, PLC, electro-pneumatic drive, vacuum technology*

1. Introduction

The technique of handling calls means or devices, which carry the flow of material from one post to another. One of the most important problems of industrial production automation is the transition from handling performed by the human operator to automatic handling [1].
The problem of developing standardized equipment systems for automatic handling of parts has become in recent years the main concern of global companies with technology concerns.
The advantages, qualities and flexibility of the pneumatic drives, the facilities offered by the interface elements have allowed a rapid improvement and adaptation to the new requirements imposed by the specifics of the processes in which they are integrated [2].
The rapid paces of technology development and advances in electronics have today enabled the development of highly efficient drive equipment and a high degree of "intelligence" built into it. Thus, the main direction of current research is to improve the control of pneumatic drives by incorporating "intelligence" [3].
Robots and manipulators are the most complex and flexible machines that have been created and used by man so far that incorporate pneumatic drives [3].
The handling of fragile parts based on vacuum technology ensures increased productivity offering maximum durability and functionality with a light, compact and robust design and the possibility to be used in any industry [4].
Taking into account these considerations, the paper presents an automatic system for handling fragile objects using a vacuum technology.

2. Structure of the handling system

The proposed automatic fragile object handling system consists of a stock of fragile plates at the entrance, an output stock and a manipulator system that transfers the plates to be processed from the input stock to the output stock (Fig.1).

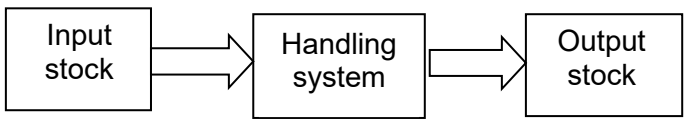

Fig. 1. Structure of handling system

Starting from the previously presented structure of the fragile object handling system, it is proposed to create a manipulating system that performs the handling operation for a single piece per work cycle, and the input stock has a capacity that can include several fragile plates.
The entire structure is integrated in an electro-pneumatic drive system with linear (pneumatic cylinder) and rotary (electric motor) actuators, controlled by monostable and bistable valves [5],[6].

The block diagram of the handling system is shown in Fig. 2.

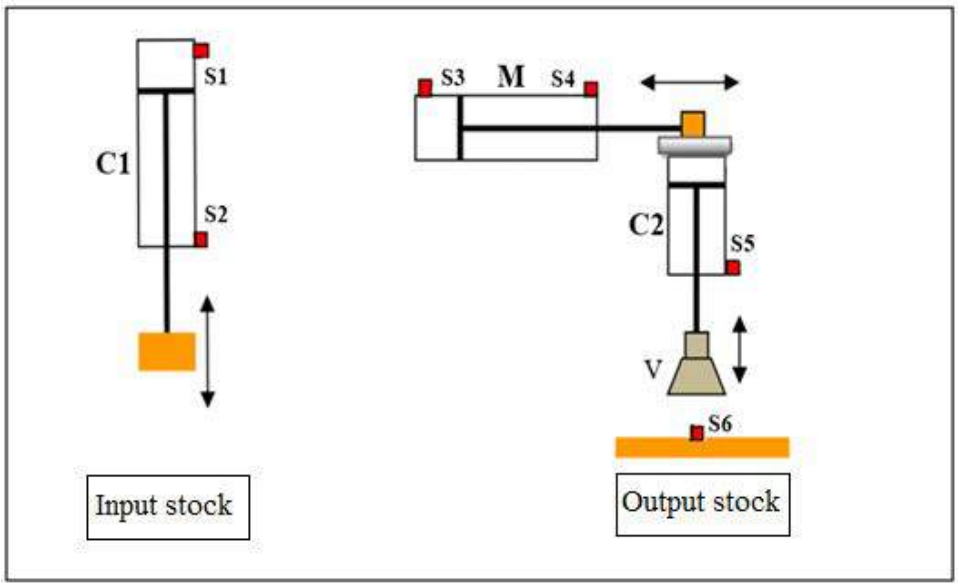

Fig. 2. Block diagram of handling system

Based on the structure of the pneumatic drive, general scheme of the automatic handling system (Fig. 3) was carried.

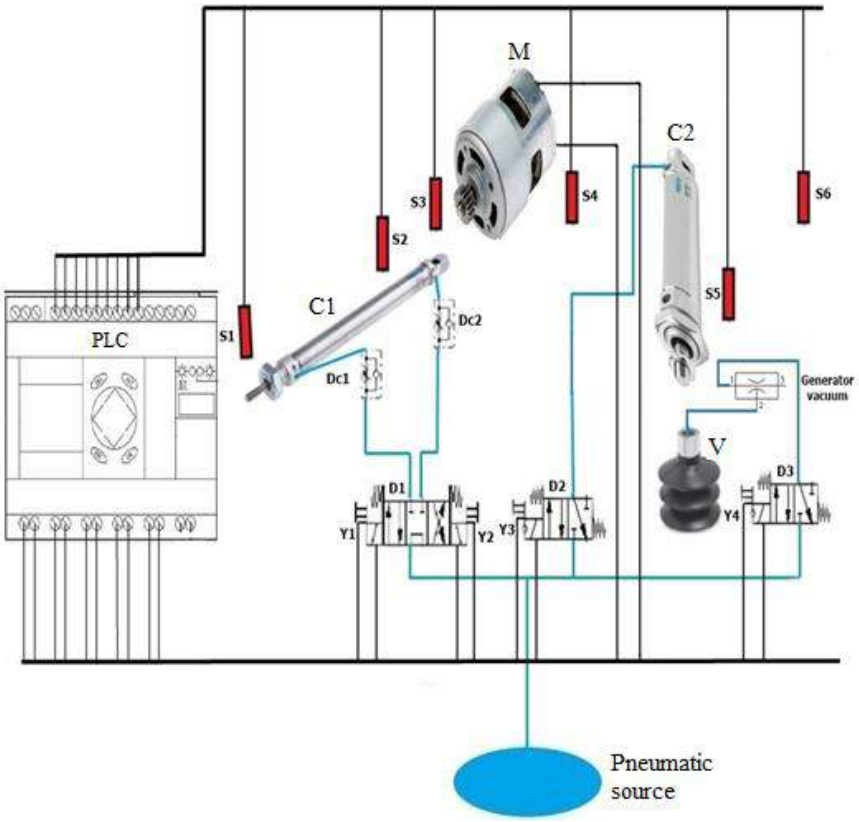

Fig. 3. Schematic diagram for the interconnection of the elements of the handling system

The meaning of the elements used in the scheme is as follows:
PLC - programmable logic controller;
D1...D3 – pneumatic valve;
C1, C2 – pneumatic cylinders;

M– electric motor;
DC1...DC3 – one-way flow control valve;
S1...S6 – sensors;
Y1...Y4 – relays valve control;
V - vacuum suction cup.

3. Modeling and simulation of the handling system

The pneumatic drive is modelled and simulated on a personal computer using the Festo FluidSim Pneumatics application [7], [8].
The modeling of the pneumatic actuator consists of two parts: shaping the power (pneumatic) part and shaping the electrical and control part. Both parts of system modeling mainly involve choosing components in the Component Library, placing them on the design sheet, setting parameters, and making connections between components [8].
If the component library is not visible in the workspace, it can be displayed by choosing Total View from the Library menu.
The model of the pneumatic part of the processing station was divided into two blocks (Fig. 4):
- the compressed air preparation unit block;
- the block of the handling system.
It is mentioned that the electric motor M in the handling system structure is replaced with a pneumatic cylinder C1.

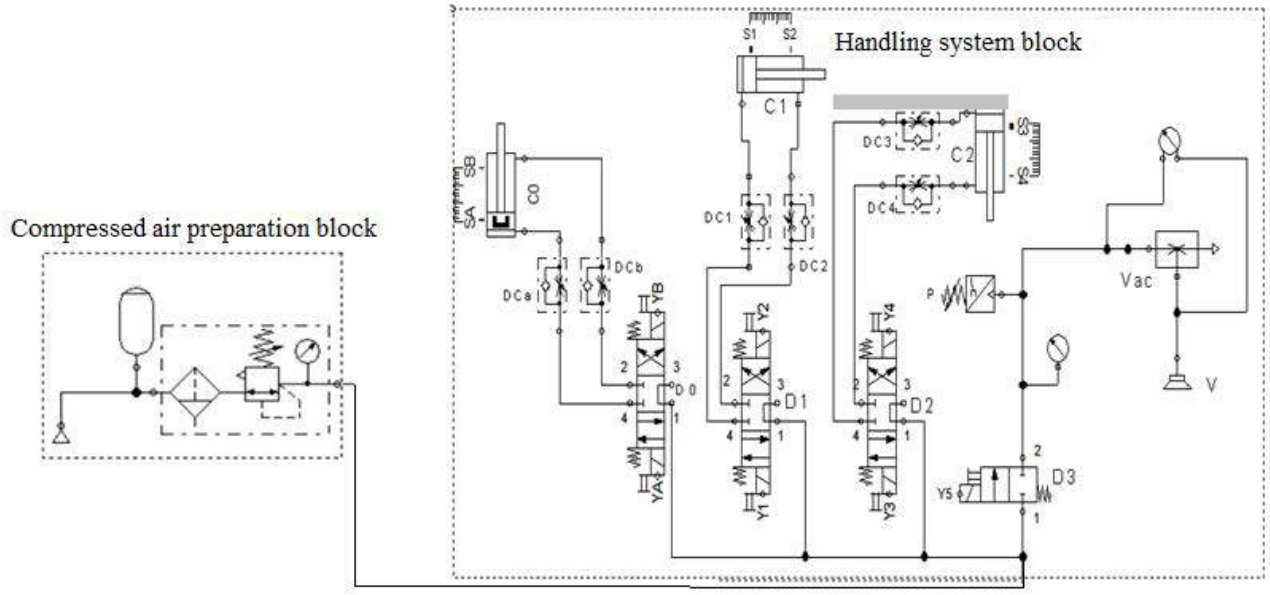

Fig. 4. FluidSim model of the handling system

A complete working cycle of pneumatic drive involves following sequences:
Stage 1:
Advance C0→Retraction C0→Advance C2→vacuum suction cup V is ON.
Stage 2:
Retraction C2→ Advance C1
Stage 3:
Advance C2 → vacuum suction cup V is OFF
Stage 4:
Retraction C2 → Retraction C1.
For simulation results, FluidSim can generate a state diagram of pneumatic drive [8]. The state diagram records the state quantity of important components and depicts them graphically (Fig. 5).

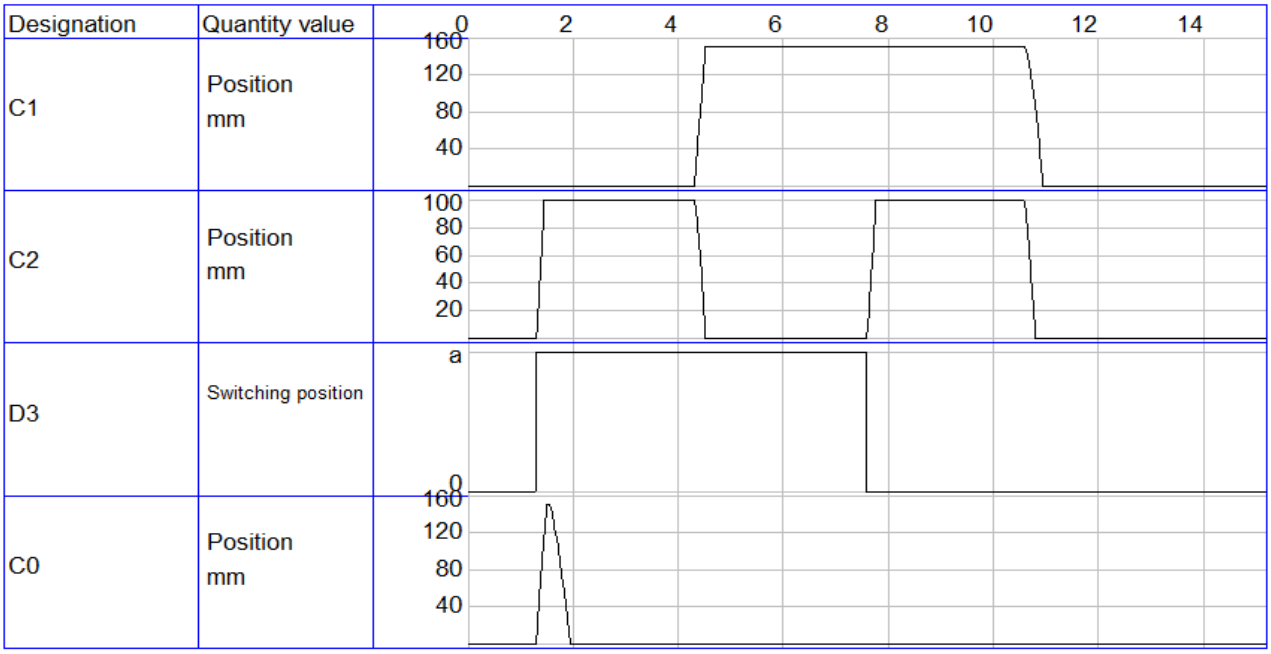

Fig. 5. State diagram of pneumatic components, in a work cycle generated by FluidSim

The status diagram is very useful for tracking and analysing the operating cycle. Based on this, anomalies, defects, irregularities in the operating cycle can be identified. Optimizations of the handling process can also be made.
The state diagram highlights the operating sequences of the execution elements in the pneumatic drive. These diagrams show the correct operation of the handling system.

4. Achievement of the automatic handling system

4.1. Achievement of the control system

The following aspects were taken into account in the implementation of the control system:
- simplifying the hard drive and using as few components as possible;
- the possibility of easy system programming.

To meet the above requirements, a PLC control system has been designed. For this purpose, the Eaton Easy AC-RC-719 programmable controller was selected [9], [10].
It offers a number of facilities including:
- small size;
- direct power supply to the 220V network;
- Keyboard and screen presence;
- a total of 14 entries.

If the Eaton Easy AC-RC-719 PLC is connected to a PC, then we can use the EASY-SOFT program. It will allow the creation and testing of the circuit on the PC, as well as the printing of the diagram made in the Ladder in DIN, ANSI format or in the own format generated by the software [9].

4.2. Achievement of the power and protection circuit

The Eaton Easy PLC is powered directly from the 230V 50Hz AC mains. A 24V DC source is required for the application to operate, as the coils of the 3 distributors, the relays and the sensors used operate at a voltage of 24V. Figure 6 shows the electrical circuit diagram of the handling system.

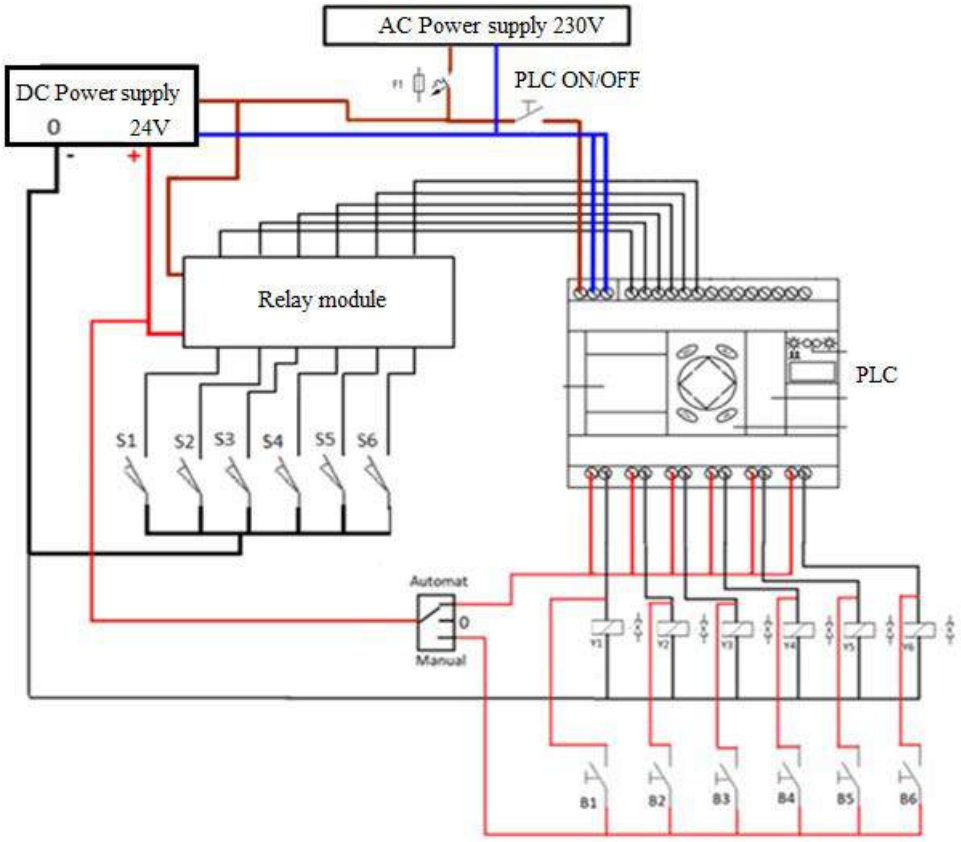

Fig. 6. Electrical circuit diagram of the handling system

4.3. Achievement of the user communication system

At the core of the control process there is the command and control unit that manages the entire process as well as the human-machine interface [11].
Based on the operating principle of a closed-loop control system [12], [13], the command and control unit takes over the position information of the system sensors from the position sensors and the presence piece sensor. After processing the information, according to a pre-set programme, control signals are generated to the pneumatic actuators.
The user communication system consists of the PLC keypad, a three-way switch, 6 buttons for manual control and the automatic display screen where one can see the activation of inputs (Fig. 7).
The keyboard allows the user to enter programs without a computer or modify certain parameters within an already created program.
The three-way switch is used to switch the mode of operation of the processing station. It allows switching from automatic mode to manual mode but also stops all pneumatic drive.
To avoid the dual simultaneous control, a separate PLC power supply switch was used which disconnects its power when the drive is operating in manual mode.
The 6 manual control buttons allow the control of the solenoid valves in the pneumatic drive.
An ejector type generator was used to create the vacuum: VN-07-H-T3-PQ2VQ2-RO1 [14].
Waircon URG 5/8 type regulators have been used to control actuator speed. The "URG" series flow regulators are produced in in-line, unidirectional versions [14].
The "URG" model [14] has a built-in control valve to control the flow in one direction, while the reverse flow is free. They are high precision regulators and can provide a high flow rate ratio and are very compact. For MK5100 IFM sensors were used to determine the position of pneumatic cylinders [14].
A Festo VASB-20 suction cup was used to hold the parts.

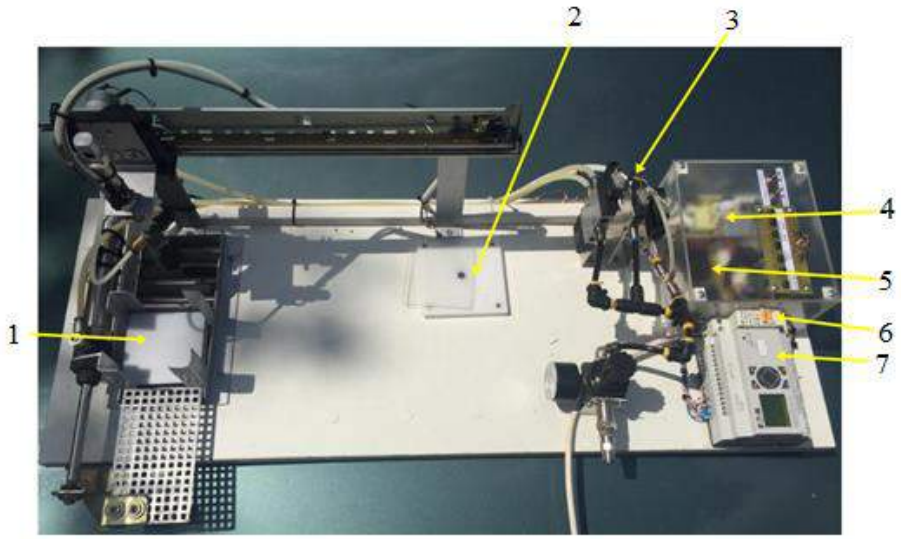

Fig. 7. Experimental model of the handling system made:
1- input piece stock; 2- output piece stock; 3- pneumatic valves; 4- DC power supply source; 5- relay module for adapting signals from sensors; 6- electrical protection 7- Eaton Easy 719 AC-RC PLC

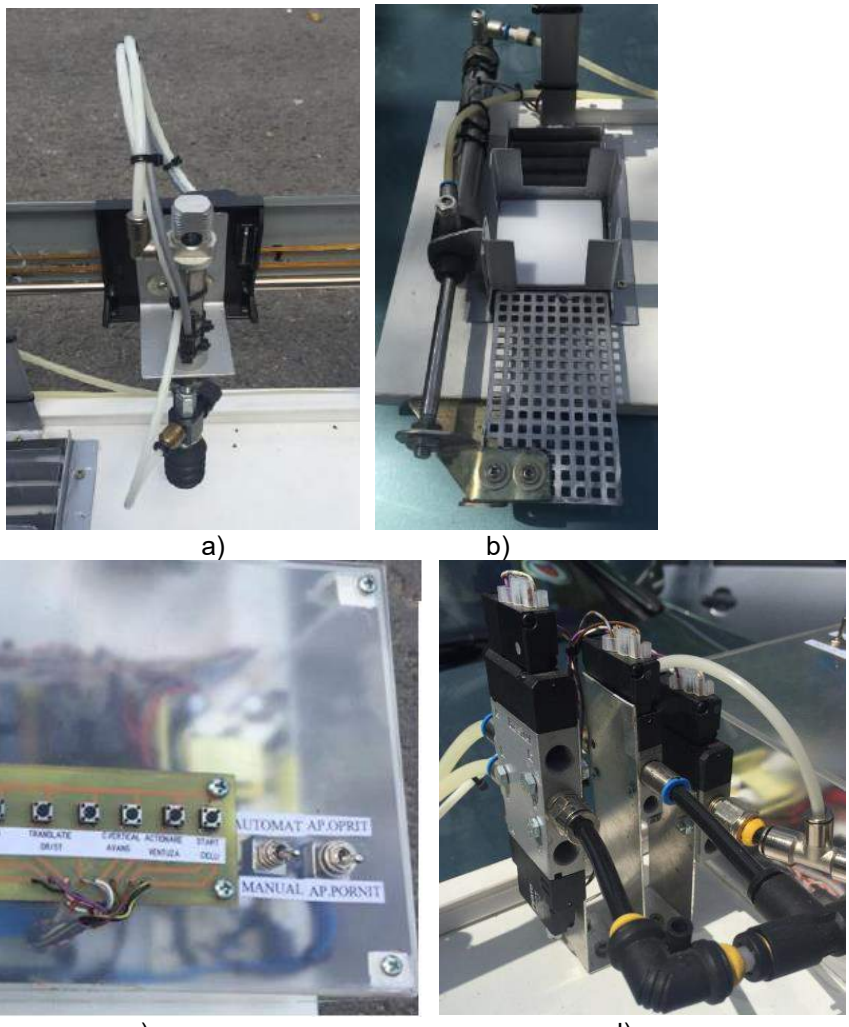

a) b)

c) d)

Fig. 8. Component modules of handling system: a) handling module; b) glass plate discharge module; c) manual control and protection module; d) pneumatic valves module

4.4. Development of the software for the Eaton Easy AC-RC-719 PLC

Starting from the simulated model, with the help of the PLC's own software, Easy-Soft, a program that respects the required operating protocol was made. EASY-SOFT is a PC program [15], with which one can create, store, simulate, document easily connection schemes that can be transferred later in an easy device ready for operation.
The verification of the software was done by simulation. The simulation of the program showed the correct operation according to the imposed protocol. After the simulation, the program was transferred to the PLC memory. The actual operation was then checked here as well. The correct operation was also verified in real conditions on the experimental system.

5. Conclusions

Industry in general and the machine construction, in particular, requires great flexibility of the manufacturing process, flexibility enabling the easy transition from the technical and cheap in terms of equipment and labour to another manufacturing. In this context, it is necessary to design and implement special equipment that will comprise flexible automation. Manipulators and robots, which ensure the construction features, functional characteristics and quality indicators for flexible manufacturing, have an important role in this equipment.
In this paper, a small-scale automatic system for handling glass pieces was designed and developed. It corresponds to the requirements and rigors imposed on a flexible manufacturing system.
Infrastructure hardware and software used allows monitoring and control of a handling system.
Both the pneumatic part of performed handling system and the electrical and command part were proven correct functioning according to the solution and protocol required.
The system designed, developed and tested can be used both in educational applications in electrical engineering and in industrial applications.

References

[1] *** https://www.buettelundmarx.de/.
[2] Drighiciu, M.A. *Hydro pneumatic drive and automation/Acţionări şi automatizări hidropneumatice*, Craiova, Publishing House of University of Craiova, 2003.
[3] ***. "About flexible production systems and complex automation." *Plant Engineering* 118, XIII Year, no. 11 (2013): 42-45.
[4] Hucknall, D.J. *Vacuum Technology and Applications*. Elsevier, 2013.
[5] Alboteanu, L., Gh. Manolea, and F. Ravigan. "Automatic sorting and handling station actuated by pneumatic drive." *Annals of the University of Craiova, Electrical Engineering Series,* no 1 (2018): 1-8.
[6] Alboteanu, L. "Automatic Processing Station Actuated by Pneumatic Drive." *Hidraulica Magazine*, no. 1 (March 2019): 16-22.
[7] Alboteanu, L. "Modeling an Automatic Processing Station Using Fluidsim Software." *Hidraulica Magazine*, no. 3 (September 2017): 27-30.
[8] ***. FESTO FluidSIM Pneumatic 4.2, Software. User manual.
[9] ****. https://www.eaton.com/us/en-us/catalog/machinery-controls/easy-programmable-relays.html.
[10] Alboteanu, I.L. "Pneumatic Tracking System for Photovoltaic Panel." *Hidraulica Magazine*, no. 1 (March 2015): 32-39.
[11] Avram, M., C. Bucşan, and V. Banu. "Innovative Systems for Incremental Positioning in Pneumatics." *Hidraulica Magazine*, no. 2 (June 2015): 52-56.
[12] Nawrocki, W. *Measurement Systems and Sensors.* London, Artech House Publishers, 2005.
[13] Toma, L. *Acquisition and digital signal processing systems / Sisteme de achizitie si prelucrare numerica a semnalelor*. Timişoara, "Vest" Publishing House, 1996.
[14] ***. http://www.festo.com/net/startpage/.
[15] ***. https://www.eaton.com/ca/en-gb/catalog/machinery-controls/easysoft.html.

Predicting the Peak Water Level of Flood Waves by Using Statistical Methods on River Rába

PhD student **Gábor KERÉK**[1]

[1] Deputy Head of Department, North Transdanubian Water Directorate, Győr, Hungary,
kerek.gabor@eduvizig.hu

Abstract: *This year, as a result of a joint Hungarian-Austrian development, an early flood warning system of the Rába river basin was completed, based on hydrodynamic model support. The warning system calculates the water flows and levels with a 6-day time advantage in the defined water gauge sections of the catchment. The system also includes a 2-dimensional flood model subsystem, which models the evolution of valley floods in case of a flood wave event.*
As a part of this project, an application was also implemented, which allows statistical-based parameter estimation onto flood peak levels. The basic mathematical method of this app is the multivariable linearized regression. Its parameters are characteristics water levels or water discharges that measured in the same water gauge sections as in the hydrodynamic model.
In this study, I describe the hydrological foundations of the database serving this application and then I evaluate the first results.

Keywords: *Hydrological statistics, Rába, Linearized regression, Flood forecasting, Numerical analysis*

1. River Rába and its catchment, Flood forecasting issues on Rába

Rába is one of the most significant tributaries of the Danube in Hungary. Its origin is in Styria province of Austria, in the Fischbach Alps, at an altitude of around 1200 m above sea level, from two branches. It crosses the Austrian-Hungarian border at Szentgotthárd, flows across Kisalföld region of Hungary, and reaches its receiving river Mosoni-Duna in the city of Győr. The total length of the river is 283 km, and its section in Hungary is 211.5 km. The catchment area is 10270 km^2. [1] One third of its catchment area is in Austria and two thirds in Hungary. The catchment area of river Rába is shown on the next figure.

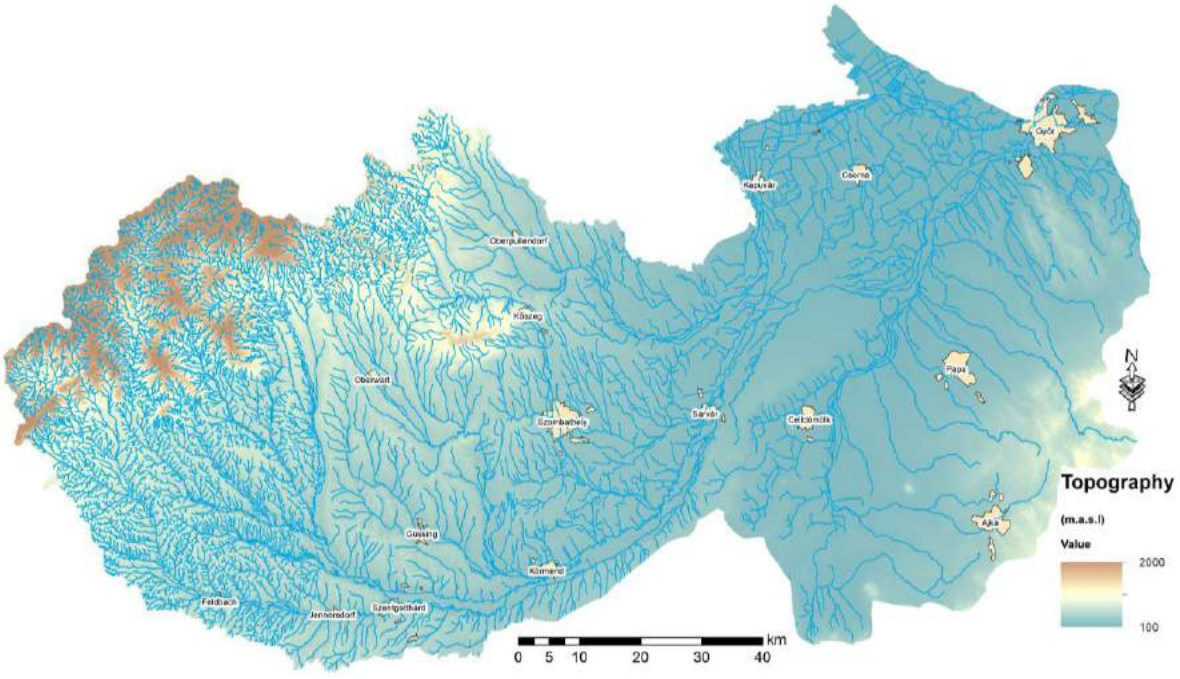

Fig. 1. Rába river basin

The current and the expected hydrological regime of our rivers is the basic of several water management tasks, and it has an essential role in the work of flood defense organizations and in disaster emergency planning. The newly developed early flood warning system on the river basin of Rába can partially fulfil this role, the hydrodynamic model system operating on meteorological boundary conditions estimates the expected water flow and water level in some cross-sections of significant rivers of the river basin for a 6 days ahead. However, in case of flood events, additional forecasts are also made in order to support the necessary measures in technical, logistical and economic sense in flood protection. This method basically not based on the river basin's meteorological forecasts, but on a statistical analysis of long-term water level time series measured in water gauge profiles. The method is based on the principle of linearized regression and it's also suitable for the continuous prediction of time series, however, with an appropriate pre-processing of the time series, the peak water levels of the flood waves can be determined with sufficient accuracy. The processed time series are derived from the long-term measured water level time series of the water system. Their location is shown in Figure 2.

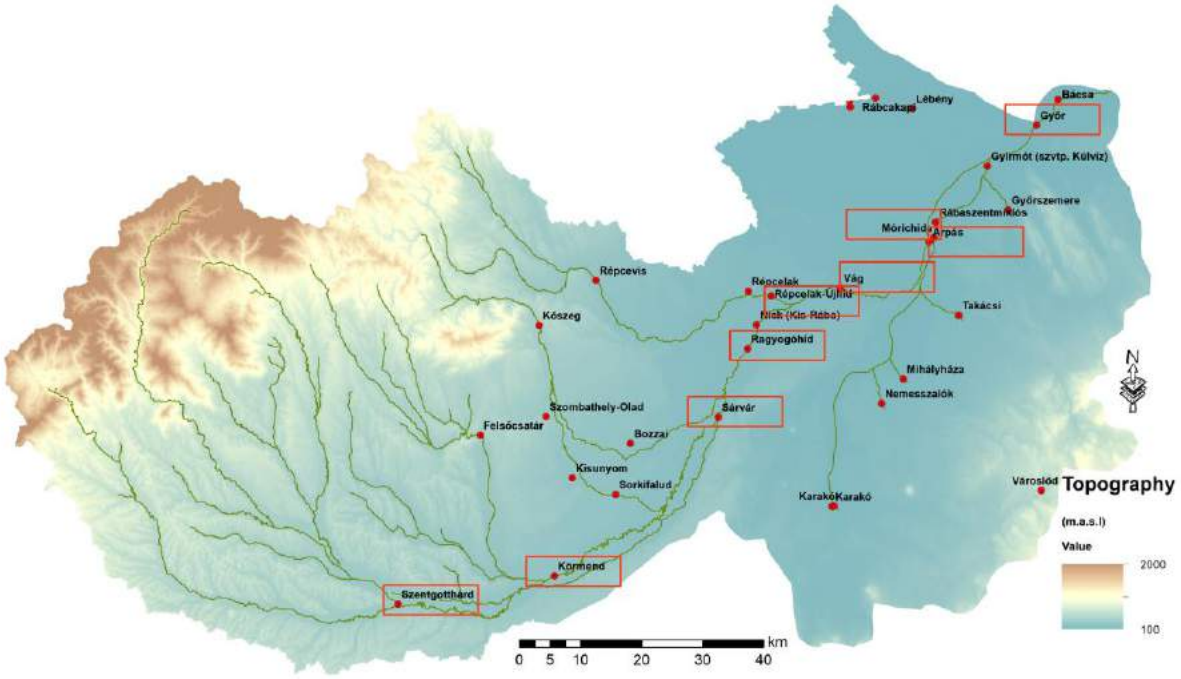

Fig. 2. Water gauges on the river basin of Rába

First, let's briefly review the mathematical foundations of regression analysis.

2. Mathematical basics of linearized regression

Due to its flexibility, this method is applicable for comparing time-invariant datasets, for parameter-estimation, if there is a physical relationship between the individual probability variables. The procedure can be used in cases where the relationship between two probability variables is not clearly defined. In this case, the values of the independent variable belong to a statistical set of the dependent variable, so that the distribution of the dependent variable together with the distribution of the independent variable changes in a specific way. In this case, there is a correlation between the variables. In a correlation relationship, the relationship can be given between the expected values of the variables; thus, the correlation occupies an intermediate space between the well-

defined function relationship and the complete independence of the variables (stochastic relationship). The closeness of the relationship is expressed by the correlation coefficient (r).

$$0<r<|1| \tag{1}$$

where the value of the correlation factor 0 refers to the complete independence of the variables and 1 refers to the exact function relationship.

The following tasks may be possible during the regression analysis:

- estimating the parameters (constants) of a function describing the relationship between two variables
- examination of the linearity hypothesis (statistical test of correlation coefficient)
- examining the assumptions about the parameters of the fitted function
- calculation of the confidence interval
- estimating the parameters of the function and the margins of error of physical quantities [2]

In regression analysis, the basic task is to fit a line or curve to a point cloud expressed by the relationship of the variables so that the difference between the points and the theoretical function is as small as possible. Obviously, no curve can be drawn that touches all points; thus, the task is to choose a relation based on theoretical considerations in the knowledge of the examined system, which enforces the physical regularities of the variables as best as possible. E.g. with the usage of power functions any point cloud can be described with an appropriate precision, but it's doubtful that the theoretical function has physical meaning, or the precision can only mathematically proved. The aim is to define an equation in which by substituting the different values of the independent variable (x), we can estimate the values of the dependent variable (y) as accurate as possible. To define this equation the least-squares-based regression analysis is used. [2]

Principle of least squares: the function describing the relationship between the variables and its parameters are defined so that the sum of the squares of the differences between the measured dependent variable values and the values calculated by substituting the same independent variable from the relationship is minimal. In the simplest case the equation of a line is fitted to the point cloud. [2]

The equation of a line is:

$$\boldsymbol{y = a + b * x} \tag{2}$$

Based on the principle of least squares, the most probable values of the parameters are: the minima of the sum of the squares of the deviations of the dependent variable calculated from the function and the measured variable

$$Q = \sum_{j=1}^{n} (y_j - f(x_j))^2 = \sum_{j=1}^{n} (y_j - a - bx_j)^2 = \min. \tag{3}$$

In the equation we consider the parameters of the function (a, b) as variable, and the measured value pairs x_j and y_j are fixed.

The condition of minima:

$$\frac{\partial Q}{\partial b}=0; \qquad \frac{\partial Q}{\partial b}=\sum_{j=1}^{n}-2(y_j-a-bx_j)x_j=0$$
$$\frac{\partial Q}{\partial a}=0; \qquad \frac{\partial Q}{\partial a}=\sum_{j=1}^{n}-2(y_j-a-bx_j)=0 \tag{4}$$

, these equations ordered and simplified are the following

$$\sum_{j=1}^{n}x_jy_j=b\sum_{j=1}^{n}x_j^2+a\sum_{j=1}^{n}x_j$$
$$\sum_{j=1}^{n}y_j=an+b\sum_{j=1}^{n}x_j \tag{5}$$

In this form the 'a' and 'b' parameters can be determined directly:

$$b=\frac{n\sum_{j=1}^{n}x_jy_j-\sum_{j=1}^{n}x_j\sum_{j=1}^{n}y_j}{n\sum_{j=1}^{n}x_j^2-\left(\sum_{j=1}^{n}x_j\right)^2}=\frac{\overline{x*y}-\overline{x}*\overline{y}}{\overline{x^2}-\overline{x}^2}$$
$$a=\frac{\sum_{j=1}^{n}y_j-b\sum_{j=1}^{n}x_j}{n}=\overline{y}-b*\overline{x} \tag{6}$$

The difference between the value pairs xj and yj and the y values calculated from the calculated equation of the line defined by the parameters a and b is called the residue. Based on this, the residual standard deviation can be calculated with the following formula

$$S^{*2}_{reziduális}=\frac{\sum_{j=1}^{n}\left[\left(y_j-a-bx_j\right)^2\right]}{n-2}=\frac{\sum_{j=1}^{n}\left(\Delta y_j\right)^2}{n-2} \tag{7}$$

, where $\sum_{j=1}^{n}(\Delta y_j)^2$ is the sum of the squares of the deviation. This quantity is the fit standard deviation and it describes the regression fit. The residual standard deviation defines a confidence interval around the regression line in both directions, which can be used to examine the quality of the fit. By using the equation of line, the standard deviation of the 'b' parameter (the slope of line) can also be determined:

$$S_b=\frac{S^*_{reziduális}}{S_x\sqrt{n}}=\frac{S^*_{reziduális}}{\sqrt{\sum_{j=1}^{n}(x_j-\overline{x})^2}}$$
$$S_x=\sqrt{\frac{\sum_{j=1}^{n}(x_j-\overline{x})^2}{n}} \tag{8}$$

The confidence interval is the following: $b \pm t_Q * S_b$ (9)

, where

t_Q is the probability value of the distribution 't' with probability 'Q', so it can be stated with probability 1-Q, that the true value of parameter 'b' is within this interval.

3. Building the database of regression parameters

The aim of the regression analysis is to predict the peak water levels of the flood waves in Rába by processing past hydrological data. In this first stage of the evaluation, I defined a regression-based forecasting model for the main water gauges of the Rába. These prediction points are marked with red squares in Figure 2.

This goal can be achieved by building and applying a well-constructed database that estimates the expected value of a selected target parameter (as dependent variable) based on a statistical sample of the behavioral characteristics of several flood waves in the past. To this end, hydrological data time series of 147 flood waves has been organized into an SQLite database from a total of 13 hydrographic stations between 1965 and 2019 [3].

The calculation parameters of the model are the peak water levels of each flood wave at the indicated water gauge profiles, as shown in Fig. 3. The physical properties of flood waves can be modeled by adding additional parameters. When a flood occurs, the magnitude of the peak water levels crucially depends on the load of the riverbed. When a flood wave arrives onto a riverbed section, and the riverbed is relatively empty, a significant part of the flood volume will be lost for filling the bed, and the longitudinal peak water discharges decreasing from section by section. This effect can be modeled by a parameter, we called 'simultaneous water levels'. This means, that additional values are stored in the database, the actual water levels in the time of an upper station's flood peak.

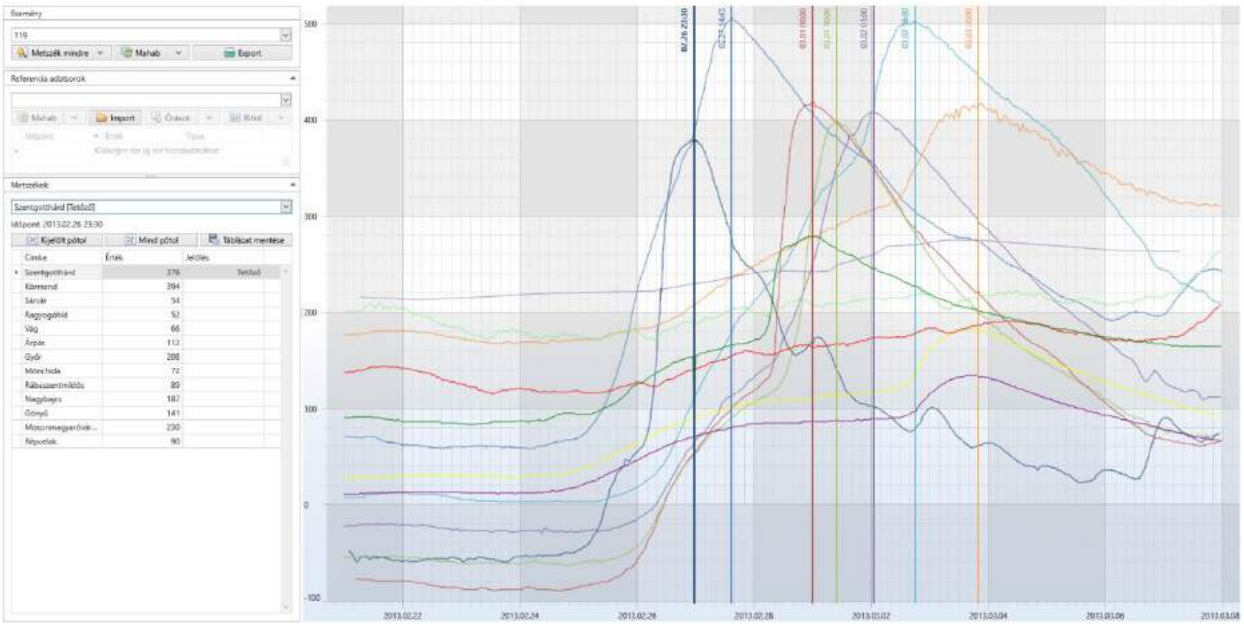

Fig. 3. Evaluation of the flood waves [4]

A part of the database numerically represented in the following figure:

Flood wave			Simultaneous water levels (cm)											Peak water levels (cm)										
ID	Time of Szentgotthárd peak	Szentgotthárd	Körmend	Sárvár	Ragyogóhíd	Vág	Árpás	Győr	Mórichida	Rábaszentmiklós	Nagybajcs	Gönyű	Répcelak	Körmend	Sárvár	Ragyogóhíd	Vág	Árpás	Győr	Mórichida	Rábaszentmiklós	Nagybajcs	Gönyű	Répcelak
1	1982.01.02 15:12	215	345	78	42	87	23	250	90	111	298	235	104	388	165	118	190	213	442	123	130	506	480	166
2	1982.05.24 23:51	182	110	-48	-63	-9	-18	318	-2	-37	416	350	70	250	68	39	90	110	385	22	-25	450	414	72
3	1982.08.09 05:02	84	218	72	41	87	72	302	72	41	309	253	202	264	97	58	134	162	319	100	84	332	284	208
4	1982.10.07 18:42	353	417	166	115	169	210	291	-13	-11	169	120	201	473	362	294	362	420	360	8	52	198	158	288
5	1982.10.07 18:42	353	417	166	115	169	210	291	-13	-11	169	120	201	473	362	294	362	420	392	30	73	198	158	288
6	1982.10.14 22:43	277	340	113	91	179	237	336	11	27	170	140	185	440	362	294	362	420	392	30	73	234	188	274
7	1982.11.14 21:00	131	181	-55	-39	7	12	157	-30	-34	103	54	100	303	106	78	150	183	260	17	14	154	99	171
8	1982.12.19 06:00	231	243	-10	-6	36	50	209	5	-4	203	157	156	392	159	118	205	234	294	80	82	266	206	250
9	1982.12.19 06:00	231	243	-10	-6	36	50	209	5	-4	203	157	156	388	173	130	212	281	366	175	181	286	252	250
10	1982.12.19 06:00	231	243	-10	-6	36	50	209	5	-4	203	157	156	388	173	130	212	281	366	175	181	286	252	250
11	1984.03.02 19:50	75	180	55	-27	20	19	168	-9	-15	128	74	90	250	67	63	127	142	273	6	-6	142	90	115
12	1984.04.04 12:25	226	252	-12	-20	23	5	183	-30	-43	237	178	103	317	100	74	142	170	260	-14	-29	259	202	143
13	1984.05.30 03:00	113	90	-48	-45	7	4	218	-8	-27	287	227	105	251	51	43	99	101	260	-1	-21	322	257	105
14	1985.03.23 05:35	296	367	101	72	147	179	260	63	61	179	119	152	438	295	238	292	381	374	87	74	301	250	211
15	1985.05.08 01:00	266	289	-40	-52	22	15	209	-12	-22	277	201	115	380	136	108	176	229	290	7	-2	310	236	169
16	1985.05.17 01:00	279	96	-42	-47	24	33	245	-18	-34	338	262	63	314	88	65	130	157	306	60	61	373	306	174
17	1985.08.07 16:00	253	87	-94	-90	-34	-30	242	-45	-60	350	268	54	263	59	39	97	126	600	14	59	659	631	126
18	1985.12.30 06:24	73	95	-84	-85	-20	-19	156	53	48	159	85	74	251	56	41	87	123	234	113	114	222	146	124

Fig. 4. Part of the database in numerical form

In the present study, I set up a regression model with multivariable linearized regression to estimate the peak water levels at Körmend, Sárvár and Árpás based on the Szentgotthárd peak water level. To perform this task, the parameters shown in the following table were used for each flood wave:

Table 1: regression parameters used for the model

Independent variable	Physical meaning of parameter
$H_{Kö\ T}$	Peak water level at Körmend (cm)
$H_{Sztg\ T}$	Peak water level at Szentgotthárd (cm)
$H_{Sá\ T}$	Peak water level at Sárvár (cm)
$H_{Ár\ T}$	Peak water level at Árpás (cm)
$H_{Kö\ T0Sztg}$	Simultaneous water level at Körmend at the time of Szentgotthárd peak (cm)
$H_{Sá\ T0Sztg}$	Simultaneous water level at Sárvár at the time of Szentgotthárd peak (cm)
$H_{Ár\ T0Sztg}$	Simultaneous water level at Árpás at the time of Szentgotthárd peak (cm)

4. Multivariable linearized regression

In the case of multivariate linear regression, the target dataset is not a function of one, but of several independent datasets. In this case, the regression result is obtained as the result of a first-order polynom; thus, the estimate is obtained as the sum of the independent variables. The aim is to determine the coefficients of the polynom, its principle is the least squares method. [2] The polynomial regression in this case takes the following form:

$$y = a_1 * x_1 + a_2 * x_2 + ... + a_n * x_n \tag{10}$$

To minimize the difference between the defined formula and the measured target time series, partial derivatives of the estimation function must be generated:

$$\sum_{i=1}^{N} (Y_i - F(x_i))^2 \tag{11}$$

, the zero positions of this partial derivatives need to be determined.

The regression model for the above-mentioned water gauges were performed with this method. The calculated function for Körmend is shown on Fig.5. As shown in the figure, a linearized function describes the relationship of the variables, which is a polygon corresponding to the equation (), and accordingly all independent variables that can be involved to the calculation has its first and second powers in the equation. Higher degree polynomials can also be fitted by the application, which describe the relationship of the parameters with a tighter fit, but this can only be verified mathematically. Knowing the physical relationship of the variables, it is advisable to approach the relationship with a polynomial with the lowest possible degree. [2]
In this first part of this study 3 main water gauge sections were involved to this multivariable regression, to estimate the peak water level of the floods. In the next chapter I describe the regression model for the estimation of their water levels.

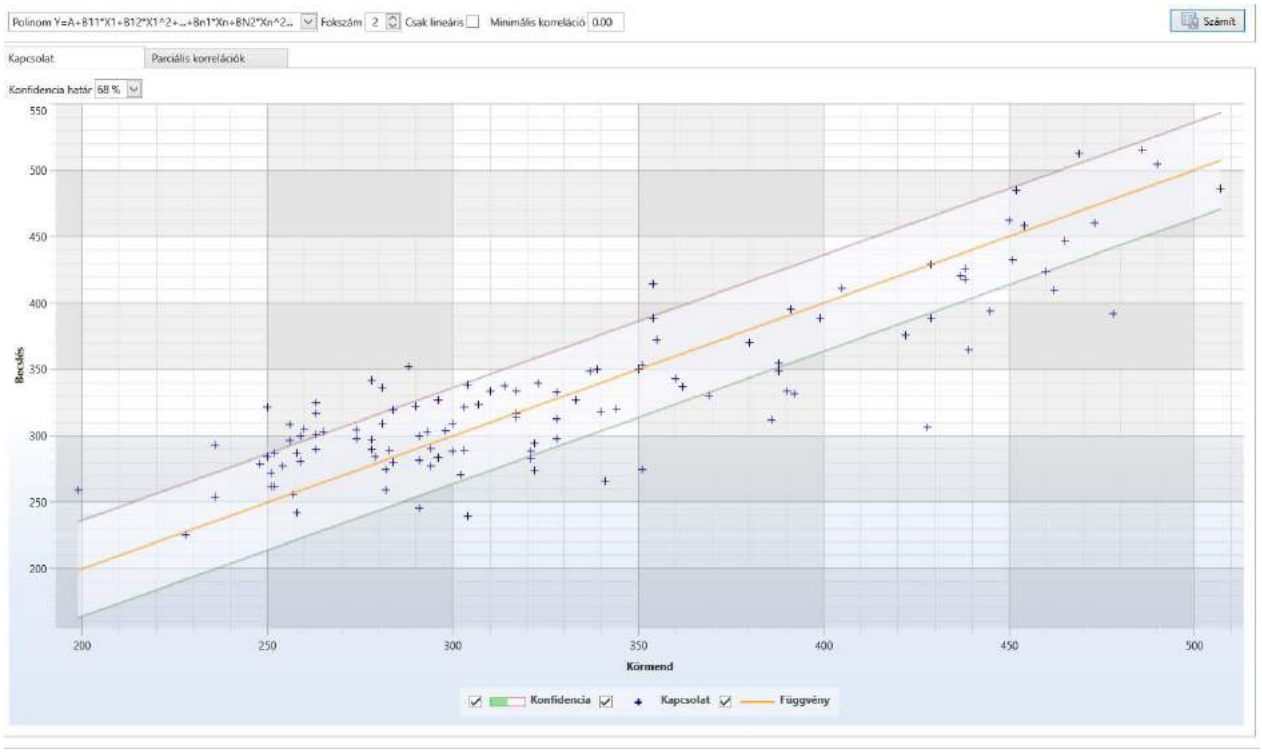

Fig. 5. Multivariable linearized regression for the predicted water level at Körmend [4]

5. Regression model for the main water gauges on Rába from Szentgotthárd peak

The polynomial regression model is shown in the following formulas. The model can be applied from the time of the peak of the Rába in Szentgotthárd. Using formula (12), the estimated peak water level in Körmend can be determined.

$$H_{Kö\,T} = 211{,}3 + 0{,}08 * H_{Kö\,T0Sztg} + 0{,}0007 * H^2_{Kö\,T0Sztg} + 0{,}11 * H_{Sztg\,T} + 0{,}00055 * H^2_{Sztg\,T} \quad (12)$$

The two lower stations' peak water level can be estimated by the following equations (13, 14). In this step, the prediction for Sárvár can be estimated on the basis of the measured Szentgotthárd and the estimated Körmend peaking from the first step. Of course, due to the usage of an estimated parameter, the result has a greater uncertainty than just the uncertainty from the regression.

$$H_{Sá\,T} = 395{,}8 - 2{,}81 * H_{Kö\,T} + 0{,}005 * H^2_{Kö\,T} + 0{,}62 * H_{Sztg\,T} + 0{,}002 * H^2_{Sztg\,T} - 0{,}00004 * H^2_{Sá\,T0Sztg} + 0{,}4 * H_{Sá\,T0Sztg} \quad (13)$$

$$H_{Ár\,T} = 54{,}1 + 0{,}11 * H_{Kö\,T} + 0{,}0005 * H^2_{Kö\,T} - 0{,}025 * H_{Sztg\,T} - 0{,}0002 * H^2_{Sztg\,T} + 0{,}35 * H_{Sá\,T} + 0{,}0006 * H^2_{Sá\,T} + 0{,}32 * H_{Ár\,T0\,Sztg} - 0{,}0004 * H^2_{Ár\,T0Sztg} \quad (14)$$

This phenomenon also valid onto the estimation for Árpás, at the lower section of the Rába (formula no. 14)

6. Conclusions

The quality of the linearized regression can be described by 2 characteristic values: the standard deviation, and the differences between the measured and the calculated values.

The standard deviation of the predicted water levels for each station is between 17… 30 cm, the average of the differences between the measured and estimated water levels is between 15… 25 cm.

The presented method can be used to predict the peak water level of discrete flood waves. The dynamics of flood waves can also be estimated by adding additional parameters (e.g., evaluating daily water level changes).

It is absolutely necessary to integrate the hydrological data measured on the tributaries of the Rába (Pinka, Gyöngyös, Strém, Perint, Lapincs), as well as to include the Austrian section of the catchment.

Further investigation is required to prepare the regression database for continuous water regime forecasting in addition to discrete flood wave forecasting.

Summarized, the linearized regression procedure, applied for both the upper and lower section of the river basin, is suitable to support flood protection with a sufficient time advantage.

The regression application was developed as a subsystem of Rába's early flood forecasting system.

The forecasting system uses hydrodynamic models to make a forecast for the already mentioned water gauges with a time advantage of 6 days.

The results of the regression procedure presented in this study may provide a good control for evaluating the results of the forecasting system.

Rába's flood forecasting system and its results are available on the website https://rf4c.vizugy.hu.

References

[1] West-transdanubian Water Directorate / Nyugat-dunántúli Vízügyi Igazgatóság. "IDENTIFICATION OF SIGNIFICANT WATER MANAGEMENT ISSUES / PROBLEMS IN THE RÁBA RIVER BASIN MANAGEMENT PLANNING UNIT” / „JELENTŐS VÍZGAZDÁLKODÁSI KÉRDÉSEK/PROBLÉMÁK AZONOSÍTÁSA A RÁBA VÍZGYŰJTŐ-GAZDÁLKODÁSI TERVEZÉSI ALEGYSÉGEN.” [Online]. Available: http://www.nyuduvizig.hu/upload/1.1.4.Raba_kesz-bovitett.PDF. Accesed December 10, 2020.

[2] Hüse, Zsolt. "Computer program for the hydrological application of nonlinear methods of univariate and multivariate regression analysis.” / „Egy-és többváltozós regresszióanalízis nemlineáris módszerei hidrológiai alkalmazásának számítógépi programja.” ATIKÖVIZIG, Szeged, 2001.

[3] National Directorate General for Water Management / Országos Vízügyi Főigazgatóság. "Hungarian Hydrological Database (Unified online hydrological data storage and data processing system).” / „Magyar Hidrológiai Adatbázis (Egységes online hidrológiai adattároló és adatfeldolgozó rendszer).” Budapest, 2015 (available: North-transdanubian Water Directorate, 28-32. Arpad St. Gyor, Hungary).

[4] H-FIT Informatikai Bt. Regress4. Regression application / Regress4. Regresszió alkalmazás, 2019. (available: North-transdanubian Water Directorate, 28-32. Arpad St. Gyor, Hungary).

Theoretical and Experimental Researches on the Determination of Pressure Losses on Bubble Generators Used for Water Aeration

PhD Std. **Marilena Monica BOLTINESCU (ROZA)**[1], Prof. Dr. Eng. **Nicolae BĂRAN**[1],
PhD Std. **Nicolae Vlad SIMA**[1], Șl. Dr. Eng. **Mihaela CONSTANTIN**[1]*

[1] University Politehnica of Bucharest

* i.mihaelaconstantin@gmail.com

Abstract: *The paper presents a theoretical and experimental analysis of pressure losses in the case of pneumatic aeration, which can be performed by:*
A. A network of pipes with orifices arranged on the tank foundation plate
B. A system of porous diffusers
C. A network of fine bubble generators
Theoretically, the pressure loss is determined when the air passes through the three constructive solutions (A, B, C); subsequently, the theoretical results are compared with the data obtained from the experimental researches carried out in the laboratory of the department of Thermotechnics, Engines, Thermal and Refrigeration Equipment.

Keywords: *Fine air bubble generator, water aeration, porous diffusers.*

1. Introduction

The process of water aeration is based on a transfer between two environments: air - water, i.e., it is an interphase process.
The air bubbles provided by the aeration equipment are introduced into a volume of water; the smaller the diameter of the air bubble, the more efficient the water aeration.
The performance of a water aeration system is specified by two parameters:
- the efficacy of the water oxygenation process;
- the efficiency of the water oxygenation process.
The water aeration process can be performed as follows [1] [2]:
1. By mechanical aeration;
2. By pneumatic aeration;
3. By mixed aeration.
In the case of mechanical aeration, the air is introduced into the water through aerators, thus realizing the surface aeration.
In the case of pneumatic aeration, the air is introduced into the water through dispersion systems, which can be:
A. A network of pipes with orifices arranged on the tank foundation plate,
B. A porous diffuser system in which the dispersion element is a rubber member with orifices,
C. A network of fine bubble generators.
Aeration systems must meet the following conditions:
- ensuring the air supply, for the existence of water fauna;
- maintaining a mixture between air and water;
- elimination of CO_2 excess resulting from the oxidation of organic matter.
In the literature [3] [4], there are several criteria for classifying aeration equipment, as follows:
a. According to the way of obtaining the interphase contact surface:
- water spray equipment and cascade equipment;
- equipment that disperses the gas in water (deep mechanical aerators, etc.);
- mixed equipment - sprays water in the form of drops and entrains the air through the jet effect at the re-entry in the water mass from the tank (mechanical surface aerators).
b. According to the mode of the aeration equipment active organ movement:
- static equipment (static aerators, ejectors, etc.);
- dynamic equipment (mechanical surface or deep aerators).

c. *By the gas type used for aeration*:
- equipment that disperses air in water (deep mechanical aerators, pneumatic aerators, ejectors, etc.);
- equipment that disperses pure oxygen in water (pneumatic type);
- equipment with the introduction of ozone or ozone-enriched air in water (such as fluid jet pumps).

2. Theoretical determination of the pressure loss in case of pneumatic aeration

For the three cases A, B, C, presented in the paper abstract, the initial data are the same, namely:
- The introduced air flow rate $\dot{V} = 600\ \mathrm{dm}^3/\mathrm{h}$:
- Compressed air pressure: p = 583 mmCA;
- Hydrostatic load: H = 500 mmCA;
- Water temperature: t = 24ºC;
- Air temperature: t = 24ºC;
- Water density: ρ = 1000 kg / m^3;
- The air density --- will be calculated in the next paragraph.

Further in the paper, the pressure losses that occur in pneumatic aeration systems are theoretically calculated.

2.1 Pneumatic aeration systems, made with orifices pipes

INKA aeration systems (figure 1) are systems based on the bubble aeration process in which the perforated pipes, located at approximately 0.8 m below the water level, represent the element of air dispersion.

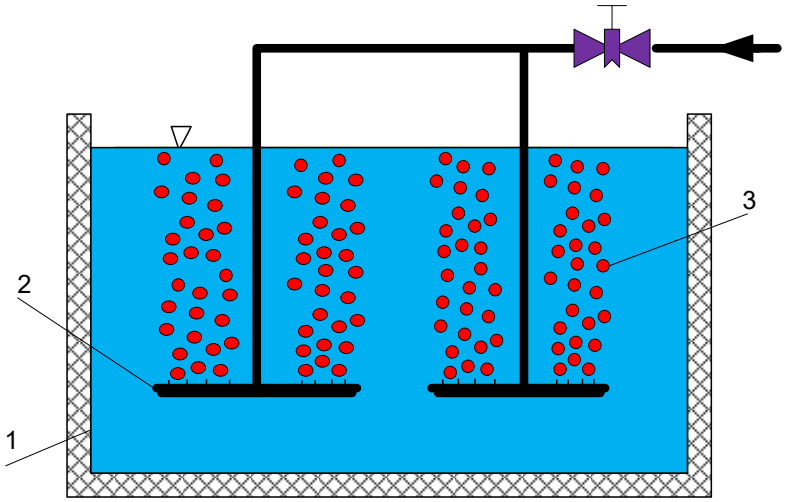

Fig. 1. INKA aeration system
1 – water tank; 2 - perforated pipes; 3 - air bubbles

Fine bubble water aeration systems (Ø <1 mm) include pneumatic generators, air transport and distribution pipes, control fittings.
Pressure loss when air passes from the piping system into the water through the orifices with Ø = 0.05 mm, is calculated with the relation [5]:

$$\Delta p = \zeta_{aer} \rho_{aer} \frac{w^2}{2} [N/m^2] \quad (1)$$

From [6], ζ = 0.6 and the air density is obtained from the relation:

$$\rho = \frac{p}{RT} \left[kg/m^3 \right] \quad (2)$$

$$p = p_{atm} + p_H \left[N/m^2 \right] \quad (3)$$

Where:
p_{atm} = 101325 N / m^2;
p_H = hydrostatic load: p_H = 0.5 mH_2O;
R = air constant: R = 287 J / kgK;
T = air temperature: T = 297.15 K;
Substituting in relation (2) one can obtain: ρ = 1.25 kg / m^3
The theoretical velocity of air flow is obtained by dividing the volumetric flow rate ($\dot{V}$) by the air outlet section in water: A = 1.2·10-6 m^2

$$w = \frac{\dot{V}}{A} = \frac{600 \cdot 10^{-3}}{3600} \cdot \frac{1}{1,2 \cdot 10^{-6}} = 138\,[m/s] \tag{4}$$

$$\Delta p = 0.6 \cdot 1.25 \cdot \frac{138^2}{2} = 7187.4 N/m^2 = 0.71 mH_2O \tag{5}$$

$$\Delta h = 0.71 mH_2O = 710\, mmH_2O \tag{6}$$

2.2 Calculation of the pressure drop when air passes through a porous diffuser

The orifices of the porous diffuser are not circular in shape, but approximately rectangular. A single orifice was measured using a modern OLYMPUS BX51M microscope, the overview of which can be seen in Figure 2.

Fig. 2. OLYMPUS BX51M microscope overview

The elastic membrane contains over 100 rectangular orifices, a single orifice was measured with a modern OLYMPUS BX51M microscope, shown in Figure 2.
The materials of which the elastic membranes are made are rubber, latex, E.P.D.M. membranes (Ethylene-Propylene-Dien-Monomer).
Figures 3 and 4 show a porous diffuser with elastic E.P.D.M membrane.

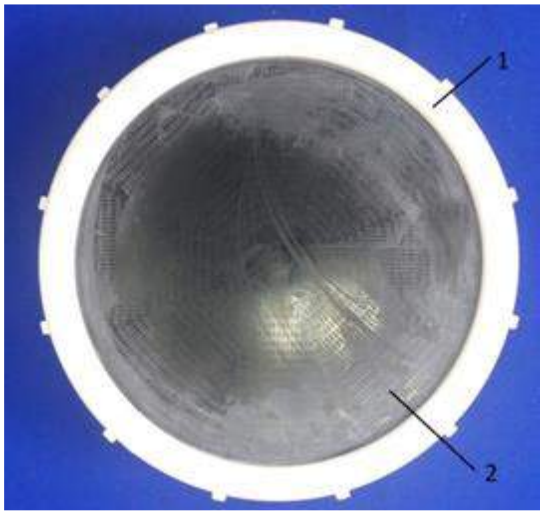

Fig. 3. Overview of the porous diffuser
1 - elastic membrane fixing ring; 2 - elastic membrane

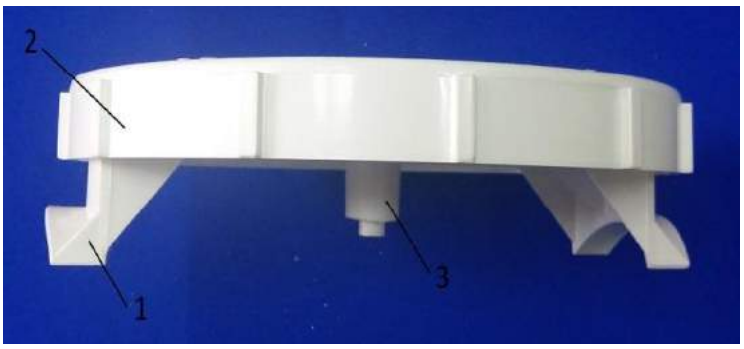

Fig. 4. Side view of the porous diffuser

The shape of the orifice in the porous diffuser is shown in figure 5.

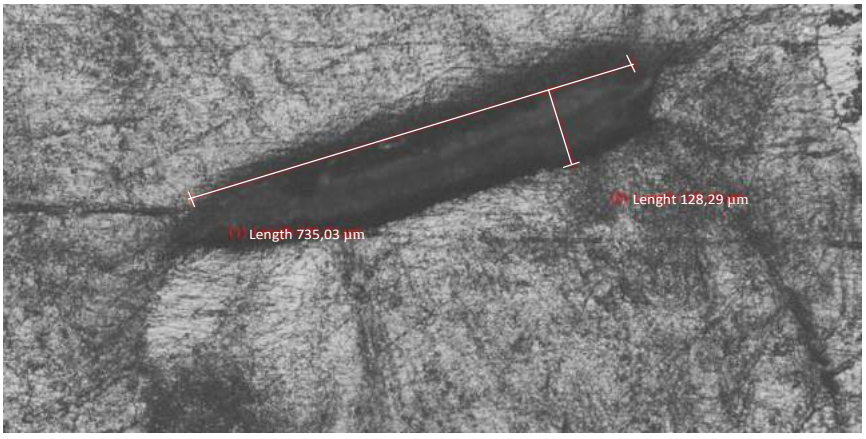

Fig. 5. View of the orifice in the porous diffuser

The orifice (figure 5) has a length of 735.03 µm and a width of 128.29 µm.
The dimensions of the orifice, approximately as a rectangle, are:

$$L \; x \; l \; = \; 735.03 \cdot 128.29 \; = \; 94296.998 \; \mu m^2 \qquad (7)$$

The equivalent diameter of the orifice will be [7]:

$$d_e = \frac{4A}{P} = \frac{4 \cdot 94296.998}{2 \cdot (735.03 + 128.29)} = 218.45\ \mu m \tag{8}$$

$$d_e = 0.21845\ mm \tag{9}$$

The value of this diameter falls within the operating range of bubble generators, which emit fine bubbles [8].
The air speed when passing through the orifice will be:

$$w = \frac{\dot{V}}{A} = \frac{600 \cdot 10^{-3}}{3600} \cdot \frac{1}{100 \cdot \frac{\pi}{4} 0.21 \cdot 10^{-3}} = 48.1 m/s \tag{10}$$

Figure 6 shows the operation of the porous diffuser; the elastic membrane has Ø229 mm.

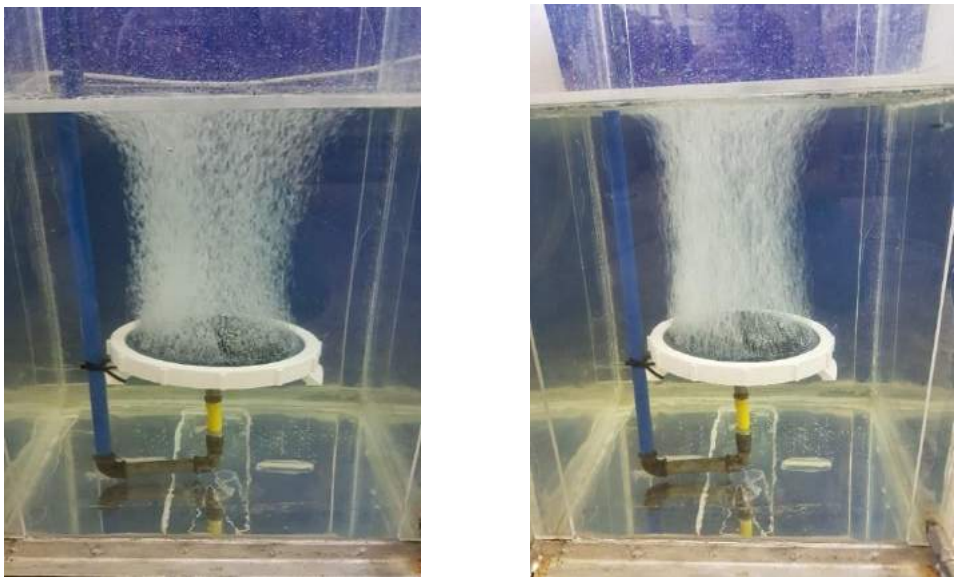

a) b)

Fig. 6. Column of air bubbles generated by the porous diffuser
a) $\dot{V} = 1400 dm^3/h$;b) $\dot{V} = 1600 dm^3/h$

The pressure drop will be:

$$\Delta p = \zeta \cdot \rho \cdot \frac{w^2}{2} = 2.4 \cdot 1.25 \cdot \frac{48.1^2}{2} = 34.102 [N/m^2] \tag{11}$$

$$\Delta p = \rho_{H_2O} \cdot g \cdot \Delta h \tag{12}$$

$$\Delta h = \frac{\Delta p}{\rho_{H_2O} \cdot g} = \frac{34 \cdot 10^2}{10^3 \cdot 9.81} = 0.351 mH_2O = 35.1 mmH_2O \tag{13}$$

2.3 Calculation of the pressure drop at a fine bubble generator

Figure 7 shows a fine bubble generator which has the orifices plate of rectangular shape. Taking into account the size of the water tank and the height of the water layer, a water outlet section of $1.2 \cdot 10^{-6}$ m^2 [6] [7] was chosen, for which a number of orifices of Ø 0.1 mm equal to:

$$n = \frac{A}{\frac{\pi d_0^2}{4}} = \frac{1.2 \cdot 10^{-6}}{\frac{\pi \cdot (0.1 \cdot 10^{-3})^2}{4}} = 152\ orifices \tag{14}$$

result.

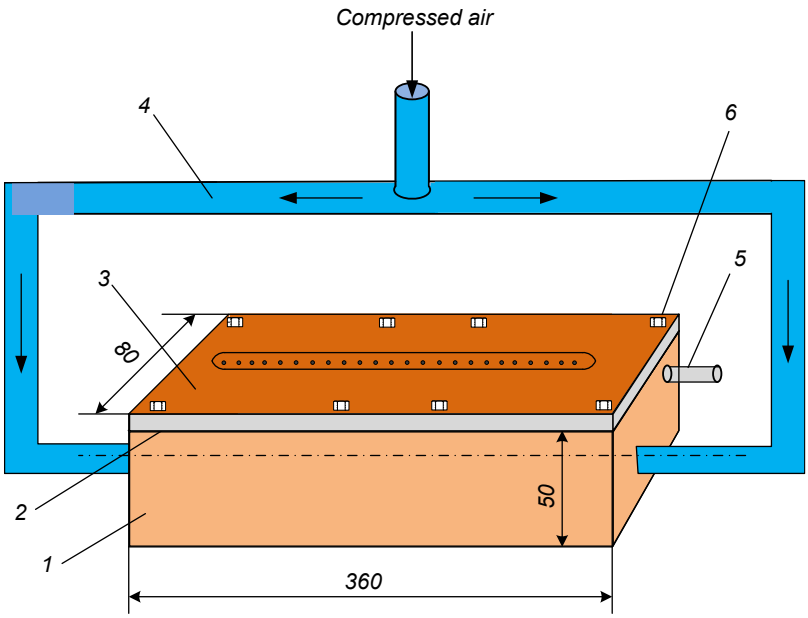

Fig. 7. Fine bubble generator with rectangular orifice plate
1 - compressed air tank; 2 - sealing system; 3 - orifices plate; 4 - compressed air pipe; 5 - connection to manometer; 6 - screws for fixing the orifices plate

The plate (3) contains 152 orifices (Ø 0.1 mm) made with the help of the KERN Micro machine; the constructive solution of this fine bubble generator is original and a very efficient constructive solution. The framing of this fine bubble generator in the experimental installation is presented in figure 8.

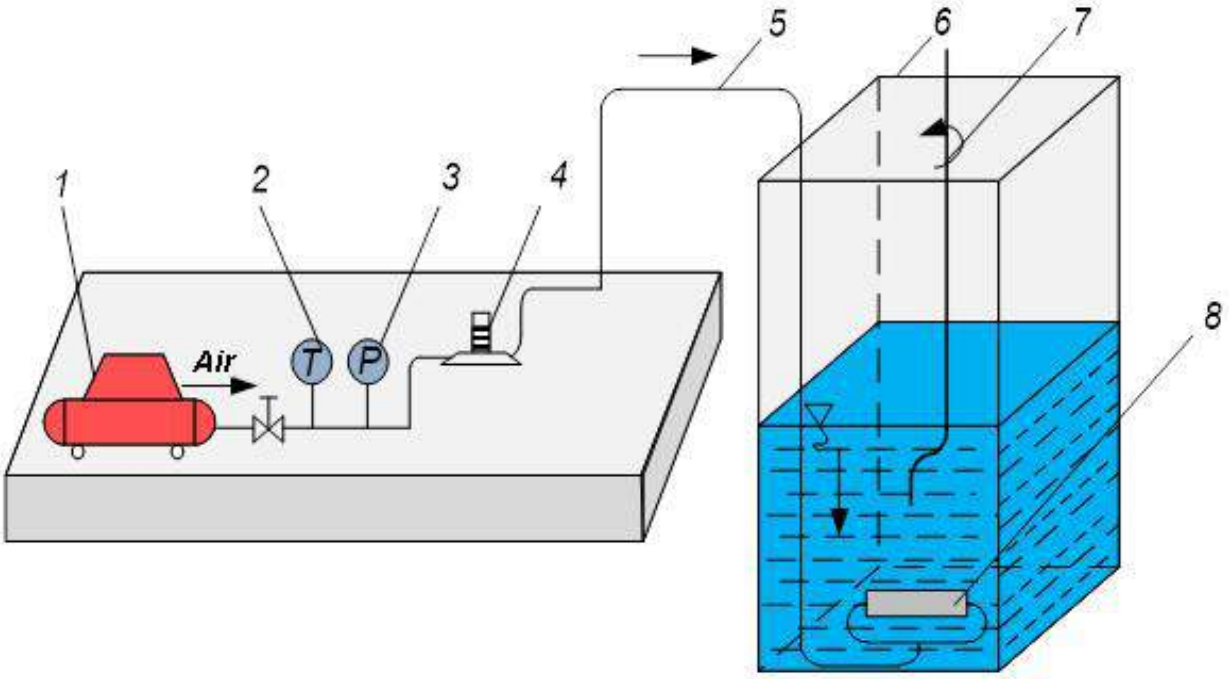

Fig. 8. Installation scheme for the introduction of atmospheric air into water
1 - electro compressor; 2 - digital thermometer; 3 - digital manometer; 4 - rotameter; 5 - air transport pipe; 6 - parallelepiped water tank; 7 - oxygenometer probe; 8 - fine bubble generator.

During the measurements, the following parameters were kept constant:
- Flow of air blown into water: $\dot{V} = 0.6\ m^3/h$;
- Air pressure at the end of the fine bubble generator: p = 573 mmH_2O;

- Hydrostatic load: H = 500 mmCA;
- Water temperature: 24º C;
- Air temperature: 24º C.

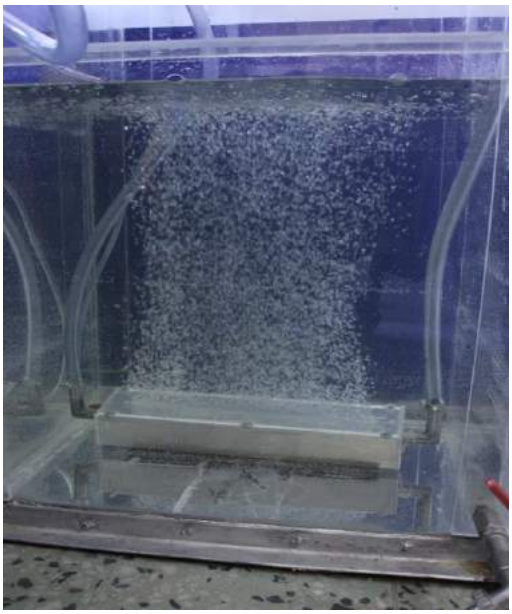

Fig. 9. Fine bubble generator in operation

To calculate the pressure drop that occurs when air passes through the fine bubble generator, the following formula is used:

$$\Delta p = \zeta \cdot \rho \cdot \frac{w^2}{2} \tag{15}$$

where:
ζ - local pressure loss coefficient; from [6] ξ = 0.82 is chosen;
ρ - air density; was previously calculated: ρ = 1.25 kg / m^3
Air passage speed through the orifices:

$$w = \frac{\dot{V}}{A} = \frac{600 \cdot 10^{-3}}{3600} \cdot \frac{1}{1.2 \cdot 10^{-6}} = 138.8\, m/s \tag{16}$$

$$\Delta p = 0.63 \cdot 1.25 \cdot \frac{138.8^2}{2} = 7498.5 \left[N / m^2 \right] \tag{17}$$

$$\Delta h = 0.749\ mH_2O = 74.9\ mmH_2O \tag{18}$$

In cases A, B, C, both the local pressure loss coefficient (ζ) and the exit speed of the compressed air in the water influence the pressure loss when the air passes through fine bubble generator.

3. Experimental researches

Next, a calculation relation of the pressure drop that occurs when air passes through an orifice in Figure 1 is established.
In capsule 1 there is compressed air with the pressure p_1 [N / m^2]; in operation, this pressure will have to overcome:

- the hydrostatic load: $\rho_{H2O} \cdot g \cdot H$;
- the surface tension: $2\sigma / r_0$
- the air pressure loss when passing through the orifice (Δp).

An equilibrium equation can be written [6]:

$$p_1 = \rho_{H_2O} \cdot g \cdot H + \frac{2\sigma}{r_0} + \Delta p \left[N / m^2 \right] \quad (19)$$

$$\Delta p = p_1 - \rho_{H_2O} \cdot g \cdot H - \frac{2\sigma}{r_0} \left[N / m^2 \right] \quad (20)$$

$\rho_{H2O} = 10^3$ kg / m^3; g = 9.81 m / s^2; $\sigma = 7.3 \cdot 10^{-2}$ [N / m] are known.
From relation (20) one can observe that, if p_1 is known, the air pressure drop can be calculated when passing through the orifice.
For different flow rates $\dot{V}$, pressure losses Δp are presented in table 1. Subsequently, water was introduced into the tank (H = 500 mmH_2O) and the pressure drops for the case of the "wet" membrane were measured; the air flow rates remained the same and the experimental results are presented in table 1.

Table 1: Pressure losses when air passes through the porous diffuser with elastic membrane

No.	"Dry" membrane		"Wet" membrane	
	$\dot{V}$ [dm^3/h]	Δp [mbar]	$\dot{V}$ [dm^3/h]	Δp [mbar]
1	400	1.47	400	57.5
2	600	2.11	600	61.1
3	800	2.70	800	62.40
4	1000	3.79	1000	64.50
5	1200	4.92	1200	66.30
6	1400	5.86	1400	68.20
7	1600	7.58	1600	71.80

For the porous diffuser the experimental values for Δp are close in size to the theoretical ones.
Based on the data in the table 1, the curves Δp = f ($\dot{V}$) were drawn for the two cases.

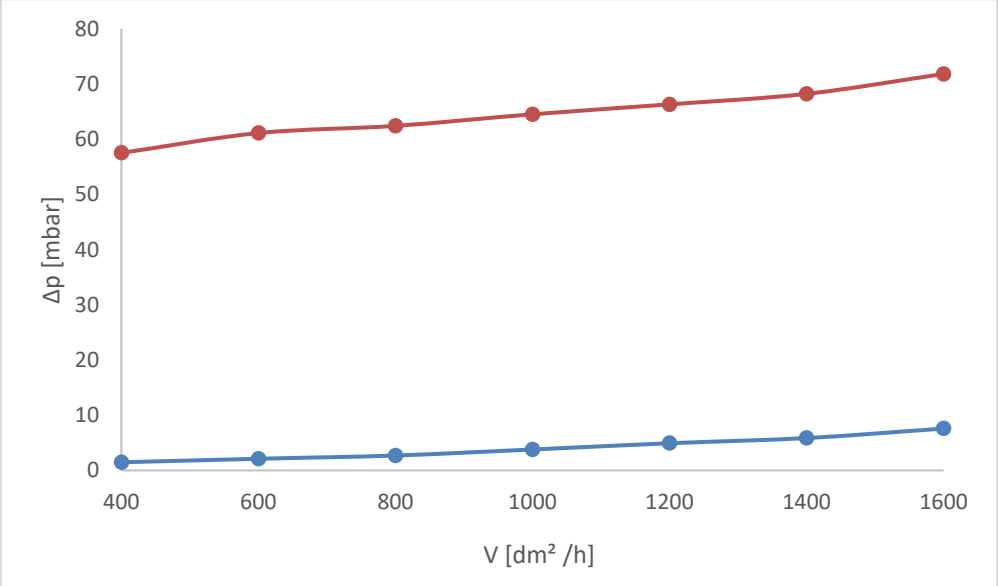

Fig. 10. The curves Δp = f ($\dot{V}$)
Δp = f ($\dot{V}$) for the "dry" membrane; 2 - Δp = f ($\dot{V}$) for the "wet" membrane

4. Conclusions

• In order to achieve a water oxygenation process as efficient as possible, it is necessary to analyse the factors involved in the equation of oxygen transfer to water, namely the speed of oxygen transfer to water increases slightly by:
- increasing the air-water contact surface, by dispersing air bubbles as fine as possible, d <0.5 mm in the water mass;
- increasing the mass transfer coefficient k_L by intensifying the turbulence;
- increase in oxygen deficiency that is increasing the difference (C_S - C)
• From the analysis of the parameters that intervene in the water oxygenation process, the following parameters have a special importance:
- the size of the air bubbles immersed in water (the smaller the diameter, the higher the concentration of dissolved oxygen in the water);
- the architecture of the bubble network - must be established in such a way as to avoid their coalescence;
- choosing an operation regime of the fine bubble generators so that the pressure losses are as small as possible; a lower pressure drop leads to saving of energy consumed for compressing the air to be introduced into the water.
Advantages of using bubble generators:
- ensure good oxygen transfer efficiency;
- ensure good mass transfer / power unit / time unit;
- can satisfy high oxygen demands;
- are easily adaptable to existing tanks.
Disadvantages of using bubble generators:
- are susceptible to chemical or biological degradation, which may lead to a decrease in mass transfer efficiency and an increase in pressure drop;
- do not ensure a uniform dispersion of air in a volume of water.

References

[1] Tănase, E.B. *Influence of the composition of the gas blown in water on the dissolved oxygen content* / *Influența compoziției gazului insuflat în apă asupra conținutului de oxigen dizolvat*. Doctoral thesis. Politehnica University of Bucharest, Faculty of Mechanical and Mechatronics Engineering, 2017.
[2] Pătulea, Al.S. *Influence of functional parameters and architecture of fine bubble generators on the efficiency of aeration installations* / *Influența parametrilor funcționali și a arhitecturii generatoarelor de bule fine asupra eficienței instalațiilor de aerare*. Doctoral thesis. Politehnica University of Bucharest, 2012.
[3] Mateescu, G.M. *Hydro-gas-dynamics of fine bubble generators* / *Hidro-gazo-dinamica generatoarelor de bule fine*. Doctoral thesis. Politehnica University of Bucharest, Faculty of Mechanical and Mechatronics Engineering, 2012.
[4] Băran, N., M. Constantin, E. Tănase, and R. Mlisan. "Researches regarding water oxygenation with fine air bubbles." *Buletinul Științific al Universității Politehnica din București*, *seria D, Inginerie Mecanică* 78, no. 2 (2016): 167-178.
[5] Constantin, M., N. Băran, R. Păun, and A.G. Roza. "Theoretical and Experimental Researches about the Pressure Loss of a New Type of Fine Bubble Generator." *International Journal of Emerging Research in Management & Technologyy* 6, no. 2 (February 2017): 115 – 120.
[6] Kiselev, P.G. *Guide for hydraulic calculations / Îndreptar pentru calcule hidraulice*. Bucharest, Technical Publishing House, 1988.
[7] Oprina, G., I. Pincovschi, and Gh. Băran. *Hydro-gas-dynamics of aeration systems equipped with bubble generators / Hidro-gazo-dinamica sistemelor de aerare echipate cu generatoare* de bule. Bucharest, Politehnica Press, 2009.
[8] Tănase, E.B., M. Constantin, R. Mlisan (Cusma), R. Mechno, and N. Băran. "Water oxygenation using gas mixtures.'' Paper presented at Septième édition du Colloque Francophone en Energie, Environnement, Economie et Thermodynamique – COFRET16, Bucharest, Romania, June 29 – 30, 2016.

Solutions for the Reuse of Rainwater in Indoor Plumbing

Assoc. Prof. PhD. Eng. **Adriana TOKAR**[1*], Lecturer PhD. Eng. **Diana FORIȘ**[2], Res. Asst. PhD. student Eng. **Dănuț TOKAR**[1], Res. Asst. PhD. student Eng. **Simona POPA-ALBU**[1]

[1] University Politehnica Timisoara

[2] Transilvania University of Brasov

* adriana.tokar@upt.ro

Abstract: *In agreement with lasting development and ensuring a sustainable future for administrative territorial units (ATUs) in Romania, the article proposes measures to support the environment with positive effects on natural freshwater resources and consumption. The study presents the context, necessity, and justification for plumbing modification from buildings, focused on the reduction of drinking water consumption through the recovery, storage, and reuse of rainwaters. The analysis of climatic parameters, quality indicators of rainwater harvested, and the proposed technical solutions was performed to justify the usefulness and the necessity of implementing the solutions for recovering and reusing this resource.*

Keywords: *Plumbing, rainwater recovery, sustainable development, freshwater protection.*

1. Introduction

The conception, the construction and the execution of the buildings have as determining factors: people, human activity, and nature. For this reason, it can be said that the human settlements can be regarded as factors of transformation for natural resources. Maintaining comfort in a building, considering the need for low energy consumption and to protect natural resources, can be achieved by ensuring efficient building functionality. On international level, we recognize the European Union's actions regarding environmental protection measures and the promotion of sustainable development. The sustainable development involves mechanisms and policies which should ensure economic development while minimizing negative impacts on consumption ecosystems [1, 2].

From the point of view of energy efficiency, the European Energy Performance of Buildings Directive requires all new buildings to have almost zero energy consumption by the end of 2020 [3], which means that these buildings need have very high energy performance. In this respect, investments are needed both for the rehabilitation and modernization of the buildings and their related facilities, as well as for the energy consumption for the inhabitants' comfort (thermal, sanitary, and lighting ones). For these reasons, the small amount of energy these buildings require will be largely derived from renewable sources and the reduction of energy and water consumption will be a priority for any consumer. Therefore, reducing energy consumption on the one hand and protecting natural freshwater resources on the other hand will become global priorities. Over time, the water, the soil, and the air have been treated at market level as free goods. Even though these issues have now been subject to some regulations, between supplying natural resources and the consumed levels, at this moment there is no clear relationship that can be regulated through the price mechanism [4, 5].

Regarding the degradation of ecosystems and freshwater resources, it has been found that they are amplified by the effects of climate change and by a wide range of disasters and crises (economic, technological, biological, etc.) [6]. One of the most urgent problems of the current society is the drinking water, which, lately, due to global warming, it is highly in demand, especially in the warm periods of the year. In Romania, there is almost no financial pressure on users for the efficient use of water resources to ensure the long-term quality and availability of this vital resource.

This can be exemplified by the approach of the water consumption in many small rural tourism destinations in Romania, where buildings are generally supplied with water by individual systems. On the other hand, public water supply systems are used by consumers to irrigate farmland. From the point of view of protecting freshwater resources in buildings from areas of tourist destination,

the design of these systems requires an integrated approach, involving a variety of stakeholders capable of overcoming sector boundary and the rural-urban limit.
Due to the impact of the climate changes, redesigning these systems in human settlements to meet the sustainability criteria, should be safely integrated into the management of water resources and the preservation of the ecosystems.
Thus, in order to reduce the consumption of potable water, it is necessary to encourage the collection, the storage and the reuse of meteoric waters [7] as well as with a new approach to the design of sanitary water supply systems for sanitary objects in the buildings. Previous studies show that replacing a portion of drinking water with meteoric water for domestic activities generates considerable savings in the drinking water resources [2, 8, 9].
Thus, for the integration of this concept, the sanitary installations will be designed taking into account the sanitary objects that require the supply of drinking water and those for which the water it does not need to be drinkable.

2. The aim of the research

Considering the fact that, in the case of environmental protection programs, in Romania, there are mainly programs aimed at improving the energy efficiency of the buildings (increasing the degree of thermal insulation, wind/solar/geothermal energy storage systems or ventilation systems with heat recovery programs), and programs which stimulate the reduction of greenhouse gas emissions, we believe that the creation and implementation of programs aimed at the protection of the natural resource - water is a topic for future approach of environmental protection.
Given that water is an important natural resource and the amount of rainfall decreases, responsible use of rainwater in an ecological and natural way is a solution for sustainable management of natural resources.
The paper deals with aspects regarding the implementation of existing financing programs in Romania to emphasize that there is no major interest in the implementation of programs aimed at saving and protecting the freshwater resource.
The study highlights the advantages of the meteoric waters' recovery and use, and the importance of providing a natural water circuit (infiltration into the soil of precipitation water).
The analysis explores the hypothesis that the meteoric waters in Romania's mountainous areas can fulfil the conditions of use for different household activities or industry, which is why solutions appeared for collecting, storing and the reuse of the rainwater, solutions that lead to the protection of the environment. In order to justify the proposal for the solutions of the reuse of rainwater, different analyses of the quality indicators were performed, regarding the water samples taken from collection systems from Brasov and Predeal.

3. Methodology of investigations

The study was conducted in two steps.
In the first stage, we consulted of the specialized literature on specialists' foresight in regard of the existing water potential in the world [1], [4], [8], [10-16].
In the second stage, possible solutions were considered for the cutback on the consumption of drinking water to protect the freshwater resource.
In this respect, was assessed the sustainability of investments in facilities for the recovery, storage, and the reuse of the meteorological waters by analysing the meteorological parameters in Romania and the captured meteorological water quality indicators.
Given that the mountain areas are much less exposed to the risk of air pollution, so that the meteoric waters that wash the atmosphere and engage pollutants to the ground, can have an adequate quality for their use in certain purposes, the study makes reference to the two mountain destinations of Romania: Brasov and Predeal.

For the analysis of the precipitation water quality indicators, were collected different meteorological water samples from rainwater collection facilities, which serve the buildings located in Brasov and Predeal.

4. Results of research

The analysis of the meteorological parameters carried out for the assessment of the precipitation potential in Romania, indicated that, generally, here, rainfall is moderate. The amount of precipitation that falls on the ground varies annually between the Danube Delta and the mountain areas. According to the statistics, most of the rainfall in the area of Romania falls between December and June, with the largest rainfall occurring in May and June, when atmospheric circulation and climatic conditions allow rapid vertical development of cloud formations [17].
The annual rainfall amounts were analysed using the Meteomanz database, available for free at http://www.meteomanz.com. The database provides data obtained from SYNOP messages issued by global meteorological stations (stations with code number assigned by the World Meteorological Organization).
For the two analysed tourism destinations, Brasov and Predeal, the annual medium rainfall rates for the last 6 years (2014-2019) are presented in Table 1.

Table 1: Annual average rainfall

Brasov Ghimbav Station - Average altitude 535m		**Predeal Predeal Station - Average altitude 1901m**	
Period	Rainfall [l/m^2]	Period	Rainfall [l/m^2]
Year 2014	362.9	Year 2014	585.5
Year 2015	631.3	Year 2015	871.9
Year 2016	701.7	Year 2016	1114.3
Year 2017	682.0	Year 2017	944.0
Year 2018	710.3	Year 2018	971.5
Year 2019	545.5	Year 2019	860.0

Source: Meteomanz database: http://www.meteomanz.com

In the Table 1 analysis we can observe the annual variation of the amount of precipitation that falls to the ground. Reported in 2014, the rainfall has increased in analysed areas. On the other hand, it can be noticed that at the altitude difference between the two areas, the rainfall increases about 1.4 times in the higher altitude zone.
Studies conducted by the National Meteorological Administration based on climate mathematical models (Ministry of Environment and Sustainable Development 2008), present the assessment of likely climate developments in the decades and even centuries to come. Thus, the map of annual rainfall estimates for the years 2001-2030 (reference interval - 1961-1990) was studied under the conditions of the A1B scenario. A1B scenario assumes a future in which growth will be rapid, which implies a weigh rate of the increase in greenhouse gas concentrations for the 21st century, in order to better estimate uncertainties.
Regarding the variability of global rainfall quantities, an important feature of the temporal variability of precipitation amounts is the pronounced interdecenial component, making it difficult to separate the long-term climatic signal [18].
As in the whole of Europe, we expect increases in the medium annual temperature in Romania compared to the 1980-1990 period (between 1.8°C and 4.0°C). Studies conducted for the period 2090-2099, regarding the pluviometric regime in Romania, indicate for the climate models that, more than 90% of them will be affected by drought in the summer (especially the southern and south-eastern region of Romania - with deviations higher than 20% relative to the reference years 1980-1990), and for winter periods, the deviations are lower, but the uncertainty is higher [19].
Although the values shown in Table 1 indicate an increase in the amount of rainfall over the last 4 years, the forecasts for the 2090-2099 indicate areas affected by drought. Therefore, to protect the future, it is necessary to think and act responsibly in the present through sustainable solutions to current problems regarding the freshwater resource.

As a conclusion of this analysis, it is estimated that the rainfall affects almost all areas of activity (mainly ecosystems, population and agriculture) and indirectly affects the freshwater resource, especially in the deficient areas, which will accentuate the consequences of the lack of water at a global scale.
For the two mountain areas considered for the study, an analysis was performed on the physical-chemical and bacteriological parameters of water samples taken from rainwater collection and evacuation facilities in order to justify the implementation of pluvial water storage and re-use facilities.
Considering that the study proposes the re-use of rainwater only for non-potable sanitary objects, only 8 physical-chemical and microbiological parameters were evaluated (total hardness, nitrates, nitrite, PH, ammonium, chlorides, total germ (NTG) at 22 °C and 37 °C, coliform bacteria, E Coli bacteria and Enterococci) on a single sample of water. The samples were analysed 12 hours after collection at the laboratories of the Public Health Department (DSP) Brasov [20-21] RENAR accredited laboratories. At the level of this study, water quality was analysed globally, the results of the analyses being interpreted by reference to national water quality limits. It is necessary to emphasize that for the internal sanitary installations for water supply of WC tanks and washing machines, it is not necessary for the water to meet drinking conditions, however the parameters analysed in this study are part of the parameters required for water quality assessment drinking.
Table 2 presents the results of laboratory analyses specifying maximum admissible concentrations (CMAs) in accordance with applicable law on drinking water quality, with subsequent modifications [22] and additions or the limit of quantification (LOQ), as well as the method used.

Table 2: Quality Indicators of Meteoric Water

Quality indicator	Measured value [UM]	Admissible values [UM]	Method
Sample rainwater Predeal			
Total hardness	2,64 German degree	Min.5	SR ISO 6059/2008
Nitrates	2,8 mg/l	50 mg/l	Fast test Spectroquant NOVA
Nitrites	0,09 mg/l	0,5 mg/l	SR EN 26777:2002/C91:2006
PH	6,2	6,5-9	SR ISO 10523:2012
Ammonium	0,21 mg/l	0,5 mg/l	Fast test Spectroquant NOVA
Chlorine free chlorine	6,3 mg/l	250 mg/l	SR ISO 9297:2001
NTG la 22° C	37 ufc/100 ml	100/ml	SR EN ISO 6222:2004
NTG la 37° C	42 ufc/100 ml	20/ml	SR EN ISO 6222:2004
Sample rainwater Brasov			
Total hardness	2,75 German degree	Min.5	SR ISO 6059/2008
Nitrates	3,2 mg/l	50 mg/l	Fast test Spectroquant NOVA
Nitrites	0,28 mg/l	0,5 mg/l	SR EN 26777:2002/C91:2006
PH	6,4	6,5-9	SR ISO 10523:2012
Ammonium	0,33 mg/l	0,5 mg/l	Fast test Spectroquant NOVA
Chlorine free chlorine	7,2 mg/l	250 mg/l	SR ISO 9297:2001
NTG la 22° C	23 ufc/100 ml	100/ml	SR EN ISO 6222:2004-
NTG la 37° C	31 ufc/100 ml	20/ml	SR EN ISO 6222:2004

Also, rainwater quality analyses did not indicate the presence of coliform bacteria, E Coli bacteria and Enterococci.
For both mountain tourism destinations the total hardness is well below the admissible drinking water level, but for the supply of non-potable sanitary items (toilet tanks, washing machines, and so on.), this indicator is favourable for the proper operation of the proposed installations.
The recorded values for nitrates, nitrites, ammonium, and chlorides fall well below the detection limits, having similar values.
PH analysis indicates a slightly acidic character, which does not adversely affect the decision to collect, to store and to use the meteoric waters. Analysing the test results for the number of colonies at 22 °C and 37 °C, it appears that this parameter does not show any abnormal change for the two samples.

In conclusion, from the analysis of the measured quality indicators, it can be said that they meet the norms stipulated by the law and there are no notable differences between the values of the parameters for the two studied mountain tourism destinations.

5. Arguments

The recovery, storage and reuse of meteoric waters can be seen in several respects, but it requires a special approach as proposed solutions must be considered by considering the local situations. A general approach may be economically inefficient and unsatisfactory in terms of the expectations of the beneficiaries.

For this reason, the study critically evaluates the importance and implications of the recovery of meteoric waters in two directions:

- For rural localities with tourism destinations, solutions are proposed for the collection, storage, and reuse of meteoric waters for indoor sanitary installations (supply of non-drinking water) and irrigation installations for the agricultural land.
- For urban localities with tourism destinations, solutions are proposed for the collection, storage and re-use of meteoric waters for indoor sanitary installations (supply of non-drinking water), irrigation facilities for green spaces, street washing and public street markets, to assure fire reserve in hard-to-reach areas.

Based on the analysis of the quality indicators of water samples taken from the mountain areas, another possible approach could be considered, providing solutions according to the type of areas (mountain areas, flat areas, industrialized areas). Depending on the results of the analysis of the quality indicators, we can come with the most efficient solutions. Therefore, the solution proposal needs to be tackled taking into consideration all relevant factors.

From the analysis of the meteorological parameters, it can be seen that the stored rainwater can provide first of all the water supply needed for the bath tanks in the bathrooms, for watering the plants in the house and the garden, and the analysis of the quality indicators provide relevant information for the use of water for washing the laundry or pots or even showers. In most areas in Romania, the water is hard and has a high salt content, however, rainwater being clean and low in salt, it does not affect the proper operation of the plumbing [8-9], [23-24].

The pluvial water storage and reuse systems must be designed so that the rainwater supply corresponds to the demand [15]. The precipitations are intermittent, so it will be necessary to store enough rainwater to avoid water depletion during periods of drought.

The Plumbing reuse outfits can be provided with the direct supply of sanitary items from an underground storage tank (Figure 1.a) or from an additional high-level water tank (Figure 1.b).

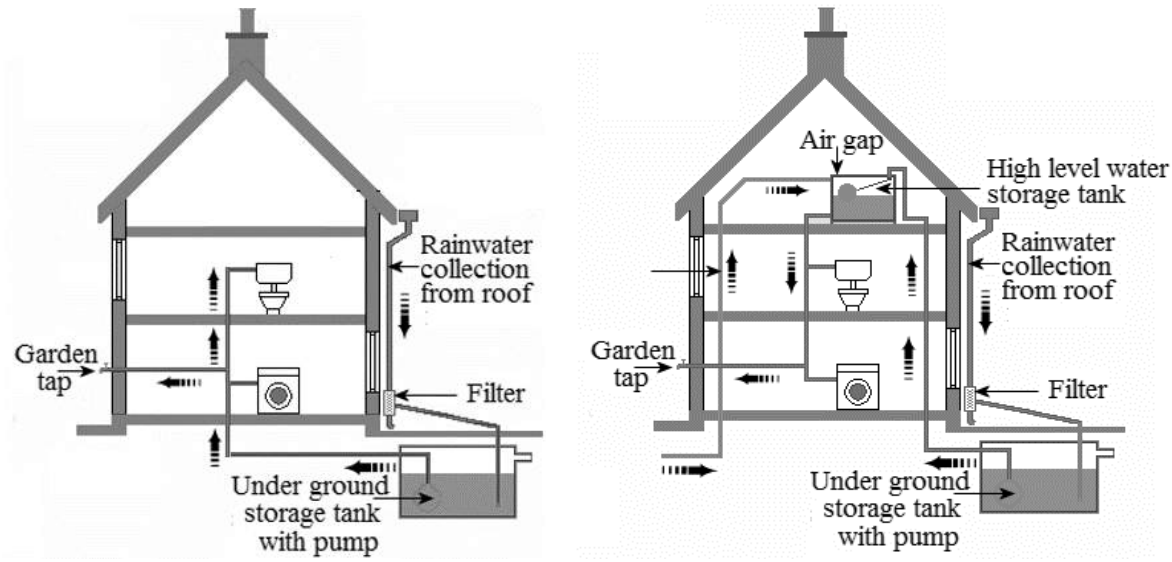

Fig. 1. Rainwater Harvesting Systems: a-direct supply, b-supply with high level water tank (Source: http://www.lowenergyhouse.com)

The extra high-level water tank will work automatically when the underground storage tank is low. The control system is programmed to fill the network storage tank when there is not enough rainwater.
For these outfits, which supply sanitary items in the buildings, it is advisable to capture the rainwater from the roofs of buildings through gutters and pipe systems. In order to maintain the quality of the collected water from the rooftop, it is necessary to inspect and clean the collection system periodically.
The water frost problem in the collection system pipelines during the cold season can be avoided by installing the de-icing systems. These systems are mounted on the roofs and on gutters and are provided with automation systems to start the heater system when sensing ice formations that can close the rainwater collection systems [25-26].
Collecting rainwater from the ground is more problematic because it can be contaminated, and it will require additional cleaning. However, contamination cannot be a problem if the rainwater is only used for watering house plants or gardens, and also when used to supply sanitary items in the buildings, it needs treatment according to the contaminants.
When water is collected from the rooftops, the simple non-disinfecting filtration is enough to allow the use of rainwater when washing toilets and feeding the washing machines. The filters can be positioned on the rainwater collection pipes or in the underground tank inlet, depending on the most economical option. The efficiency of a filter mounted on the rainwater collection pipes is high when water is clean, but it will decrease significantly if it is not cleaned regularly.
The storage tanks will be mainly placed underground because light and high temperature favour bacterial growth. However, annually, tanks should be inspected to check for sludge accumulation and need to be washed with calcium hypochlorite.
Pumps are required to raise water pressure in sanitary plumbing re-use outfits.
From the point of view of the safety of the sanitary supply which require drinking water, the rainwater re-use facilities will be properly marked, and no connections will be made between the two installations.
The systems presented are principally described and can be complemented with safety and automation systems depending on the local situation, on the area where they are installed and the type of sanitary items.
Consequently, the recovery and re-use of rainwater can play a major role in ensuring water supply availability and that of water saving in draught areas and not only.

6. Conclusion

A sustainable development includes the preservation of ecosystems, and their protection conditions a sustainable development. Through its core coordinates, the strategy for environmental protection is therefore found in the Strategy for Sustainable Development.
Increasing the number and the complexity of safety problems regarding freshwater resources, due to an increasing water consumption, requires new actions to be taken to protect this vital resource. The study shows the sustainability of solutions to reduce drinking water consumption by collecting, storage and using rainwater in the buildings. In this respect, the analysis of the meteorological parameters and that of the rainwater quality indicators, at least for the mountain areas, indicates as a viable solution the use of rainwater in non-drinking sanitary fittings. The proposed technical solutions can be implemented in both new and existing buildings, as they do not require major changes to the existing domestic water supply installations.
The study concludes that, for the rural and urban areas, the main benefits that rainwater can bring can be quantified by reducing dependence and demand for water supply from the public networks, lowering costs, protecting the natural freshwater resource, protecting the environment, reducing the amount water collected by sewage systems requiring treatment, diminishing soil erosion due to the floods. The actions for the protection of this vital resource are defined in close connection with the economic development policy, the medium and long term economic and social forecasts. Society and the economy must work, and the protection of freshwater and, implicitly, the environment must be done at all costs.

References

[1] Stănescu, Rodica, Mihai Sene, and Clara Volintiru. *European Union Policy Guide, no.4 (Ghidul Politicilor Uniunii Europene, nr.4)*. European Institute of Romania Publishing, 2012.
[2] Foris, Diana, Adriana Tokar, Danut Tokar, and Tiberiu Foris. "A New Dimension on Sustainability of Tourism Destinations: The "Green Water" Program". Paper presented at the XI International Tourism Congress ITC'19, Funchal, Ilha da Madeira, Portugal, November 05 - 07, 2019.
[3] European Commission (EC). "Energy Performance of Buildings Directive". *Energy: Nearly zero-energy buildings*. Accessed January 24, 2017. https://ec.europa.eu/energy.
[4] Falkenmark, Malin, and Johan Rockström. "The New Blue and Green Water Paradigm: Breaking New Ground for Water Resources Planning and Management." *Journal of Water Resources Planning and Management* 132, no.3 (May 2006): 129-132.
[5] Dimitriou, Christina. "From theory to practice of ecotourism: major obstacles that stand in the way and best practices that lead to success." *European Journal of Tourism, Hospitality and Recreation* 8, no. 1 (January 2017): 26-37.
[6] Ural, Mert. "Risk Management for Sustainable Tourism". *European Journal of Tourism, Hospitality and Recreation* 7, no. 1 (May 2016):63-71.
[7] Bahri, Akiça. *Managing the other side of the water cycle: Making wastewater an asset.* Mölnlycke, Elanders Publishing House, 2009.
[8] Foris, Diana, Mihaela Plesca, Tiberiu Foris, and Danut Tokar. "Protecting sweet water Resources from Mountain Area through Ecological Investments in Tourism Industry". Paper presented at the 4th International Multidisciplinary Scientific Conference on Social Sciences and Arts SGEM2017, Sofia, Bulgaria, August 24 - 30, 2017.
[9] Foris, Diana, and Mihaela Plesca. "Sustainable tourism through the protection of sweet water resources in montain area." *Bulletin of the Transilvania University of Braşov* 10, no.1 (January 2017): 107-112.
[10] Graham, Jewitt. "Integrating blue and green water flows for water resources management and planning." *Physics and Chemistry of the Earth, Parts A/B/C* 31, no. 15 (December 2006): 753-762.
[11] Liu, Junguo, Alexander Zehnder, and Hong Yang. "Global consumptive water use for crop production: The importance of green water and virtual water." *Water Resources Research* 45, no. 5 (28 May 2009): 1-15.
[12] Liu, Junguo and Hong Yang. "Spatially explicit assessment of global consumptive water uses in cropland: Green and blue water." *Journal of Hydrology* 384, no.3-4 (30 April 2010): 187–197.
[13] Rockstrom, Johan, Mats Lannerstad, and Malin Falkenmark. "Assessing the water challenge of a new green revolution in developing countries." *Proceedings of the National Academy of Sciences of the United States of America* 104, no. 15 (10 April 2006): 6253–6260.
[14] Tokar, Adriana, and Arina Negoițescu. "Treatment Solutions for Rainwater Contaminated with Various Pollutants." *Annals of the University "Eftimie Murgu" Reşiţa* 22, no. 1 (2015): 405-414.
[15] Tokar, Adriana. *Sanitary and gas installations. Part I (Instalații sanitare și de gaze. Partea I).* Timisoara, Politehnica Timisoara Publishing, 2016.
[16] Vörösmarty, Charles, Pamela Green, Joseph Salisbury, and Richard Lammers. "Global Water Resources: Vulnerability from Climate Change and Population Growth." *Science* 289, no. 5477 (14 Jul 2000): 284-288.
[17] Ministry of the Environment. "*Report on the state of the environment in Romania, year 2018 (Raport privind starea mediului în Romania, anul 2018)*." Accessed January 26, 2019. http://www.anpm.ro.
[18] Busuioc, Aristita, Mihaela Caian, Roxana Bojariu, Constanța Boroneanț, Sorin Cheval, Mădălina Baciu, and Alexandru Dumitrescu. *Climate Change Scenarios in Romania for the period* 2001-2030 (Scenarii de Schimbare a Regimului Climatic în România pe perioada 2001-2030)." National Meteorological Administration, 2012.
[19] Ministry of Environment and Sustainable Development. "Guide on adapting to the effects of climate change. Appendix (Ghid privind adaptarea la efectele schimbărilor climatice. Anexă)." *Official Monitor*, September 29, 2008. Accessed January 26, 2018. http://www.meteoromania.ro/anm.
[20] Public Health Directorate Brasov (Laboratory DSP). "*Analysis Report - Water quality indicators (Raport de analiza – Indicatori de calitate a apei)*." 2017.
[21] Public Health Directorate Brasov (Laboratory DSP). "*Analysis Report - Water quality indicators (Raport de analiza – Indicatori de calitate a apei)*." 2018.
[22] The Romanian Parliament. "Law no. 458/2002 on the quality of drinking water modified by Ordinance no. 22/2017 (Legea nr. 458/2002 privind calitatea apei potabile modificată prin Ordonanța 22/2017)**."** *Official Monitor*. September 03, 2017. Accessed January 26, 2018.
[23] Spiridon, Razvan. "What you can do with rainwater? (Ce poti face cu apa de ploaie?)". *Environmental Magazine Greenly*, May 28, 2012. Accessed January 26, 2018. http://greenly.ro/apa/ce-poti-face-cu-apa-de-ploaie.

[24] Puchianu, Gheorghe, Vasile Pădureanu, Dorin Valter Enache, and Valentin Necula. "Research on microbiological quality and physico – chemical Azuga spring water and exploitation of results obtained by identifying potential health benefits to consumers." Paper presented at the 3rd North and East European NEEFOOD Congress on Food. Global and Local Challenges in Food Science and Technology, Brasov, Romania, May 20 - 23, 2015.

[25] Law, Dave. "How to Safely Thaw a Frozen Gutter." *Renovation Roofing & Remodeling Inc.,* January 13, 2020. Accessed November 14, 2020. https://www.renovationsroofing.com/blog/thaw-frozen-gutter.

[26] Rusen, Alexandra, Alin Scurtu, and Alexandru Crăciun. "Alternative Methods for De-Icing Dangerous Parts of the Road." Paper presented at the 7th edition of the Symposium Energy - Resources - Environment of the Students from Oradea SERMStudo2017, Stana de Vale, Romania, May 18-20, 2017.

Consideration on Hydraulic Modelling and Evaluation of Surface Waters with Environmental Risk

Prof.phD.eng. **Mariana PANAITESCU**[1*], Prof.phD.eng. **Fănel-Viorel PANAITESCU**[1]

[1] Constanta Maritime University

* panaitescumariana1@gmail.com

Abstract: *All groundwater catchments in a basin must be protected against pollution by establishing sanitary and hydrogeological protection areas, in order to ensure a good use of groundwater resources. The most precise method of determining the protection zones is the mathematical modeling. The paper presents a modeling of an erodible riverbed with environmental risk in the Dobrogea hydrographic Basin, as well as the assessment and analysis of environmental risk for the related.*

Keywords: *Surface water, protection, risk factor, assessment, vulnerability, probability*

1. Introduction

Dobrogea is composed of three major structural blocks namely: Dobrogea South, Central Dobrogea and North Dobrogea separated by faults Capidava -Ovidiu and Peceneaga - Camena (Fig. 1) [1]. More than 80% of Dobrogea appears to be siliceous rocks [2].

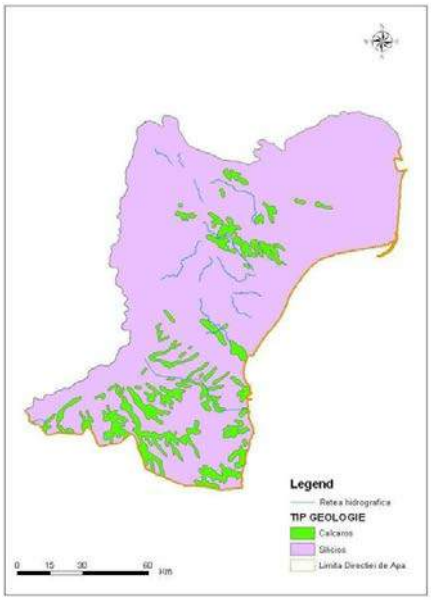

Fig. 1. The structural blocks from DOBROGEA

Dobrogea catchment area is very poor in own surface resources. Basically, they consist of several major rivers surface (so far there is no use in rivers due to low water flow permanently) and in coastal lakes and related Danube [3].
The catchment area Dobrogea identifies 16 rivers with areas greater than 10 km², 18 natural lakes and four water storages that are larger than 0.5 km².
DOBROGEA ARIA consists of Seaside and streams tributary to the Danube River catchment area corresponding Dobrogea (Figure 2) [4].

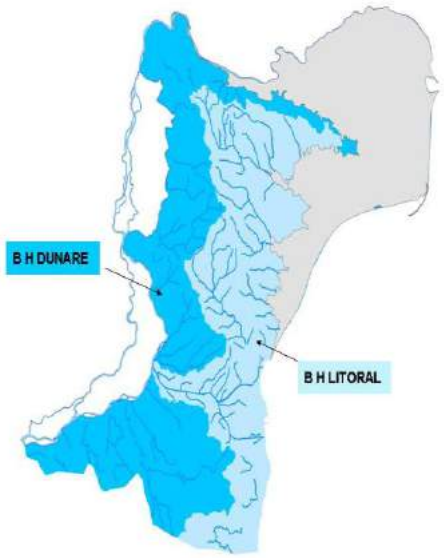

Fig. 2. DOBROGEA hydrographic basin

To characterize a basin is necessary to know its characteristic elements-morphological variables of the watercourse system (Fig. 3) [3].

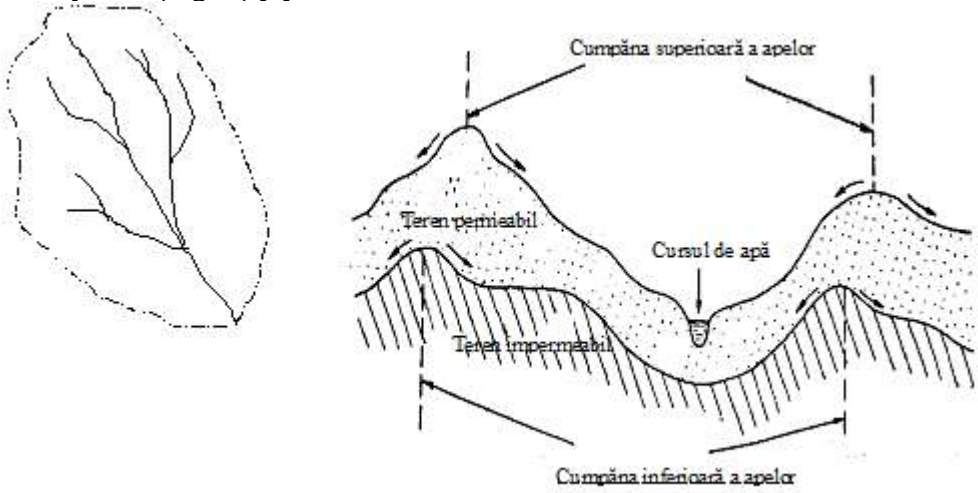

Fig. 3. Hydrographic basin-schematization and water scale

These can be divided into:

- Elements of hydrology and river network
- Geological features
- Features on vegetation.

2. Modeling the river bed with environmental eroding risk in DOBROGEA area

Modeling the riverbed with environmental eroding risk the following elements need to be studied:

- Data location and description of the catchment area, applicable to chosen location;
- Data on power sources aquifer basin, applicable to chosen location;
- Balance river flows in the basin area for a chosen period;
- Reporting to the climatological normal space basin [5].

Hydrometeorological regime for chosen catchment area reported to County statistics [6].

2.1 Choosing a white space erodible river in Dobrogea

The analysis will be done for the creek Nuntasi. Supply aquifer - is mainly from rainfall and the loss of irrigation water systems.
Balance flow to the hydrographic area Dobrogea (for 1999, 2004, 2007 and 2010) is shown in Table 1.

Table 1: Balance flow to the hydrographic area Dobrogea

Year	Balance flow	Feed rate [m^3/s]	Discharge rate [m^3/s]
1999[27]	Northern limit	-	5417.58
	Western limit	-	7 869.45
	Southern boundary	-	17 98.06
	Black Sea	-	60 800.55
	Input from the surface	91 367.34	-
2004	Northern limit	-	5923.72
	Western limit	-	8104.57
	Southern boundary	-175.33	1945.27
	Black Sea	-	67845.13
	Input from the surface	98 452.89	-
2007	Northern limit	-	6123.48
	Western limit	-	8765.41
	Southern boundary	-189.37	2006.39
	Black Sea	-	69929.16
	Input from the surface	99 321.23	-
2010	Northern limit	-	2 320.63
	Western limit	-	4 248.47
	Southern boundary	143.28	8 579.01
	Black Sea	-	24 998.52
	Input from the surface	39 987.25	-
TOTAL		329 636.69	286675.83

Nuntasi Lake River Basin lies between 280 37''30' NV and 280 45' N-E and also parallel 44° 30 'latitude and parallel 44° 35' [6].
Morphometric parameters are shown in Table 2 (River Data hydraulic).

Table 2: River Data hydraulic

River	Average depth (mdM)	Area (km^2)	Volume (mil. m^3)	Maximum Depth (m)	Length (m)	The diameter of the granules r (mm)	Specific gravity of the alluvium [N/m^3]	Friction slope
Nuntasi	10	145	9.8	2.3	14 000	8	26.5	0.002

3. Numerical modeling and flow simulation for riverbed

Study of modeling assumptions are:

- flow-permanent, two-dimensional, parallel throughout the riverbed,
- incompressible fluid and homogeneous,
- slope small bed, small variations in the parameters of cross sections
- hydrostatic pressure distribution date [7].

The equations for the flow cross-section are the Saint-Venant equations and for along the riverbed flow, the turbulent flow equations, i.e. equation for turbulent kinetic energy.

For the flow modeling we select a sector and we will note the geometric and hydraulic parameters and related to this sector, the settling flow diagram (Fig. 4) by hydraulic modeling [8]. In our case, the modeling will be done by using software MIKE 11 [8].

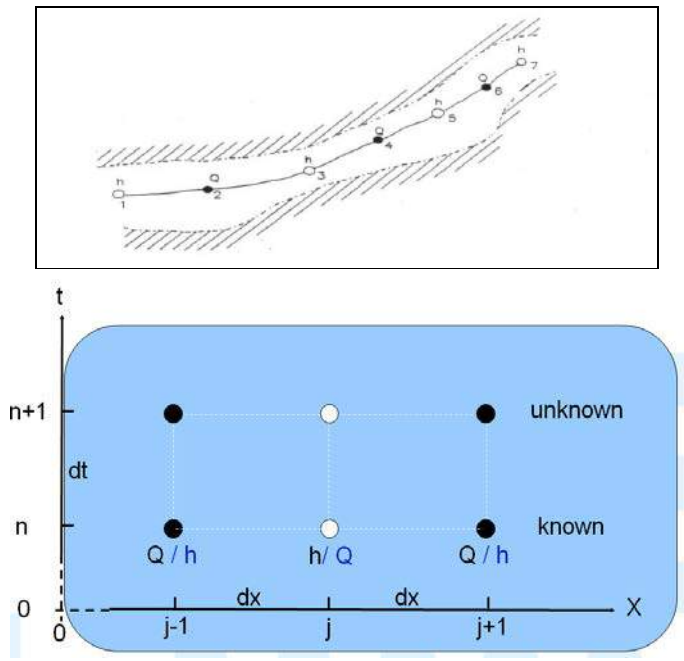

Fig. 4. The geometric and hydraulic parameters and the settling flow diagram

Flow stability is required for the convergence of the solution achieved by modeling, given the initial conditions and the approximation by finite differences that need to be consistent.
Explicitly provided stability is the number Courant (eq. 3.20) [8], where Cr <1.
Boundary conditions of the flow are:

- discharge flow upstream of the control section, downstream;
- tributaries flow;
- condition for convergence solution-end flow, Q = 0;
- water depth, h (1 ÷ 2.3) m;
- weather-wind, currents;
- conditions for Q / h downstream flow (never upstream).

Input data are: topographic data, hydraulic data. There was used information provided by operating with ArcGIS software (Fig. 5) [8], software MIKE Zero (Fig. 6) [8] and Nuntasi topographic map of the basin (Fig. 7) [9].
Study parameters sections; limnimetric key to riverbeds (Figure 8); elementary hydrograph (Figure 9); values for peak flow conditions (Table 3, Table 4).
In the Nuntasi riverbed were analyzed aspects necessary for sizing the riverbed by means of graphic-analytical (flow, roughness, depth initial slope bottom and sloping embankment) (Table 5, Table 6), rising variation in the width b depending on the depth h (Figure 10) and changes the width b by block debit K (Figure 11).

These elements will help us to shape both flow into the riverbed and to analyze risk in the event of floods.

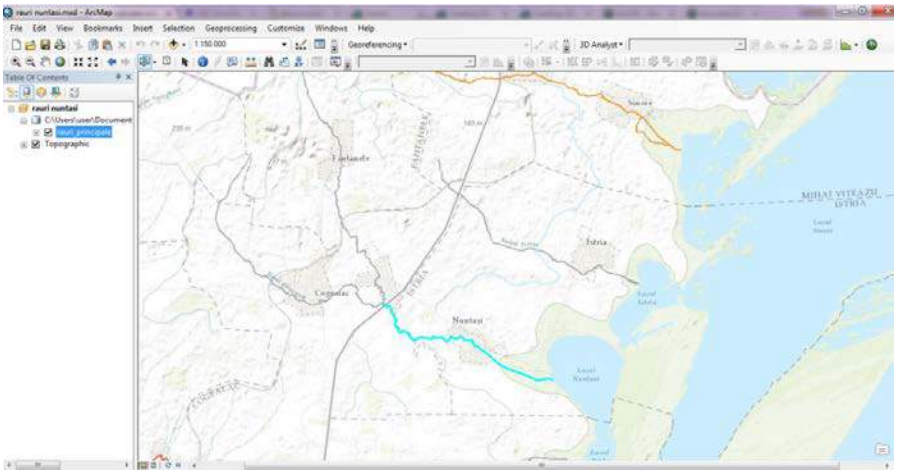

Fig. 5. Localization with the ArcGis program

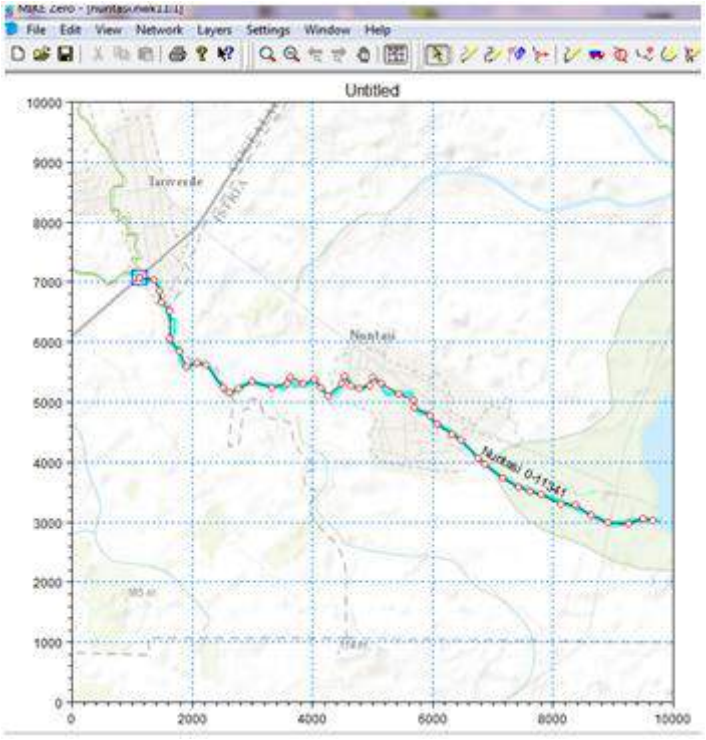

Fig. 6. Map construction with MIKE Zero program

Fig. 7. Location on the map of the Nuntasi hydrographic space

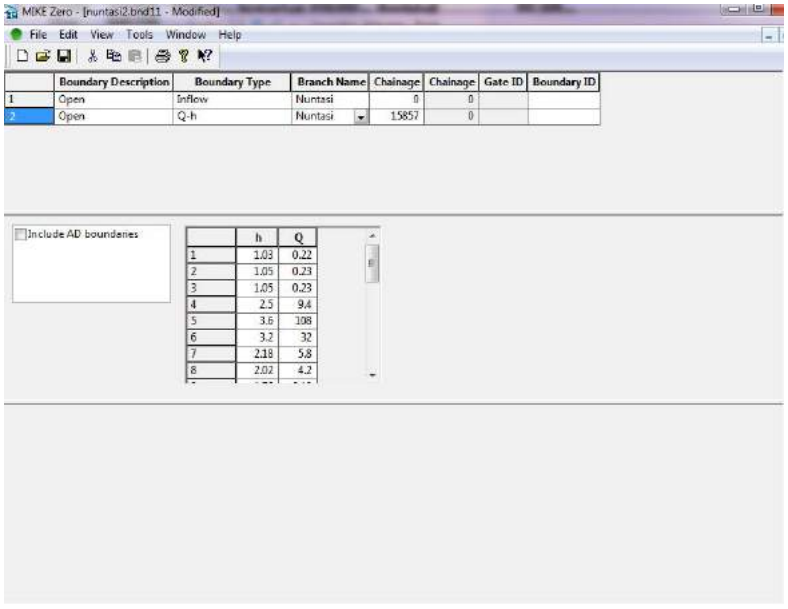

Fig. 8. The limnimetric key to riverbeds

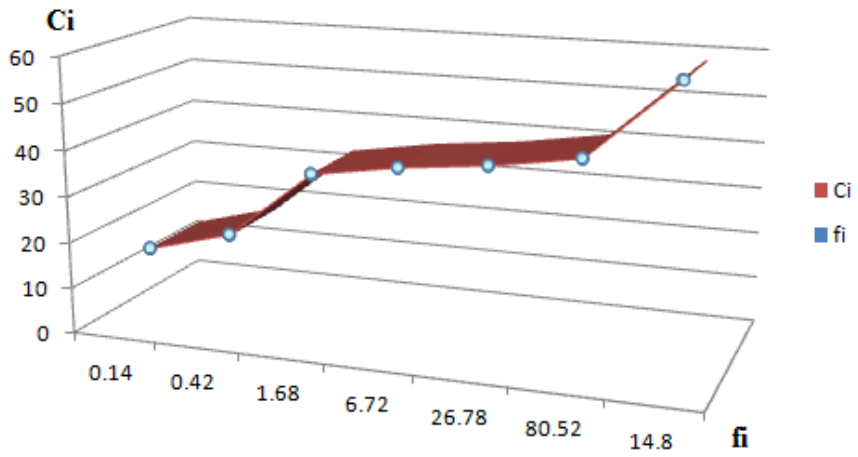

Fig. 9. The elementary hydrograph

Table 3: The values of the elevations of the curves of the surfaces between two contours

Curve	C_i [mdM]	f_i [km^2]
1	15	0.14
2	20	0.42
3	35	1.68
4	38	6.72
5	40	26.78
6	43	80.52
7	60	95.40

Table 4: The Pool characteristics

River	L, km	Total volume, mil. m^3	S, km^2	Alt, mdM	Q_{medma} (m^3/s)	$Q_{minlmedma\ asig}$ 80% (m^3/s)	$Q_{minlmedma\ asig}$ 90% (m^3/s)	$Q_{minlmedma\ asig}$ 95% (m^3/s)	Q_{min}/Q_{max}^*
Nuntasi	14	9.3	145	10	0.473	0.280	0.200	0.140	1/2250

Table 5: Initial data

Initial data	Q_i [m³/s]	n	h_0 [m]	i	m=ctgθ
Values	0.02	0.015	1.2	0.0165	1.732

Table 6: Grapho-analytical method [41], [42] for width variation as a function of flow modulus

No.	b [m]	A [m²]	P [m]	R [m]	C	K [m³/s]	h [m]
2.	7.2	4.033	9.1999	0.438374	58.103	155.1491	0.5
3	5.2	3.743	7.5999	0.5131	59.2452	155.656	0.6
4	3.85	3.54368	6.6499	0.5328	60.0272	155.28	0.7
5	2.9	3.42848	6.099	0.56205	60.5626	155.66	0.8
6	2.17	3.35592	5.769	0.5816	60.9091	155.88	0.9
7	1.5700	3.302	5.569	0.5928	61.103	155.347	1
8	1.0800	3.2837	5.479	0.5992	61.212	155.597	1.1
9	0.65	3.27408	5.449894	0.60076	61.23865	155.4052	1.2

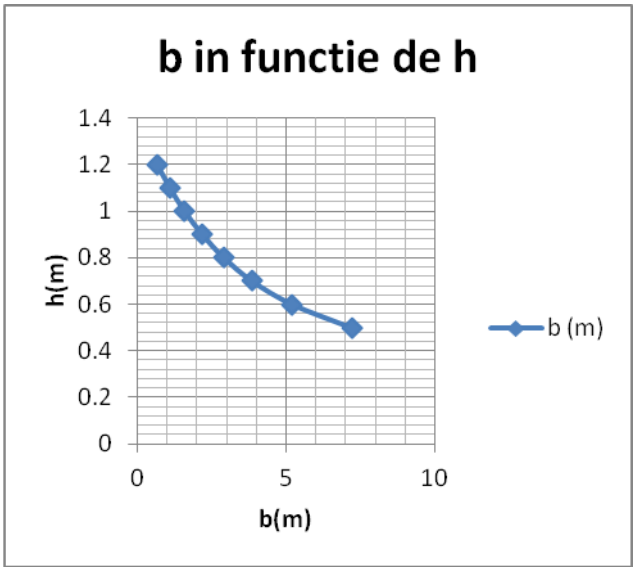

Fig. 10. Variation in width as a function of depth

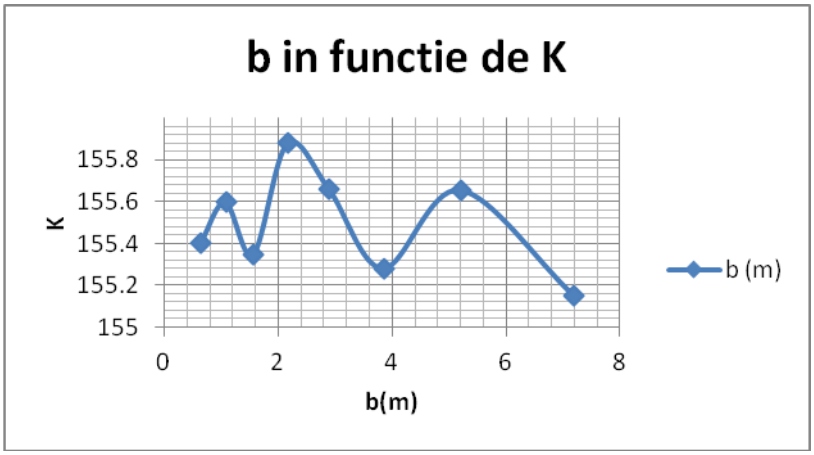

Fig. 11. Width variation depending on the flow module

3.1 Flow simulation in the riverbed by MIKE 11

Based on topographic data, initial hydraulic data and data obtained by graphic-analytical and also the limnimetric key of Nuntasi riverbed using MIKE 11 software was simulated a flow specific to a situation of flood in 2007 (Fig. 12) and compared to the level of 1999 (Fig. 13).

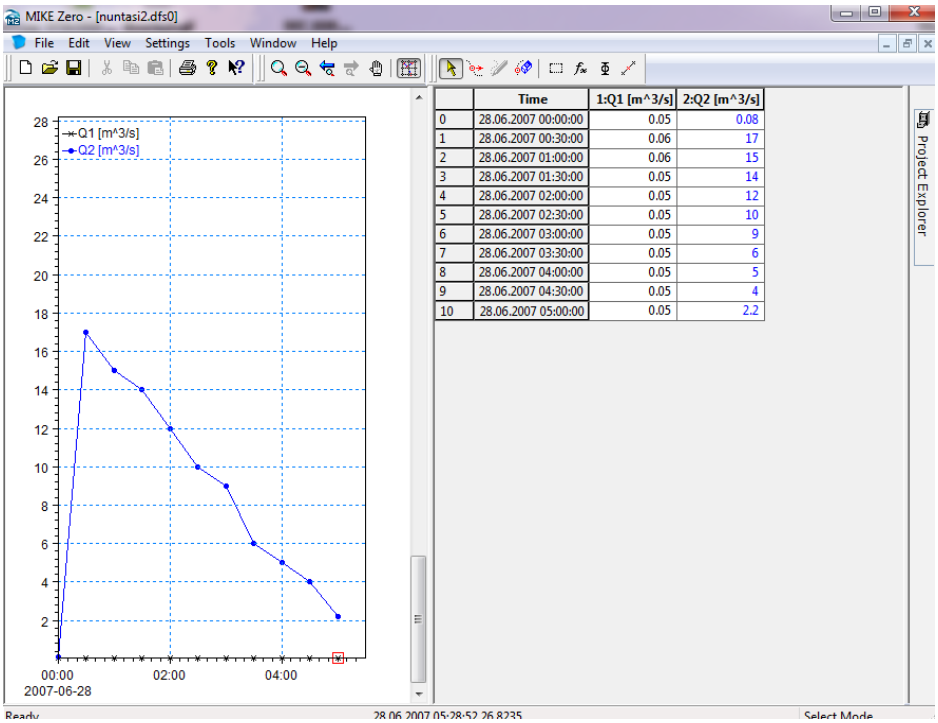

	Time	1:Q1 [m^3/s]	2:Q2 [m^3/s]
0	28.06.2007 00:00:00	0.05	0.08
1	28.06.2007 00:30:00	0.06	17
2	28.06.2007 01:00:00	0.06	15
3	28.06.2007 01:30:00	0.05	14
4	28.06.2007 02:00:00	0.05	12
5	28.06.2007 02:30:00	0.05	10
6	28.06.2007 03:00:00	0.05	9
7	28.06.2007 03:30:00	0.05	6
8	28.06.2007 04:00:00	0.05	5
9	28.06.2007 04:30:00	0.05	4
10	28.06.2007 05:00:00	0.05	2.2

Fig. 12. Flow simulation for two flow discharge in 2007

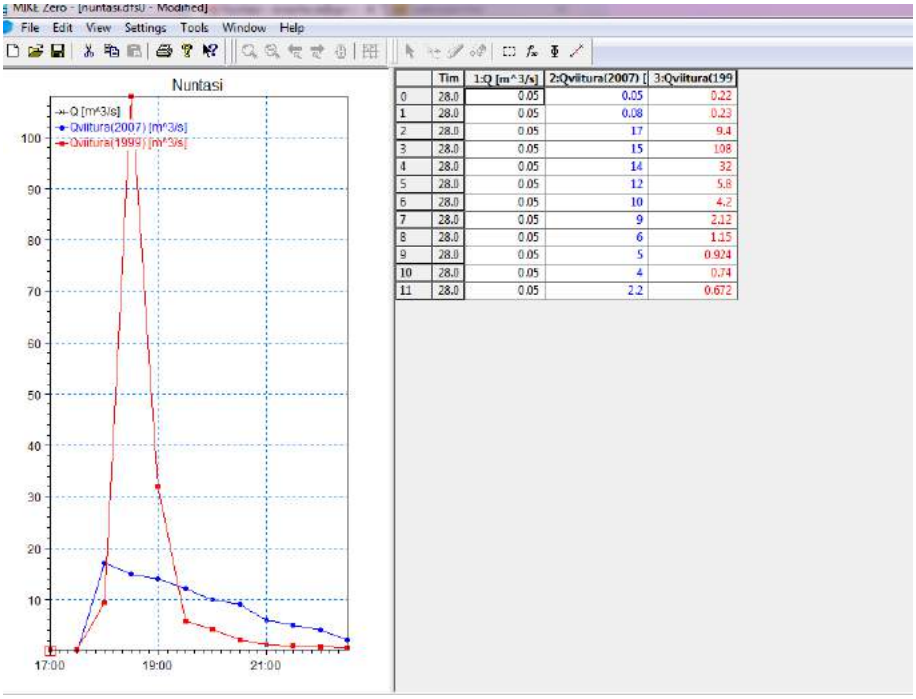

	Tim	1:Q [m^3/s]	2:Qvilitura(2007) [	3:Qvilitura(199
0	28.0	0.05	0.05	0.22
1	28.0	0.05	0.08	0.23
2	28.0	0.05	17	9.4
3	28.0	0.05	15	108
4	28.0	0.05	14	32
5	28.0	0.05	12	5.8
6	28.0	0.05	10	4.2
7	28.0	0.05	9	2.12
8	28.0	0.05	6	1.15
9	28.0	0.05	5	0.924
10	28.0	0.05	4	0.74
11	28.0	0.05	2.2	0.672

Fig. 13. Flow simulation for two discharge flow (flood in 1999 and 2007)

The result of the MIKE 11 simulation program consists of a contemporary representation while during flood flow path on the Nuntasi course, viewing velocity vector (green, Fig.14) for the entire length of the river.

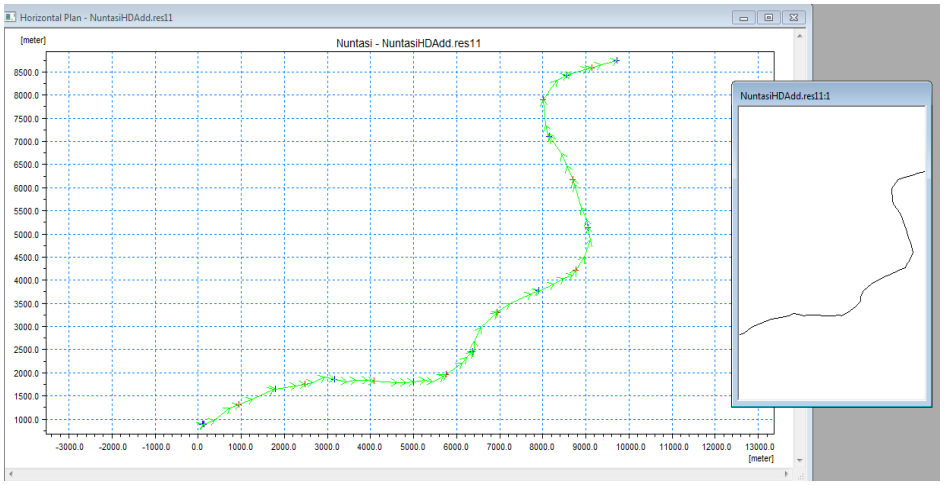

Fig. 14. Flow visualization and velocity vector along the riverbed Nuntasi.

The final results of modeling with MIKE 11 program are plotting and maximum rates for the flood of 2007 (Fig. 15) and flow profile along the riverbed Nuntasi (Fig. 16).

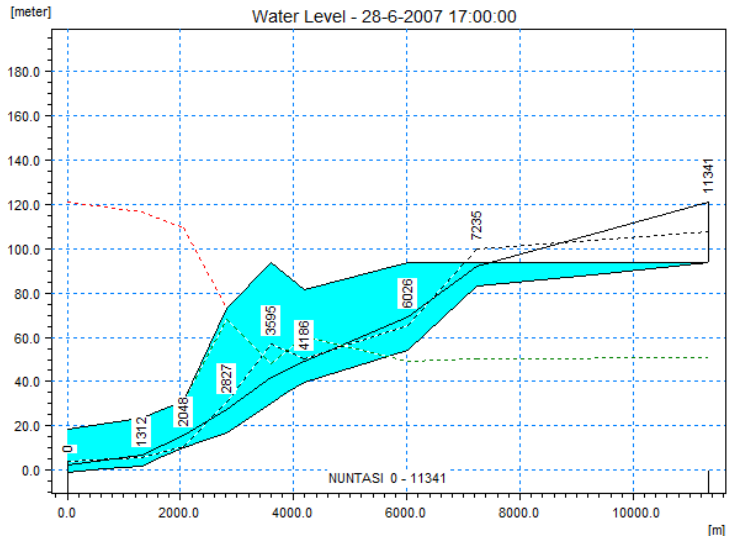

Fig. 15. Shares riverbed for flood in 2007

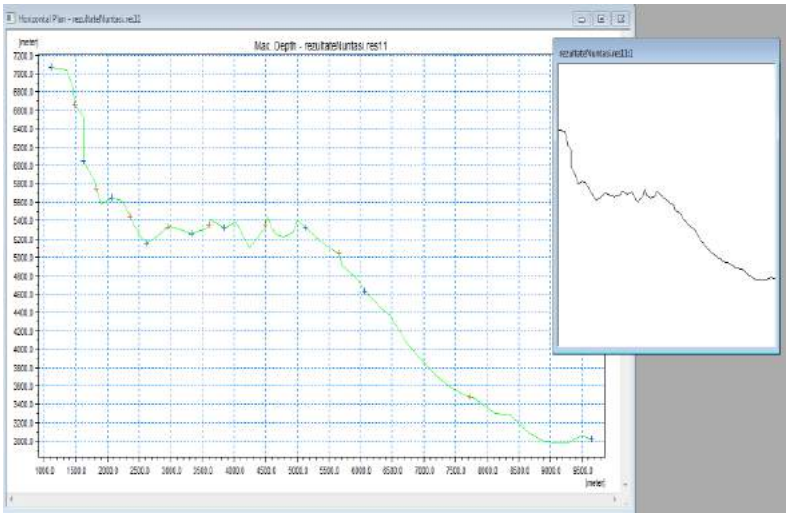

Fig. 16. The final flow profile along the riverbed

4. Assessment and risk analysis of environmental basin

The risk factors for chose catchment are the flooding and anthropogenic pollution.

4.1 The floods

One of the risk factors is represented by the floods. Approaching to flood hazard in Area Hydrographic Dobrogea consists of a first stage group watercourses cadastral three degrees of detail depending on the frequency of floods in recent years, the magnitude of their manifestation, the level of equipment with works flood protection, economic or social objectives subject to flooding hazard, etc (Fig. 17) [8]: level A - very detailed; Level B - detailed; Level C.

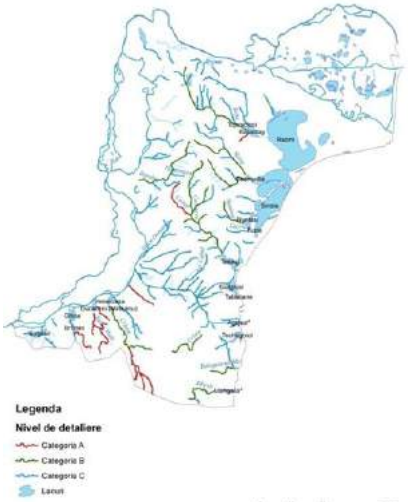

Fig. 17. Map of the hydrographic network Dobrogea Water Basin Administration

There were analyzed areas Nuntasi Basin - Nuntasi, Nuntasi Basin - Fantanele. In terms of structural measures, imposed costs on urban river engineering on the section Nuntaşi- Fantanele Basin and river engineering costs for the urban section Nuntaşi- Nuntasi Basin, aiming finally to avoid casualties. [12].

4.2 Anthropogenic pollution

Human activities lead to alterations in the riverbed morphology and dynamics to change its hydraulics. Aspects should be considered amending the short term (dams, bridges, erosion, etc.) and long term (changes generated by the embodiment Management work).

4.3 Risk analysis of hydrographic area

With the method of analysis of the possibilities of risk RFMEA (failure mode risk evaluation analysis) are measured and quantified four parameters [13], [14], [15], [16], [17]:

• vulnerability (exposure) (R);
• the probability (P);
• the effect of being an instrument of control / measurement / control / share (N);
• efficiency indicator of a new measure (F).

The first three provide the level of risk or risk factor (RPN). Parameter (F) of the method of analysis is an indicator of the effectiveness or urgency of a new measure or a series of prevention and control measures. It includes the economic effect of the control measure and compares the estimate of the consequences of a probable accident or disaster with the financial and human loss. All these four parameters form the complex risk factor (RPNF).

Vulnerability characterize exposure to risk factors analyzed location. The probability (P) an event in a year can be classified with another likely in the coming year, when more accurate data are available. The same is true with other factors in the selection process (Table 7).

Table 7: The probability

Probability for a disaster event	Probability (caz/ani)	Value
Very high, very often	>1 ... 2	10
	1 ... 3	9
High : repeated accidents	1... 5	8
	1 ... 10	7
Average: from time to time	1 ... 15	6
	1 in 20	5
	1 in 25	4
Low: very rare accidents	1 in 35	3
	1 in 50	2

Measures of control- the means of prevention and protection present actions and active policies. These are defined mainly by preventing complex parameter-control measure (N) (Table 8).

Table 8: Control measures

The measure of prevention, control or effect of the action	Description of the effect	Value
Nothing; Without measure	Absolutely no measures, controls or actions are currently in place	10
Almost no effect	Almost no effective measures for control or prevention, impact on system protection against destruction, loss of life or warning	9
Very low effect	Extremely inefficient or unproven for all measures to control, prevent and protect human lives and long-term consequences	8
Quite low effect	Quite low effect of the measure, control or action to protect human lives and long-term consequences	7
Low	Low effect, but there are some chances of protecting human lives and long-term consequences	6
Relative	Relative effectiveness of the measure, control or action to protect loss of human life, but protect human victims and mitigate long-term consequences	5
Relatively high	Relatively high effect of the measure, control or action to protect human lives, and diminishes the long-term consequences	4
High	High insurance which means a measure, control or action that prevents losses and reduces long-term consequences.	3
Very high	Very high insurance, which means a measure, control or action that prevents losses and reduces long-term consequences.	2
Safe effect	Safe measure, control or action that prevents losses and reduces long-term consequences. In the case of NUNTASI, the execution of a covered trapezoidal section was proposed which involves: • regularization of the riverbed on the urban section Bazinul Nuntaşi-Fântanele in the amount of 3,767,390.90 € • regularization of the riverbed with dams in the amount of € 2,029,612.20 • regularization of the riverbed on the urban section Bazinul Nuntaşi-Nuntaşi in the amount of € 3,737,263.25 • regularization of the riverbed with dams in the amount of € 666,872.58	1

The level of risk can be simply determined (RPN), or determined by the efficiency factor F (complex level of risk, RPNF).
Automatic calculation of the level of risk (value RPN) is done by multiplying the three values.

The risk levels based on RPN values are chosen so (Table 9):

- High (marked in red) for RPN values> 250;
- Intermediate (marked in yellow) є RPN values (41 .... 250);
- Low (marked in green) for RPN values є (1 .... 40).

Table 9: Calculation of values for RPN and F

Economic factor of efficiency F - costs for damage and prevention	Damage rate / prevention costs	Value F
Very high - the estimated damage is considered higher than the prevention budget	>50 1	10
	>20 to 1	9
High - the estimated damage is considered much higher than the prevention budget	10 1	8
	5 to 1	7
Almost equal - the estimated damage is slightly above the prevention budget	2 to 1	6
Equal	1	5
The prevention budget is higher than the estimated damage	1 to 5	4
The prevention budget is considerably higher than the estimated damage	1 to 20	3
	1 to 100	2

5. Conclusions

For studying the flow in the Nuntasi riverbed eroded with environmental risk were analyzed elements: location and description of the hydrographic area, data sources feeding the aquifer basin data sources feeding the aquifer basin balance flows to the hydrographic area Dobrogea for 1999, 2004, 2007 and 2010, reporting to the climatological normal catchment area Dobrogea; hydrometeorological regime for the guests catchment area reported at Constanta County; morphological and morphometric elements of the bed of the guests; Nuntasi riverbed proper flow modeling; risk analysis in the event of floods.
The conclusion of the risk analysis was: Nuntasi riverbed fits at "low risk prevention measure without any serious urgent implementation RPNF with values between (1 ... 150)". Following theoretical and experimental findings about river conditions change in response to the liquid phase flows and sediments are:

- current depth is directly proportional to fluid flow and inversely proportional to the flow of solid material dragged;
- limits the embankments of river bed varies in direct proportion to the flow of liquid and solid material;
- varying flow is directly proportional to the variation solid ratio width / depth;
- slope of the river bed varies in direct proportion to solid and grain alluvial flow and inversely proportional to fluid flow;
- river meanders rate is directly proportional to the variation in relief and inversely proportional to the solid flow.

References

[1] Zotta, Benone. *Geography of Constanța Municipality / Geografia Municipiului Constanța.* Constanța, Muntenia Publishing House, 1995.
[2] Ielenicz, Mihai, and Iulian Săndulache. *Romania - plateaus and hills / România - podişuri şi dealuri*. Bucharest, University Publishing House, 2008.
[3] Scradeanu, D., and A. Gheorghe. *General hydrogeology / Hidrogeologie generală* (chapter *Natural factors of groundwater supply and regime* / *Factori naturali ai alimentarii si regimului apelor subterane*). Bucharest, Bucharest University Press, 2014.
[4] ***. *Plan for the prevention, protection and mitigation of the effects of floods in the Dobrogea-Coastline hydrographic area / Planul pentru prevenirea, protecţia şi diminuarea efectelor inundaţiilor în spaţiul hidrografic Dobrogea-Litoral*. Constanta, 2014.
[5] Panaitescu, Mariana. *Hydraulic modelling and evaluation of surface waters with environmental risk.* Constanta, Nautica Publishing House, 2016.
[6] ***. *Planul de analiză şi acoperire a riscurilor al judeţului Constanţ*a, 2015. Accessed November 9, 2020. http://www.isudobrogea.ro/wp-content/uploads/2016/03/Planul-de-Analiz%C4%83-%C8%99i-Acoperire-a-Riscurilor-al-jude%C8%9Bului-CONSTAN%C5%A2A-2015.pdf
[7] Enache, Iulia-Alina. *Modeling the components of water flow in the Dobrogea-Litoral river basin / Modelarea componentelor scurgerii apelor din bazinul hidrografic Dobrogea-Litoral*. Bachelor thesis, Constanta, 2014.
[8] ***. Hydro-Informatics. *Modelling tools MIKE 11, Part 1-Introduction*. IHE, 2001-2003.
[9] http://www.hartastrazi.info/harta-localitate-nuntasi-judet-constanta. Accessed November 9, 2020.
[10] Hâncu, Simion. *Guidelines for hydraulic calculations / Indreptar pentru calcule hidraulice*. Bucharest, Technical Publishing House, 1989.
[11] Trofin, E. *Hydraulics and hydrology / Hidraulica si hidrologie*. Bucharest, Didactic and Pedagogical Publishing House, 1974.
[12] ***. "Plan for prevention, protection and mitigation of flood effects, scenarios for planning and prioritizing measures in the Dobrogea coastline hydrographic area" / "Planul pentru prevenirea, protecţia si diminuarea efectelor inundaţiilor, scenarii de amenajare si priorizare masuri în spaţiul hidrografic Dobrogea litoral", version 3. http://www.rowater.ro/dadobrogea/Lists/Anunturi1/Attachments/61/PPPDEI-ABADL-ver3.pdf, pp. 329-337. Accessed November 9, 2020.
[13] Kanev, V. *System and web application for risk assessment of oil spill in black sea and prevention management – covered hazards and risks, users' response and further development*. Final Book of IUCRISKMAN project. Constanta, Nautica Publishing House, 2015.
[14] ***. Apl. Ref. 2.2.1.73194.264, "Creation of Interuniversity centre for risk management and assessment for prevention of ecological and technological risks in the Black Sea" (IUCRISKMAN). *Training on RISK Monitoring & Database Software WEB Application for the RkFMEA System for Risk Assessment and Prevention Management*, *Guidebook and Application Manual*. Constanta, 2015.
[15] Manescu, M. *Hydraulics of bridges and footbridges / Hidraulica podurilor si podeţelor.* Timisoara, University Horizons Publishing House, 2002.
[16] ***. A.N.C.O.L.D. *Guidelines on risk assessment. Position paper on revised criteria for acceptable risk to life*. A.N.C.O.L.D. Working Group on Risk Assessment, 1998.
[17] Popa, R. *Elements of river hydrodynamics / Elemente de hidrodinamica râurilor*. Bucharest, Didactic and Pedagogical Publishing House, 1997: 253-300.

Aspects regarding the Operation of PELTON Turbine Model Used in Energy Recovery from Water Streams

Assistant professor **Fănel Dorel ȘCHEAUA**[1]

[1] "Dunărea de Jos" University of Galați, MECMET Research Center, fanel.scheaua@ugal.ro

Abstract: *It is highlighted the major potential of natural water flows that can supply large amounts of electric energy when the necessary conditions are met regarding the water flow rate and height. In order to achieve this goal, different models of hydraulic turbines have been developed over time that are capable of taking over and using the nature provided water flow rates for the energy production. The constructive PELTON turbine type represents a special model having fixed or variable blades which can ensure an axial rotation mode when there is a low water flow rate and high drop height values. The theoretical aspects are presented in this paper, characteristic for the turbine type and a fluid flow analysis is made on a PELTON turbine virtual model emphasizing the flow parameters when the operation conditions are simulated. The virtual model describes a scaled turbine type which can be used on a low height water stream and specific flow rate values.*

Keywords*: Water flow, energy recovery, three-dimensional modelling, CFD*

1. Introduction

The continuous increase in energy demands is the challenge that human communities must face in the near future. That is why the opportunities that lead to the objectives achievement of producing energy from renewable sources which also avoids environmental damage must be considered. One of these opportunities is the use of the water flow force on level differences that can ensure a necessary potential energy in order to obtain rotational motion at a turbine shaft, mounted directly on the water stream.
Several solutions for water energy recovery are presented in producers offer presently worldwide comprising the main components needed for energy production represented by turbine and generator in compact mode. The turbine can achieve the take over of water energy and conversion into the mechanical energy described by rotational motion and shaft torque, while the generator is the component which converts the mechanical energy into electric energy according with the rotation velocity received.
The energy obtaining principle based on water flow is the traditional method but it is the provided power value that makes the difference based on water flow rate and height.
For the PELTON turbine type the water fall height is of major importance in comparison with water flow rate. A solution for energy recovery based on water flow using a PELTON turbine type is presented. It represents a model that can be used for capturing water source flow energy of reduced flow rate values ensuring the energy generation possibilities. 00

2. Water stream recovery energy concept based on PELTON turbine model

For water streams that have a low flow rate but high drop height, it is preferable to use the water capture solution through a PELTON turbine type. In order to achieve this, the initial design of the basic turbine model must be considered in order to perform an optimal energy conversion function. The used PELTON turbine model under optimum conditions has a quite high efficiency in operation with values slightly exceeding 90% depending on provided water flow rate and the height of fall. The main parameters related to the operation of the turbine are the power at the turbine shaft, the maximum torque, the rotation velocity, as well as the specific values for sizing the model of water dosing at the entrance to the turbine enclosure. 000

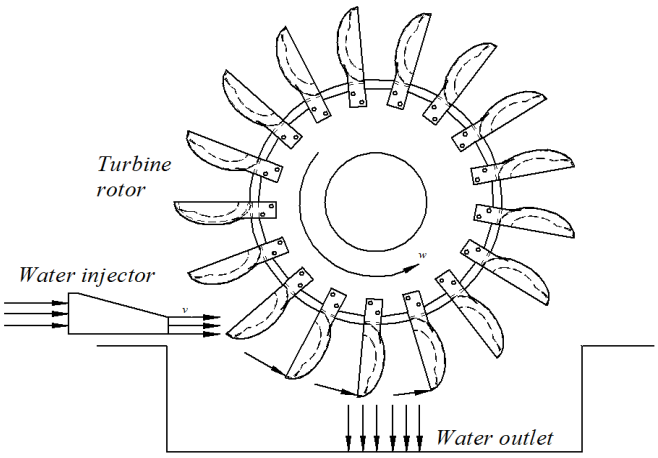

Fig. 1. Schematical representation of PELTON turbine operation

By means of this constructive turbine model it is possible to convert the water mechanical energy into shaft rotational energy. Shaft power is a proportionality relation between turbine drop height, water flow and turbine output:00

$$P_T = 9.81 Q H \eta \tag{1}$$

The fundamental equation that underlies the turbine operation is represented by Euler's equation and expresses the relationship between the specific energy transmitted to the rotor by each mass unit of water that is driven through the turbine enclosure and the mediated velocities parallelograms at the inlet and outlet sections of the turbine rotor. 00

$$E_T = H\eta_h = \frac{v_{r1}v_1 \cos a_1 - v_{r2}v_2 \cos a_2}{g} \tag{2}$$

where:
E_T - the specific energy transmitted to the turbine;
H - the height of fall;
η_h - hydraulic efficiency.

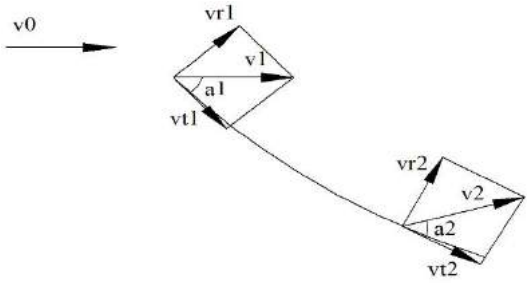

Fig. 2. Velocity components description for turbine rotor

Considering the velocity dimension which for the axial-symmetrical water flow type is described by the relation: 00

$$\mathrm{K} = \pi D v \cos a \tag{3}$$

The Euler equation can be rewritten based on the angular velocity of the turbine rotor , (w) and the turbine circulation velocity before and after the turbine (K_1, K_2) as follows: 00

$$H\eta_h = \frac{w}{2\pi g}(K_1 - K_2) \tag{4}$$

The optimal operating regime of the turbine (maximum efficiency) can be defined based on the fulfillment of the following conditions:

- The water entry into the rotor enclosure should be made without shocks (the relative velocity to the entry edge being tangent to the rotor blade);
- The outlet water stream direction from the rotor is so positioned as to ensure minimal load losses.

The calculation relations for the change case in fall height and turbine diameter under the similarity conditions of the operating regimes are the following: 00

$$\frac{n_1}{n_2}=\frac{D_2}{D_1}\frac{\sqrt{H_1\eta_{h1}}}{\sqrt{H_2\eta_{h2}}}$$
$$\frac{Q_1}{Q_2}=\left(\frac{D_1}{D_2}\right)^2\frac{\sqrt{H_1\eta_{h1}}}{\sqrt{H_2\eta_{h2}}} \quad (5)$$
$$\frac{N_1}{N_2}=\left(\frac{D_1}{D_2}\right)^2\frac{H_1\eta_1}{H_2\eta_2}\frac{\sqrt{H_1\eta_{h1}}}{\sqrt{H_2\eta_{h2}}}$$

The total yields (η_1,η_2) and hydraulic yields (η_{h1},η_{h2}) are taken into account. If the variation of the yield value is neglected, the relations can be written as follows: 00

$$\frac{n_1}{n_2}=\frac{D_2}{D_1}\frac{\sqrt{H_1}}{\sqrt{H_2}}$$
$$\frac{Q_1}{Q_2}=\frac{D_1^2}{D_2^2}\frac{\sqrt{H_1}}{\sqrt{H_2}} \quad (6)$$

The turbine-specific parameters can only be recalculated if the principle of geometrical similarity of the turbine component elements in direct contact with water is respected. The unit values for the calculation parameters describing a diameter rotor of 1m operating at a drop height of 1m are thus introduced. The parameter equations become: 00

$$n=n_1^*\frac{\sqrt{H}}{D}$$
$$Q=Q_1^*D^2\sqrt{H} \quad (7)$$

In order to describe the specific velocity regime of the turbine rotor for which the velocity values, water drop height and shaft power are known, the following relation can be written: 00

$$n_{sp}=\frac{n}{H}\sqrt{\frac{1.36N}{\sqrt{H}}} \quad (8)$$

If the values for the unit parameters $\left(n_1^*,Q_1^*\right)$ are known, the following relation can be used to calculate the specific velocity at the turbine shaft: 00

$$n_{sp}=3.65n_1^*\sqrt{Q_1^*\eta} \quad (9)$$

Different values for the specific velocity regime for PELTON type turbines with one or more nozzles are shown in table 1.

Table 1: Specific PELTON turbine rotor velocity function of mounted nozzle number 0

Number of turbine rotor nozzles	Specific rotor velocity $\left(n_{sp}\right)\left[rot/\min\right]$
1	3-24
2	20-34
4	32-47
6	38-58

Table 2: Velocity values for PELTON turbine rotor type with one nozzle based on $\left(n_1^*\right)$

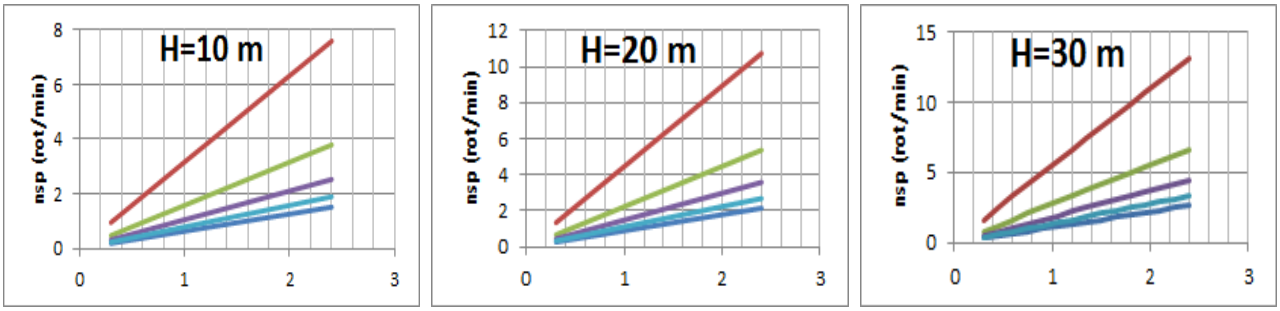

3. Water flow analysis on turbine rotor model

A three-dimensional turbine rotor model is constructed with a number of 17 double blades and a 5.135 m in diameter.
The model is placed in a closed enclosure having an VENTURI injector model with an outlet of 0.5 m diameter for water discharge.
The assembly represents the basic model for a PELTON turbine type and the surrounding fluid region of 10.29 cubic meters in volume.
A water flow analysis is made on the virtual rotor model using ANSYS CFX software, in order to highlight the flow parameters at the level of the blades operated by water gravitational motion.

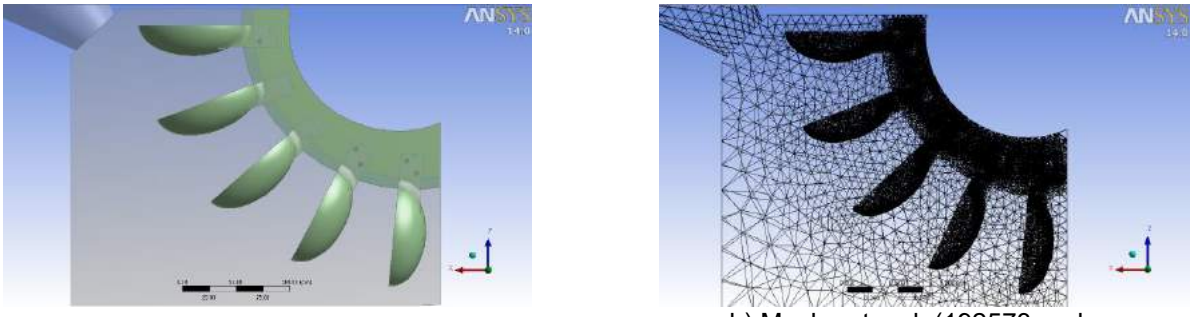

a) Analysis assembly model

b) Mesh network (192573 nodes, 969475 elements)

Fig. 3. Turbine model used for flow analysis and mesh network

Based on the analysis initial values declared for the turbine enclosure inlet and outlet regions the specific flow values at the analyzed fluid region level are calculated. The water values are used as the working fluid.
The assumed water inlet velocity value is of max 5 m/s, while for the output region the reference pressure of zero value is declared.
The results are presented as pressure and velocity distribution inside the fluid domain emphasizing the active contact region where the water is directed mainly on the rotor blade, having the role of motion entrainment basing on the values obtained, tending to move the blade through the direct action of hydrostatic forces.

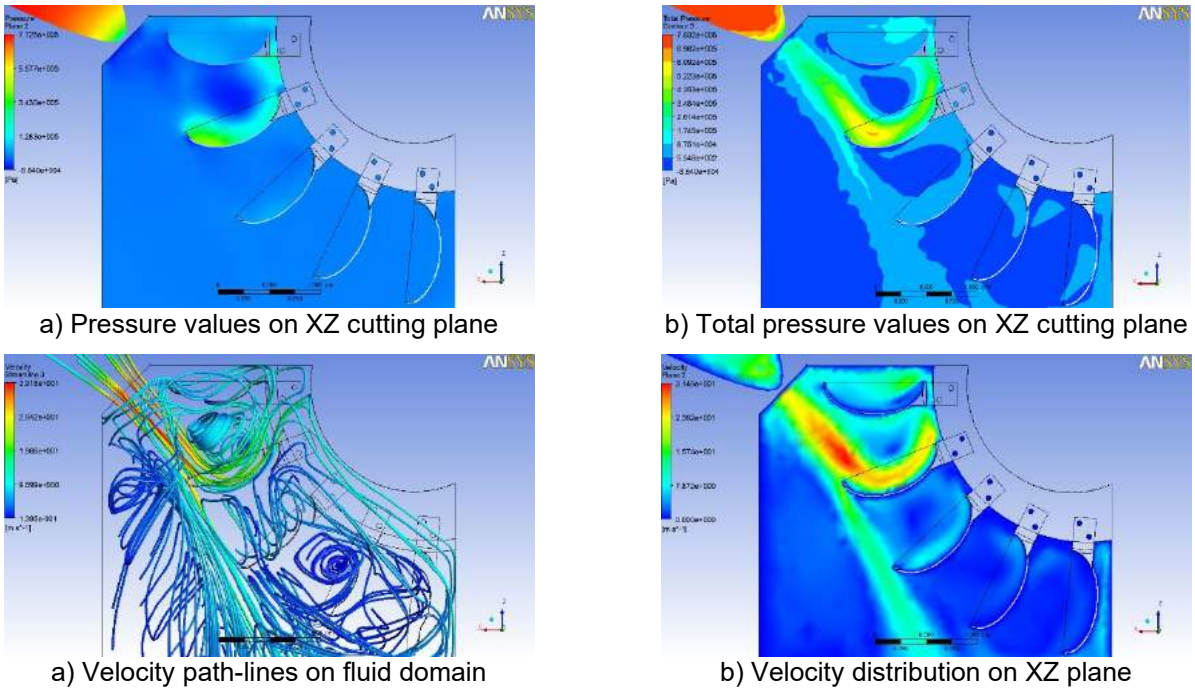

a) Pressure values on XZ cutting plane

b) Total pressure values on XZ cutting plane

a) Velocity path-lines on fluid domain

b) Velocity distribution on XZ plane

Fig. 4. Results obtained from water flow analysis on virtual model

Based on the obtained results, the main fluid stream flowing through the turbine enclosure can be identified.
Are highlighted the recorded values for water pressure and velocity starting from the fluid region inlet area and up to the contact with the turbine blade, determining the appearance of the hydrostatic forces at the level of the blade surface.
The resultant hydrostatic forces are acting for the blade forced displacement enabling the rotational movement of the turbine rotor.
The continuous water circulation ensured through the optimum dosage realized by the injector have results in a continuous action on the rotor blades which by successive modification of the position provide the possibility of taking over the hydraulic flow in a continuous cycle thus ensuring the rotor rotational movement with a certain velocity.

Table 3: The result values recorded at the fluid region for velocity and total pressure

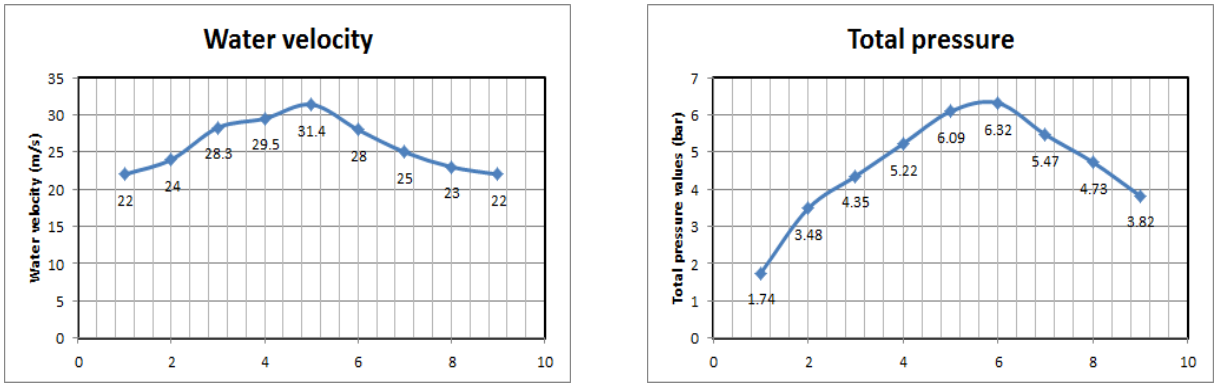

The specific values recorded at the fluid region level for water velocity and total pressure are presented in table 3.
Water velocity and total pressure are increasing from the inlet region up to rotor propeller at maximum values.
The specific values recorded determine the occurrence of the hydrostatic pressure forces whose tangential result has the role of pressing the blade in the downward vertical direction so that the movement conditions of the turbine rotor are fulfilled.

4. Conclusion

The methods of capturing the water courses energy have been developed and improved over time, so that at present it represents a significant percentage in the total energy produced in the favorable areas that benefit from water courses with significant flow rate values and an optimum flow difference level.
Several turbine constructive types have been designed and used over time in water-flow plants all being able to retrieve and transform the flowing water energy into mechanical energy of the rotating shaft.
A constructive version of PELTON turbine has been presented in this paper. Represents a turbine model with large diameter rotor with blades for which an overall virtual model assembly was developed and analyzed from the water flow point of view in order to highlight the flow pattern inside the rotor enclosure and the values obtained for water velocity, pressure and water stream path-lines. Thus, specific values are obtained for the water velocity and pressure characteristic for the flow energy required for the rotational movement of the turbine rotor, with a certain speed value.
It should be emphasized that the PELTON turbine types are used mainly in the case of low water flow rates and high fall heights ensuring a high operating efficiency of over 90%.
An optimum rotor operation efficiency can be obtained by adjusting the constructive parameters of the rotor blades so that the radial component of the water velocity is acquired at minimum values.

References

[1] Kiselev, P.G., and S. Hancu. *Guide for hydraulic calculations / Indreptar pentru calcule hidraulice*. Bucharest, Technical Publishing House, 1988.
[2] Axinti, G., and A.S. Axinti. *Hydraulic and pneumatic drives - Components and systems; functions and characteristics / Actionari hidraulice si pneumatice – Componente si sisteme; functii si caracteristici*. Chisinau, Tehnica-Info Publishing House, 2008.
[3] Vasilescu, Al.A. *Fluid Mechanics / Mecanica Fluidelor*. Galati, Ministry of Education, University of Galati, 1979.
[4] Kim, Jeong-Won, Inchan Jo, Joo Hoon Park, and Youhwan Shin. "Theoretical method of selecting number of buckets for the design and verification of a Pelton turbine." *Journal of Hydraulic Research* 55, no. 5 (2017): 695-705.
[5] Thake, Jeremy. *The micro-hydro Pelton turbine manual*. Warwickshire, UK, Practical Action Publishing, 2000, 136-142.
[6] Scurtu, I.C., C. Clinci, and A. Popa. "Water interference effect on ship due to square shaped object shielding." *IOP Conference Series: Earth and Environmental Science* 172, no. 1 (2018): 012030 .
[7] Popa, A., and I.C. Scurtu. "CFD Results On Propeller Analysis." *"Mircea cel Batran" Naval Academy Scientific Bulletin* 20, no. 2 (2017): 124-131.
[8] Eisenring, M. *Micro Pelton turbines*. SKAT, 1991.
[9] Perrig, Al., F. Avellan, J.-L. Kueny, and E. Parkinson. "Flow in a Pelton turbine bucket: numerical and experimental investigations." *Journal of Fluids Engineering* 128, no. 2 (2006): 350-358.
[10] Zoppe, B., C. Pellone, T. Maître, and P. Leroy. "Flow analysis inside a Pelton turbine bucket." *Journal of Turbomachinery* 128, no. 3 (2006): 500-511.
[11] Jošt, D., P. Mežnar, and A. Lipej. "Numerical prediction of Pelton turbine efficiency." *IOP conference series: Earth and Environmental Science* 12, no. 1 (2010): 012080.
[12] Perrig, Al. *Hydrodynamics of the free surface flow in Pelton turbine buckets*. Doctoral Thesis. École Polytechnique Fédérale de Lausanne, 2007.
[13] Scheaua, F.D. "Design Details of a Turbine Model Used for Energy Conversion in Low Flow Rate Water Streams." *Hidraulica Magazine*, no. 2 (June 2018): 29-32.

Using the Fractional Derivative of Grundal Letnikov to Approximate the Profile of a Rectangular Channel

Dra. **Maritza Liliana ARGANIS JUÁREZ**[1*], M.Eng. **Margarita PRECIADO JIMÉNEZ**[2], B.S. Student **Carlos SANTAMARÍA DÍAZ**[3], Dr. **José Luis HERRERA ALANÍS**[4], Dr. **José Luis ARAGÓN HERNÁNDEZ**[5], M.A. Eng. **Jesús Javier CORTÉS ROSAS**[5], M.A.Eng. **Miguel Eduardo GONZÁLEZ CÁRDENAS**[5], M.A. Eng. **Víctor Damián PINILLA MORÁN**[5], Eng. **Alfonso SALAZAR MORENO**[5]

[1] Universidad Nacional Autónoma de México. Instituto de Ingeniería, Av. Universidad 3000 Ciudad Universitaria Edificio 17 Cub.328. Coyoacán CDMX México 04510

[2] Universidad Nacional Autónoma de México. Facultad de Ciencias, Av. Universidad 3000 Ciudad Universitaria Coyoacán CDMX México 04510

[3] Instituto Mexicano de Tecnología del Agua. Blvd. Paseo Cuauhnáhuac 8532, Progreso, 62550 Jiutepec, Mor México

[4] Sistema de Aguas de la Ciudad de México. Calle Nezahualcóyotl Colonia Centro (Área 8), Cuauhtémoc, Ciudad de México. Edificio 109, Piso 4CDMX. 06080

[5] Universidad Nacional Autónoma de México. Facultad de Ingeniería, Av. Universidad 3000 Ciudad Universitaria Edificio 17 Cub.328. Coyoacán CDMX México 04510

* MArganisJ@iingen.unam.mx

Abstract: *A two-term numerical scheme was used from the fractional derivative Grundal Letnikov, considering order a means to find the M-type profile of the water of a rectangular channel. Factors were used that associate the one-half derivative with the one-order derivative as a function of the chain x. The factors obtained from considering polynomial functions of degree 3 allowed to obtain better approximations to the flow profile at some points far from the critical depth.*

Keywords: *Derivative of Grundal Letnikov, gradually varied flow, rectangular channel, fractional calculus*

1. Introduction

The fractional calculus [1] applied in mechanical, physics and engineering problems [2,3,4,5], recently in science health [6]; is a useful and relatively simple tool when combined with numerical analysis [7], in the field of physics fractional calculus has begun to be used to solve diffusive equation problems [8,9]. [10] present factors that relate the behavior of the fractional derivative one-half with the derivative of order one, when simple polynomial functions are used. In this study, the equations that relate the proportion factor of the one-half derivative with the one-order derivative were obtained, as a function of the independent variable x, said factor was used in the result that gave a finite difference scheme fractional based on the fractional derivative of Grundal Letnikov, it was used to solve the equation of gradually varied flow applied to a rectangular laboratory channel, of which measurements and calculations were carried out with the direct passage method. The results obtained are presented by assuming that the derivative one means allows a better approximation of the variation of the flow profile, with respect to the chain x. The previous assumption was only fulfilled in some points far from the control section for the estimation of the M-type profile that the rectangular channel used has.

2. Methodology

According to [8], the first derivative y'(x) of a continuous function y (x) can be approximated with the concept of backward finite differences as

$$y'(x) = \frac{y(x)-y(x-\Delta x)}{\Delta x} \quad (1)$$

If the function is derived again using finite differences backwards, we obtain:

$$y'(x) = \frac{y(x)-2y(x-\Delta x)+y(x-2\Delta x)}{\Delta x^2} \quad (2)$$

By mathematical induction the numerical derivative of order n proposed by [8] results:

$$y^n(x) = \sum_{r=0}^{n}(-1)^r \binom{n}{r} y(x-\Delta x) \quad (3)$$

Where

$$\binom{n}{r} = \frac{n(n-1)(n-2)..(n-r+1)}{r!} \quad (4)$$

[8] proposes that if n is not an integer, the form of the fractional derivative of Grundal Letnikov in finite differences results:

$$y^\gamma(x) = \frac{1}{(\Delta t)^\gamma}\sum_{r=0}^{n}(-1)^r \binom{\gamma}{r} y(x-\Delta x) \quad (5)$$

In the previous equation γ is the order of the fractional derivative that can be a real number. The function is considered defined in a closed interval of values [x_i, x], where $n\Delta x = x-x_i$.

2.1 Fractional finite difference scheme of a term based on the derivative of Grundal Letnikov

Taking into account equation (5), if the value of the function y(i-1) is known and it is desired to estimate its value at an instant y(i), knowing the derived function $f(x,y) = y^\gamma(x)$, with n=1 a scheme similar to Euler's method is obtained, but for fractional finite differences:

$$y(i) = \binom{\gamma}{1} y(i-1) + (\Delta x)^\gamma f(x_i, y_i), i = 2,3,\dots m \quad (6)$$

In this study a value of γ=1/2 was considered.

2.2 Derivative factor that associates one-half with derivative of order one as a function of x

According to [10] factor $f=y^{1/2}/y'$ was calculated for each point of 2 and 3 degrees polynomials, and it was drawn against the independent variable x, with which following equations were found:

$$f1 = 0.0243x^2 + 0.9795x - 1.9499 \quad (7)$$

$$f2 = -0.001 + 0.116x + 0.7474 \quad (8)$$

Where x is an independent variable x, f1 and f2 are factors that relate mean derivative with order 1 derivative considering 2 and 3 degrees' polynomials, respectively.

2.3 Gradually varying flow equation

Gradually varied flow equation for a prismatic channel is given by [11]:

$$y'(x) = \frac{(S_0-S_f)}{1-Fr^2} \quad (9)$$

Where S_0 is dimensionless channel slope bottom, S_f is dimensionless friction slope (in this paper its average value was considered between two successive points and using Manning equation), F_r is Froude number, (also for calculation was taken average value between two successive points).

3. Application and results

Equation 6 scheme was applied considering γ = 1/2 and Δx = 0.5 m, to obtain water profile (Figure 1) of a hydraulics laboratory rectangular channel from Faculty of Engineering, UNAM, with geometric data and hydraulic conditions given in Table 1. Starting from critical condition y_c = 0.12 m, to normal condition y_n = 0.192, slope S_0 = 0.00128 and critical slope S_c = 0.0046, channel profile type was estimated from type M because $y_n > y_c$ and $S_0 < S_c$. For calculation purposes, an initial chain xi = 10 m was used. One-half derivative f (xi, yi) using t equation scheme of 6 was obtained

by multiplying order 1 derivative from equation 9 multiplied by f_1 factor or f2 for each interest point from equations 7 and 8.

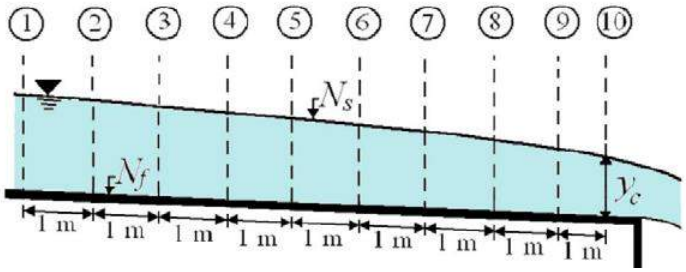

Fig. 1. Water profile to be calculated. Rectangular Chanel (Source: [12])

Table 1. Experimental rectangular channel data

Variable	Value	Units
Q	0.0192	m^3/s
n	0.009	
S0	0.00128	
b	0.2	m
g	9.81	m/s^2

In Table 2 we show x chaining reported at each meter by laboratory measurements were made; the data of the depth measured in laboratory y_{lab}, calculated data with direct step method y_{step}, and depths estimated values with scheme and factors f_1 and f_2, represented by yf_1, 0.5y f_2 and 0.25 f_2; equation 6 the latter correspond to a Δ_x = 0.5m and Δ_x = 0.25 m, respectively. Figure 2 shows graphical comparison of these results.

Table 2. Measured and calculated profile Results from rectangular channel

x Section, m	ylab, m	ystep	y_{f1}, m	$0.5y_{f2}$,m	$0.25y_{f2}$,m	%errorstep	%errorf1	%error0.5f_2	%error0.5f_2
10	0.109	0.109	0.116	0.116	0.116	0.00	6.4	6.4	6.4
9	0.13	0.137	3.069	0.488	0.08054287	5.38	2260.5	275.3	38.0
8	0.133	0.137	2.125	0.014	0.12029287	3.01	1497.8	89.3	9.6
7	0.139	0.143	1.161	1.008	0.13054361	2.88	735.0	625.3	6.1
6	0.141	0.145	0.034	0.729	0.20255578	2.84	75.7	416.8	43.7
5	0.146	0.149	0.878	0.423	0.12024771	2.05	501.0	189.7	17.6
4	0.15	0.152	0.177	0.049	2.35906407	1.33	18.2	67.6	1472.7
3	0.153	0.155	0.040	0.049	0.14462849	1.31	73.9	68.0	5.5
2	0.155	0.157	0.158	0.034	0.13669956	1.29	1.9	78.3	11.8
1	0.162	0.162	0.220	0.070	43.8272592	0.00	36.1	56.8	26953.9

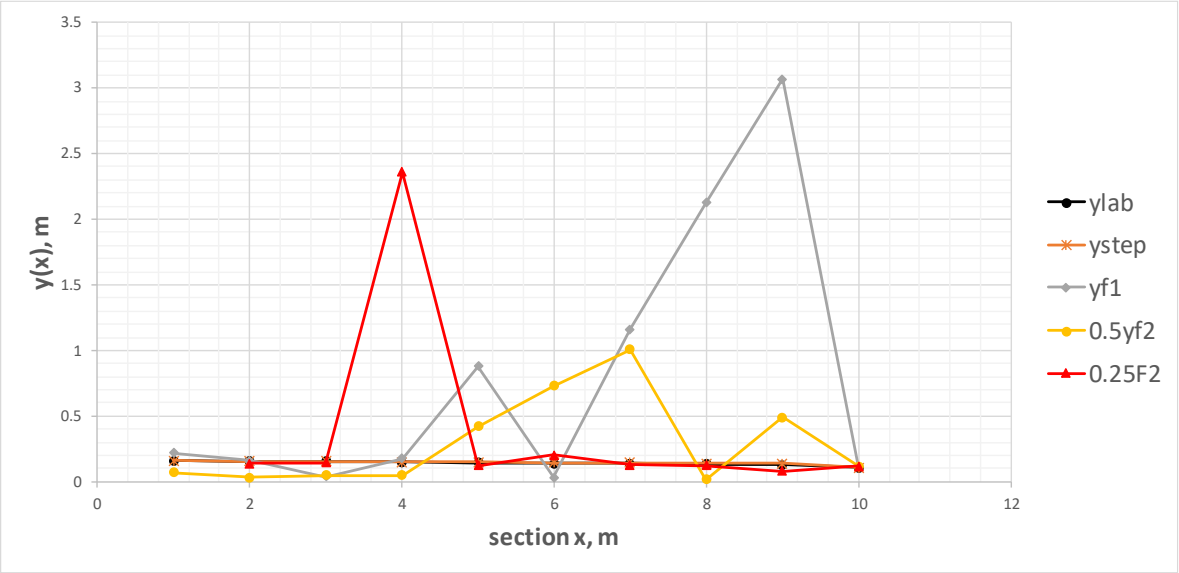

Fig. 2. Comparison between measured and calculated depths. Rectangular channel

From Table 2 and Figure 2 it is observed that the assumption of a behavior of the variation of the depth considering the derivative a mean and under the assumption of a polynomial behavior of degree 2 (factor f_1) of the depth and with respect to the chain x gives high errors, although smaller compared to the assumption of a third degree polynomial behavior (factor f_2); but on average the behavior of $_{0.5}y_{f2}$ gave a behavior with less oscillations than $_{yf1.}$ Due to the above, the $_{025}y_{f2}$ calculation was made, which was observed a little more attached to the behavior of the flow in the sections, except in sections 4 and 1 (this last data was not drawn since the figure was deformed a lot when the vertical scale was expanded). The method of the direct step considering the derivative of order one gave the best answer in this case, with respect to the measured laboratory data. There was only almost coincidence in the depth measured with that calculated in the section x = 2 m, with respect to what the direct passage method gave with what the scheme in fractional finite differences with the factor f_1 gave. Higher oscillations were observed in the case of 0.25 and f_2.

4. Conclusions

Considering hypothesis that M profile flow variation from a rectangular channel with laboratory data, with respect to x position corresponds to a derivative of order ½, was not corroborated in this study using fractional finite difference scheme, although result using lowest error was with the Δx = 0.25 m considered, except in two sections of profile in which scheme gave very high depth values. Oscillations were observed in numerical solution scheme that show new calculations are required with other proposals both order γ fractional derivative and Δx in order to seek a reduction of these oscillations and with it derivative order can best represent flow behavior. Up to this point in this line of research, direct step method and order one consideration derivative report the best numerical response with respect to profile measured at laboratory.

References

[1] Guía-Calderón, Manuel, J. Juan Rosales-García, Rafael Guzmán-Cabrera, Adrián González-Parada, and J. Antonio Álvarez-Jaime. "The differential and integral fractional calculation and its applications"/" El cálculo diferencial e integral fraccionario y sus aplicaciones." *Acta Universitaria* 25, no. 2 (2015): 20-27.doi: 10.15174/au.2015.688.

[2] Rossikhin, Yuriy A, and M.V. Shitikova. "Application of Fractional Calculus for Dynamic Problems of Solid Mechanics: Novel Trends and Recent Results." *Applied Mechanics Reviews ASME* 63, no. 1 (January 2010): 010801.

[3] Lai, Jinxing, Sheng Mao, Junling Qiu, Haobo Fan, Qian Zhang, Zhinan Hu, and Jianxun Chen. "Investigation Progresses and Applications of Fractional Derivative Model in Geotechnical Engineering." *Mathematical Problems in Engineering* 2016 (2016): 9183296. http://dx.doi.org/10.1155/2016/9183296.

[4] Dönmez Demir, D., N. Bildik, and B.G. Sinir. "Application of fractional calculus in the dynamics of beams." *Bound Value Problems* (2012): 135. https://doi.org/10.1186/1687-2770-2012-135.

[5] Su, Ninghu. Fractional *Calculus for Hydrology, Soil Science and Geomechanics*. Flo, USA, Taylor & Francis Group, 2021.

[6] Sweilam, N.H., A.M. Nagy, and L.E. Elfahri. "Nonstandard finite difference scheme for the Fractional order salmonella transmission model." *Journal of Fractional Calculus and Applications* 10, no. 1 (January 2019): 197-212.

[7] Li, Changpin, and Fanhai Zeng. "Finite difference methods for fractional differential equations." *International Journal of Bifurcation and Chaos* 22, no. 4 (2012): 1230014. doi: 10.1142/S0218127412300145.

[8] Quintana Murillo, Joaquín. *Numerical methods in finite differences for the resolution of fractional diffusive equations*/*Métodos numéricos en diferencias finitas para la resolución de ecuaciones difusivas fraccionarias*. Doctoral thesis. Bajadoz, España. Universidad de Extremadura, 2016.

[9] Yang, Xiao-Jun, J.A. Teneiro Machado, Dumitru Baleanu, and Feng Gao. "A new numerical technique for local fractional diffusion equation in fractal heat transfer." *J. Nonlinear Sci. Appl.* 9 (2016): 5621–5628.

[10] Santamaría Díaz, Carlos A., Maritza L. Arganis Juárez, José L. Aragón Hernández, José L. Herrera Alanís, Jesús J. Cortés Rosas, Miguel E. González Cárdenas, Víctor D. Pinilla Morán, and Margarita E. Preciado Jiménez. "Gradually Varied Flow in a Trapezoidal Channel, towards a Hydraulics with Fractional Calculation and Finite Differences." *Hidraulica Magazine,* no.1 (March 2020): 40-46.

[11] Sotelo Avila, Gilberto. *Open Channel Hydraulics/Hidráulica de canales*. México, UNAM, Faculty of Engineering, 2002.

[12] Aragón Hernández, José Luis. *Channel hydraulics practice. Hydraulics Laboratory./Práctica de hidráulica decanales. Laboratorio de Hidráulica*. Faculty of Engineering, UNAM, June, 2016.

2D Numerical Embankment Dam Breach Modeling due to Accidental Highwaters Transitation

Assist.prof.dr.eng. **Marie Alice GHIȚESCU**[1], Assoc.prof.dr.eng. **Gheorghe I. LAZĂR**[2], Assoc.prof.dr.eng. **Albert Titus CONSTANTIN**[3], Lect.dr.eng. **Șerban-Vlad NICOARĂ**[4]

[1] POLITEHNICA University Timişoara, alice.ghitescu@upt.ro

[2,3,4] POLITEHNICA University Timişoara

Abstract: *The safety in operation of the hydrotechnical constructions, in the case of the retention ones from local materials, is a particularly important issue, involving numerous technical, economic and social implications. The phenomenon of failure, an event of utmost importance, is particularly complex both in terms of genesis and development. Leaving aside the exceeding of the resistance capacity of the materials, the partial or total failures of the earth dams and / or boulders, the most numerous due to the accessible materials, can be due to infiltrations through the construction body, generating suffusions and leaks.*
The paper presents a 2D numerical modeling of the liquid flow transit on the Gladna River, Timiș County, Romania, in the Surduc accumulation section, at the appearance of an accidental flood wave.
The reservoir has a maximum volume of over 51 million cubic meters and is created by an embankment dam with a concrete mask with a maximum height of 35 m. The peak flow hydrograph used is similar with the peak flow hydrograph of April 2012 flood event.
The discrete numerical modeling of the transition of flood event is made with the help of the HEC-RAS 5.0.7 software package, assuming a fictitious scenario of accidental overtopping of the embankment dam, which determines a possible failure of this hydraulic structure. The geometric development of the dam breach is estimated with the help of a specific additional facility from the employed software.
Apart from the position of the yield section and its final geometric shape, the numerical simulation estimates the development over time of specific phenomenon's hydraulic parameters - flows, levels, velocities - in all points of the modelled domain.

Keywords: *2D hydraulic modeling, embankment dam, highwaters flow, crest overflow, dam breach, numerical modeling*

1. General considerations

The embankment dam and the online reservoir are situated on River Gladna, tributary of River Bega, located in Poiana Rusca Mountains, in Timiș County. Surduc embankment dam construction was done in two steps, started in 1972, and finalised in 1986, retaining 51 million cubic metres. The main purpose of the reservoir is to provide drinking water, to protect against floods, and for recreation. Having an appreciable water surface of approx. 460ha, is the largest reservoir in Timiș County. The valleys along Gladna River are with steep slopes and river sections' width up to 200 meters. Upstream of Surduc dam, the valley opens suddenly and can reach important widths of approx. 1500 ~ 2000 meters.

The retention embankment dam Surduc (Fig.1) has a maximum height of 35m. The dam has two bottom circular outlets, with a length of 70m and diameter of 1.40m each, with a maximum capacity to discharge of approx. 2x17.0 m^3/s= 34 m^3/s. The spillway channel width is B=6 m, located on the right slope of the valley (Fig.2) the spillway is a concrete structure, free, without any flow control structure. The downstream end of the spillway channel a stilling basin connects with Gladna River.

In order to model the reservoir, the embankment dam and River Gladna reach (reach length of approx. 9235m), a 3D surface was considered (Fig.3). HEC-RAS 5.0.7 [3] software was used to build the numerical model discretisation.

Along the River Gladna study reach, and the adjacent areas, a database was created based on 2823 topographic survey points and 204 profiles (from the channel towards the flood plain).

Fig. 1. Upstream view of Surduc Dam

Fig. 2. Spillway channel and Surduc Dam downstream view

Fig. 3. Plan view of Surduc dam and reservoir – "GOOGLE MAPS" 2019

2. Numerical modeling - general presentation

In order to graphically represent a 3D terrain, Earth Explorer utility is usually used. In the documentation [1], a very useful and easy method of graphical processing of known topographic data from the actual topographic surveys is presented.

This method uses a specialized topographic program of 2D graphical interpolation, in two directions (Ox, Oy), from which a 3D shape surface (shx extensions) can then be generated [1]. In this case, too, a known file from the topographic database was used (it includes approx. 2823 points: x, y and z coordinates - point elevation) resulting in a 3D surface (Fig.4a). This surface is loaded into ArcMAP 9.3 [2], divided by discrete triangular elementary spatial surfaces of a triangular shape and then a final digital form results in the real 3D space of type TIN (Triangulated Irregular Network - (Fig.4b) - here, in addition, several updates were made in the cross sections related to the area downstream of the dam, in the channel and floodplain, excluding some defects due to the small number of cross sections in the downstream area).

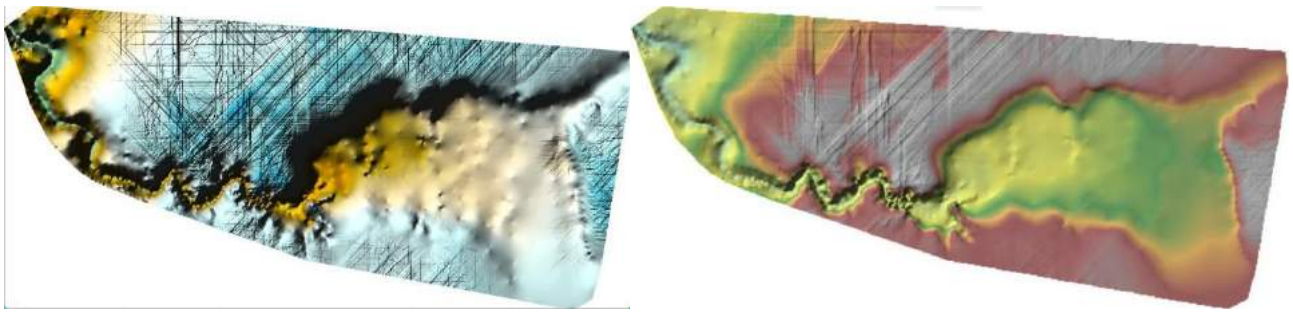

Fig. 4. a. (Left) – 3D topographic plan view of Surduc establishment; b. (right) – 3D updated DTM plan view

In order for this shape to be recognizable by the RAS Mapper module (HEC – RAS 5.0.7 graphics post-processing module), it has been converted to an accessible grid-type file - DTM (Digital Terrain Model) [1, 4, 6]. At the beginning, the geographic coordinate system was chosen, then, this

final form of the natural terrain (extension ".FLT") is loaded with the RAS Mapper module within the HEC – RAS 5.0.7 program. The 3D spatial surface thus obtained is also observed in the graphic presentation in (Fig.5). If more information is desired, respectively the sequential generation procedure, as well as the conversion mode, it is recommended to consult the documentation [6] and / or the presentation work [1].

It can be said that on the "satellite" model of 3D representation, the discretization of the arranged land is almost realistic, even if it is obtained by this easy method of data processing. Although the representation of the discretized model is based on a small number of points (obtained from topographic processing – 2823 points), it still satisfactorily meets most of the requirements in the system arranged by 3D graphic representation. Therefore, the initial terrain model was used (Fig.4b) considering the same project name and then the 2D analysis domain called: surduc_gladna is generated. From the Explorer Window area (Fig.5) the 2D Flow Areas facility was chosen and then draw the discretization contour of the 2D analysis domain and final name Perimeter 1. The grid spacing points in meters (Dx = 50m, Dy = 50m) were chosen, the points associated with the facility are generated (Generate Computations Points) as well as the related tables that include the associated properties for discrete points (Compute Property Points). A grid thickening operation is then performed in the channel and floodplain area, (Fig.5) with new distinct spacing points in meters (Dx = 20m, Dy = 20m)

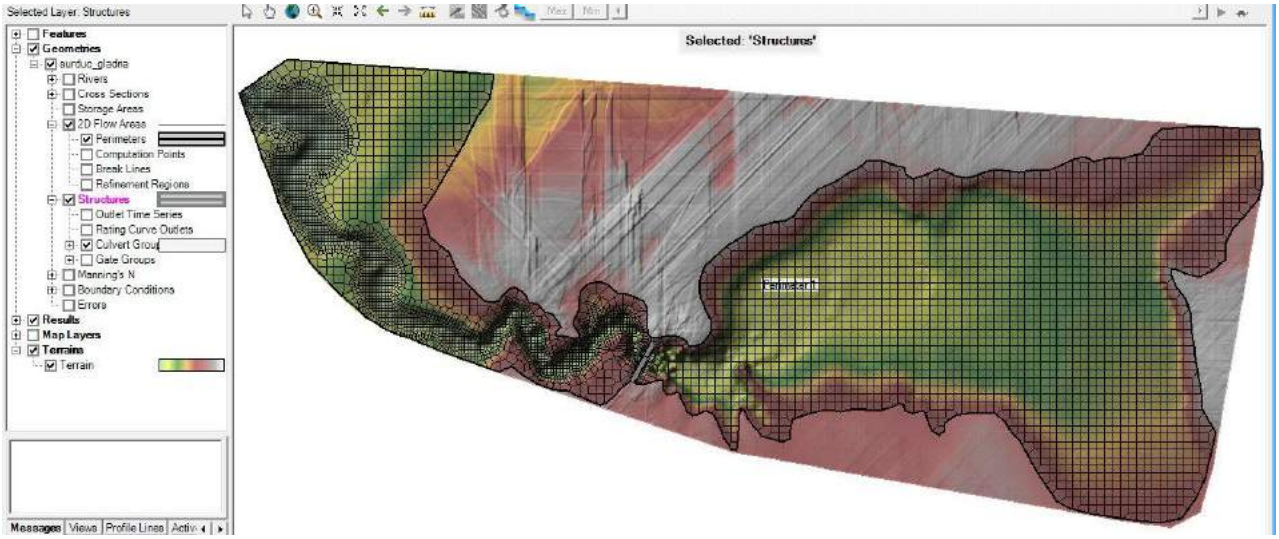

Fig. 5. 3D plan view of grid network representation of the area of interest

Define a grid line in the direction of the dam axis and similarly, a cell thickening operation is performed in the area associated with the dam, choosing additional and distinct spacing points in meters (Dx = 5m, Dy = 5m) as seen in (Fig.6).

The Break Lines have two important and distinct purposes. The first goal is to align the grid cells according to the direction of the dam axis. The second purpose is the most important and necessary at the same time when, it is desired to define a connection structure (it is an internal connection area on a 2D model and represents a subdivision inside the discretized interior of a surface that can be: an area - 2D Area or a polder - SA).

For this reason, a connection structure will be inserted on this line (in the main menu the SA / 2D Area Conn facility is used) which will represent the geometry of the dam.

Therefore, this option defines the connection between the two close areas that include the construction of the Surduc dam, in the discrete 2D numerical model (the present case is 2D Area).

From the upper area Geometric Data choose the facility with which to draw the direction of the connection structure – SA / 2D Area Conn (this direction overlaps the grid break line – Break Lines) and then define the geometric shape of the dam crest using the facility on the left main menu (Fig.7).

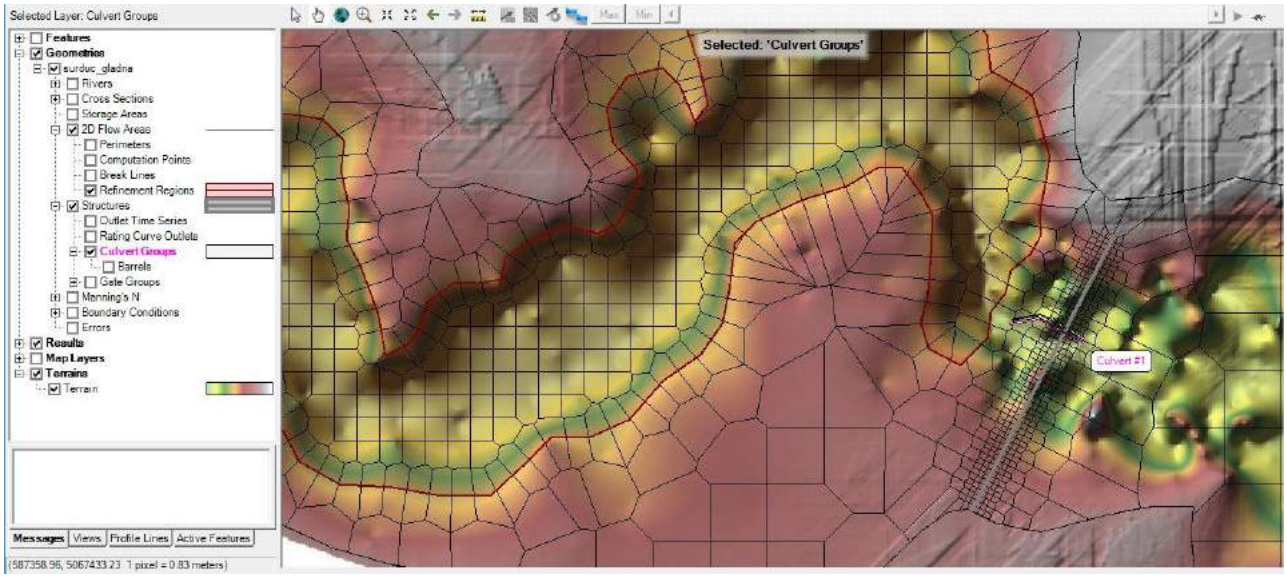

Fig. 6. Detailed model network discretization, at Surduc Embankment Dam and River Gladna

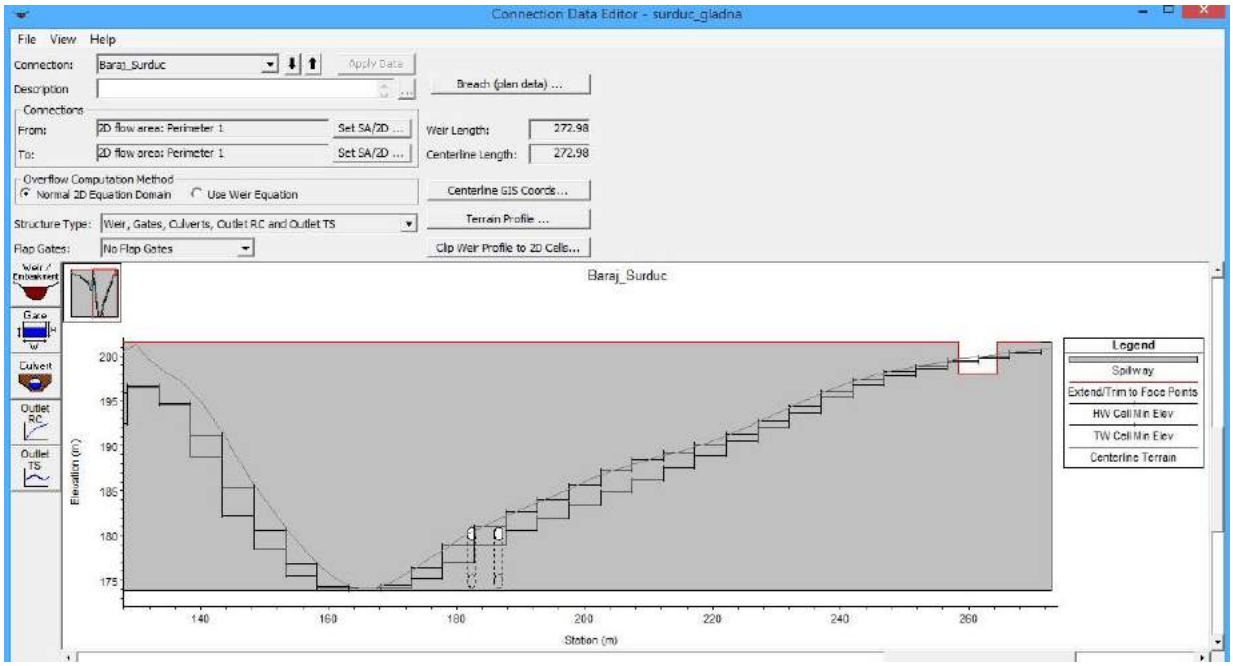

Fig. 7. Geometric elements used to define the connection structure of Surduc Dam on River Gladna

Choose the Culvert tool from the left menu, and enter the two outlet pipes with the available known geometric coordinates (X, Y) of the route definition points, respectively, enter the geometric and hydraulic characteristics of the pipes as seen in figure 8.

When selecting Breach tool (plan data), a graphic window opens (Storage Area Connection Breach Data, figure 9), from which we chose the Parameter Calculator tool. This last tool creates the breach section geometry (calculates width, slope, breach hydrograph and cross section selection method – Froehlich 2008) by user through hydraulic and geometric parameters user specification.

Therefore, after specifying the parameters that define the dam breach (it is also necessary to enter in the left side boxes by the user the selection elements: Center Station 167.5; Final Bottom Elevation 180.5; Breach Weir Coef. 2.6; selection of failure mode Piping; Initial Piping Elevation 185.5; Starting WS 197.5) as well as method selection: Froehlich (2008). The Breach Plot option is

chosen, which will lead to the appearance of the graphical window in which both the chosen and the calculated parameters are presented.

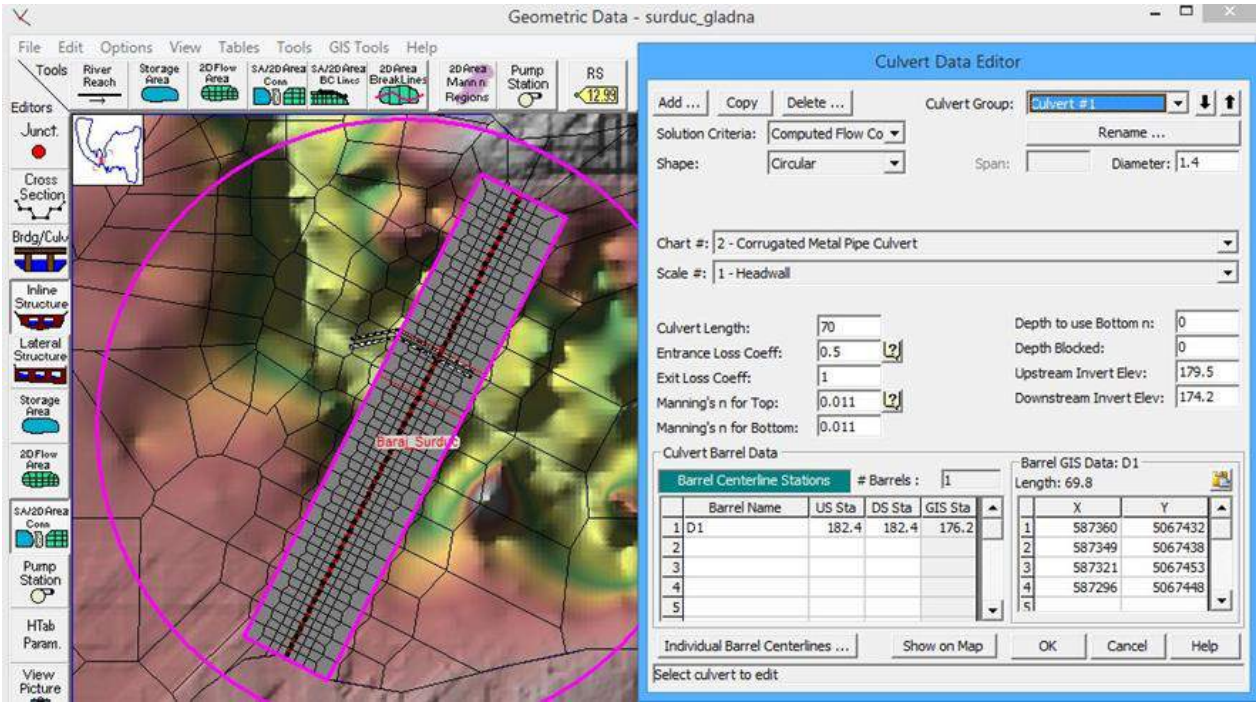

Fig. 8. Geometric elements to define the river reach and the hydraulic and geometric bottom outlet parameters

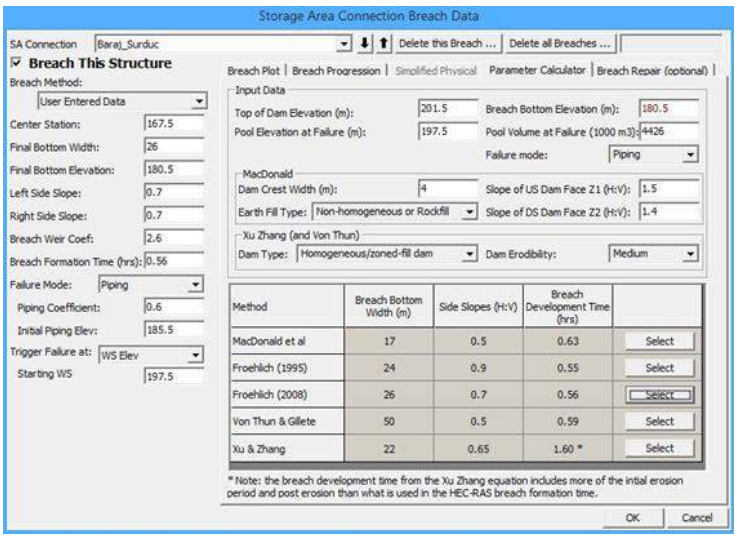

Fig. 9. Dam breach computation section and selected parameters

These parameters define the geometric shape and position of the yield section as seen in the graphical representation in Fig. 10.

3. Initial and boundary conditions

With the selection tool, two sections were defined for roughness coefficient Manning's n (downstream of the dam) comprising some discrete cells to which are attached the new numerical values appreciated for the Manning roughness coefficients (left floodplain: n = 0.075 and right floodplain: n = 0.082), as can be seen in the graphical representation in (Fig.11).

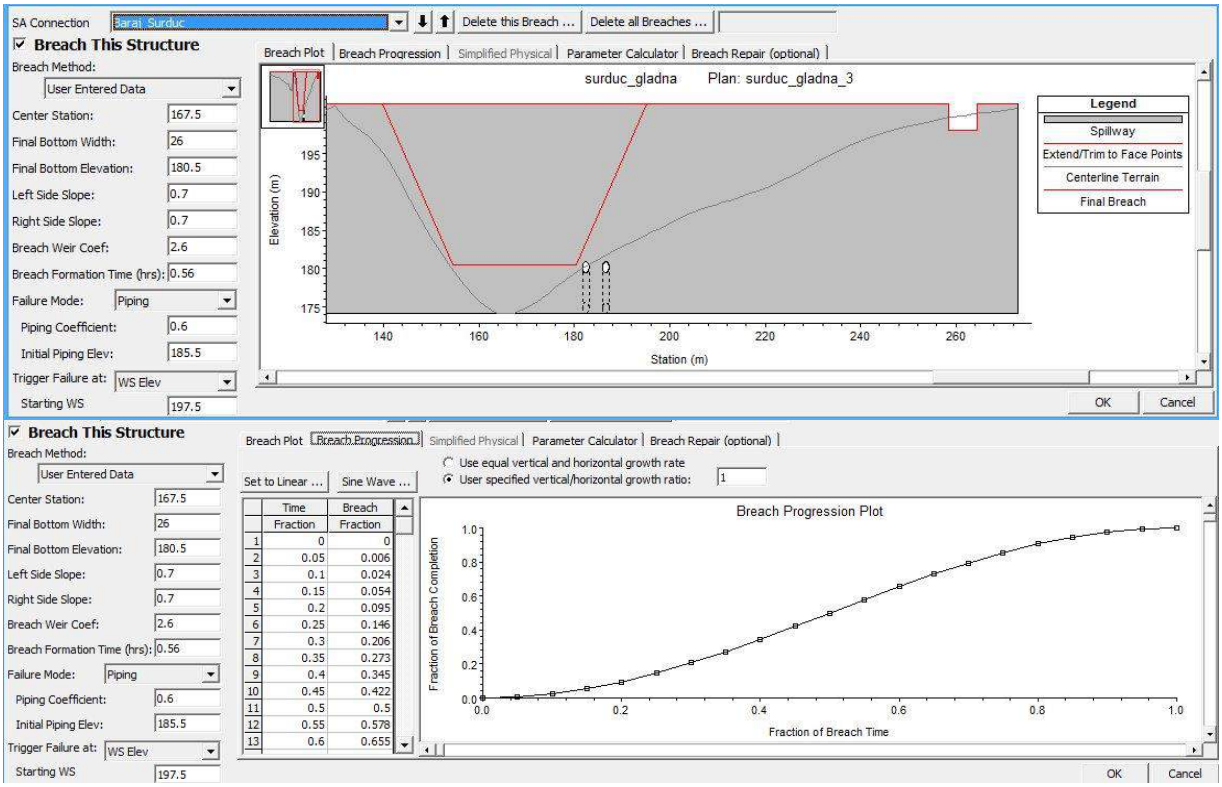

Fig. 10. Dam breach parameters, Surduc Embankment Dam

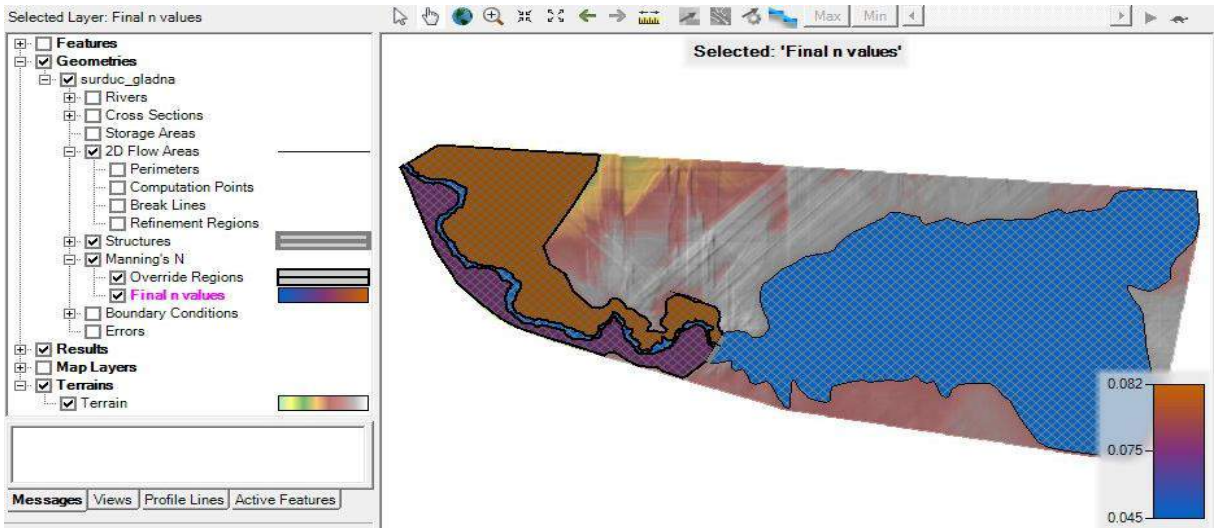

Fig. 11. Manning's n roughness coefficients distribution

The 2D numeric model requires the definition of the boundary conditions from the main menu in Geometric Data using the facile line type edge condition (BC Line) and therefore the option SA / 2D Area BC Lines (Fig.12). In the case of this 2D domain, two routes have been defined: a route in the upstream area BC_S2D_11, in which the flood hydrograph with the energy slope of the water is introduced and a route in the downstream area, respectively, BC_S2D_22, on which the hydrodynamic slope of the water is introduced downstream.

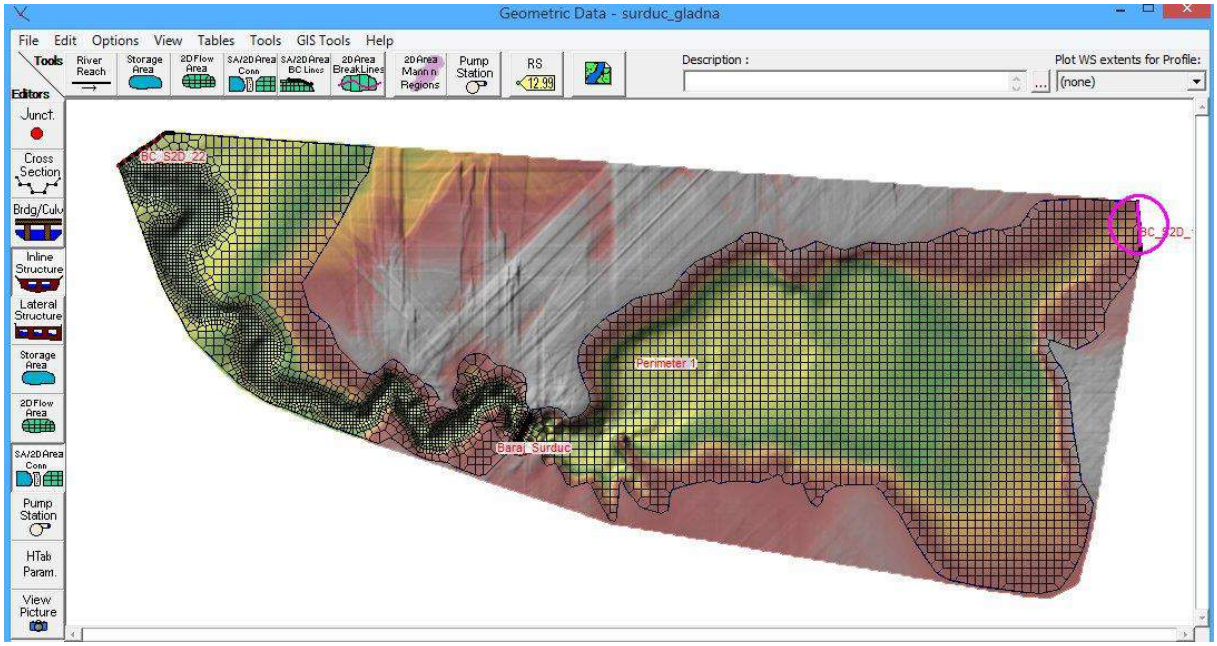

Fig. 12. Model plan view with boundary condition locations

The configuration of the flood hydrograph on the Gladna River associated in numerical modeling reaches the maximum value of 106.72 m^3/ s, and the energy slope in the entrance area is 0.0015205 and is applied on the associated line - BC_S2D_11 (with this energy slope the HEC-RAS 5.0.7 program will final distribution of the input flow on the edge condition line).

The hydrodynamic slope with the numerical value 0.000852 was introduced in the downstream area and is applied on the associated line - BC_S2D_22.

4. Numerical simulation. Results summary

The actual numerical simulation of the transit of flood flows takes place in known time and period, starting on April 15, 2012 at 1.00, until May 1, 2012 at 7.00.

The actual execution analysis is performed, however, in the short time interval, from April 15 at 1.00 to April 17 at 23.00, has a time step Δt = 5 seconds, a mapping interval of 1 minute, and storage of results final is done at an interval of 1 minute.

Following the execution of the numerical simulation, constant or time-varying parameters were obtained, referring to: levels, flow rates and speeds, on each cell of the 2D numerical model. Following graphical post-processing operations, the numerical results are stored in separate files which can then be viewed for each cell or on specific and user-set paths (usually only in the 2D area), using the options in the RAS Mapper area [6].

When presenting the results in 2D graphic form obtained after post-processing, two significant representations – distribution of level surfaces in 2D presentation and model longitudinal outline – are selected at predetermined time moments over April 16, 2012 (figure 13): at 12:23, before the initiation of the piping breach, when the bottom outlet discharge is approx.36m^3/s; at 12:45, when the flow through the breach is already approx.613m^3/s; at 12:51, when the breach is completely formed and the flow through it is approx.4053m^3/s; at 12:58, when the breach discharges approx.3806m^3/s; at 13:25, when the flow by the breach is approx.3069m^3/s and the maximum height of the flood in the Surducu Mic area is reached; at 16:19, when the breach discharge drops to approx.512m^3/s; and at 19:52 and at 23:00 respectively, when the breach discharge diminishes to approx.7.3m^3/s and 5.9m^3/s.

In the graphic representations with predilection, the level surface and the level configuration were chosen in a longitudinal outline that crosses the entire route through the area of the trough.

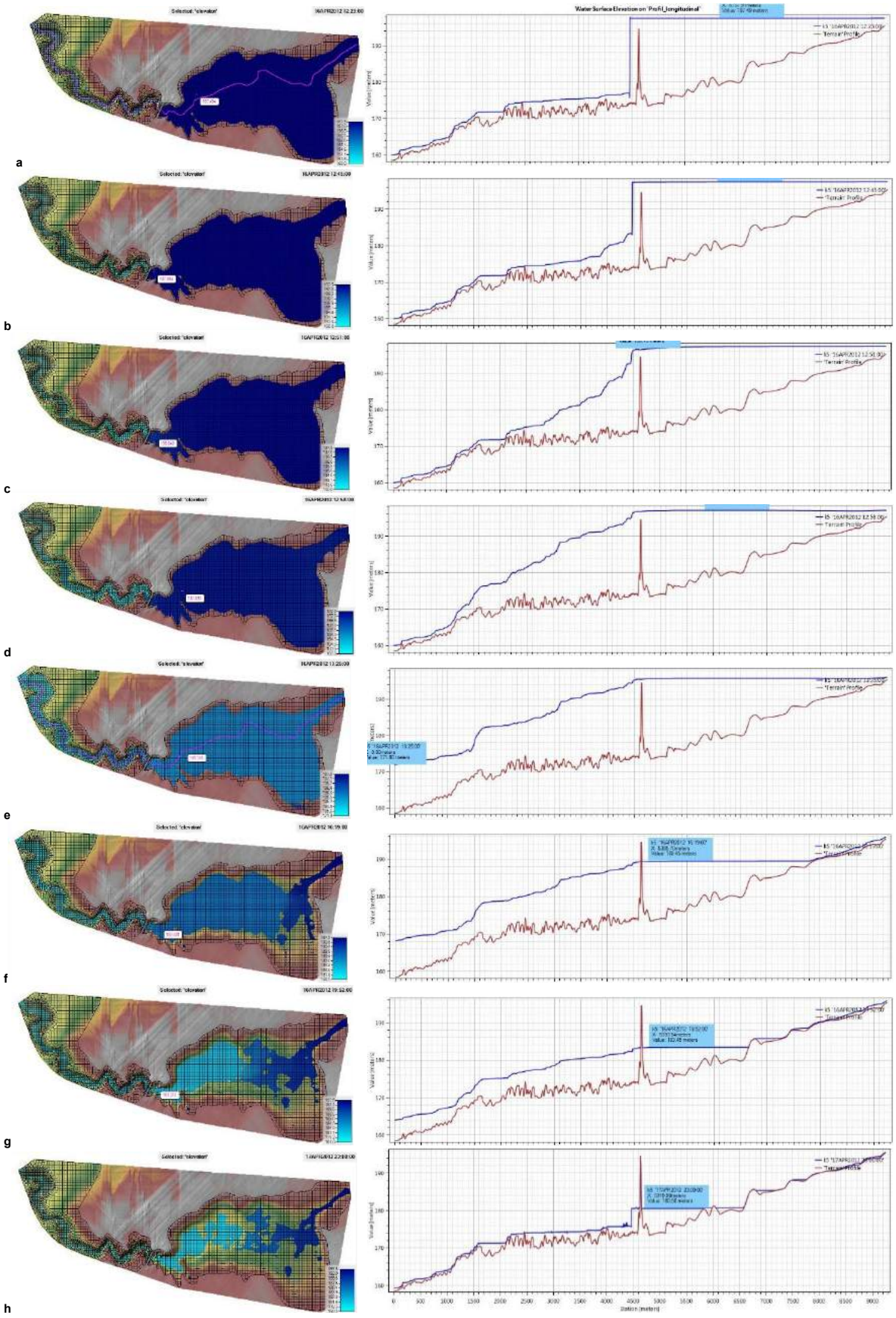

Fig. 13. Distribution of level surfaces in 2D presentation (in maSL) and water surfaces level longitudinal outline with respect to terrain profile, at significant predetermined time moments

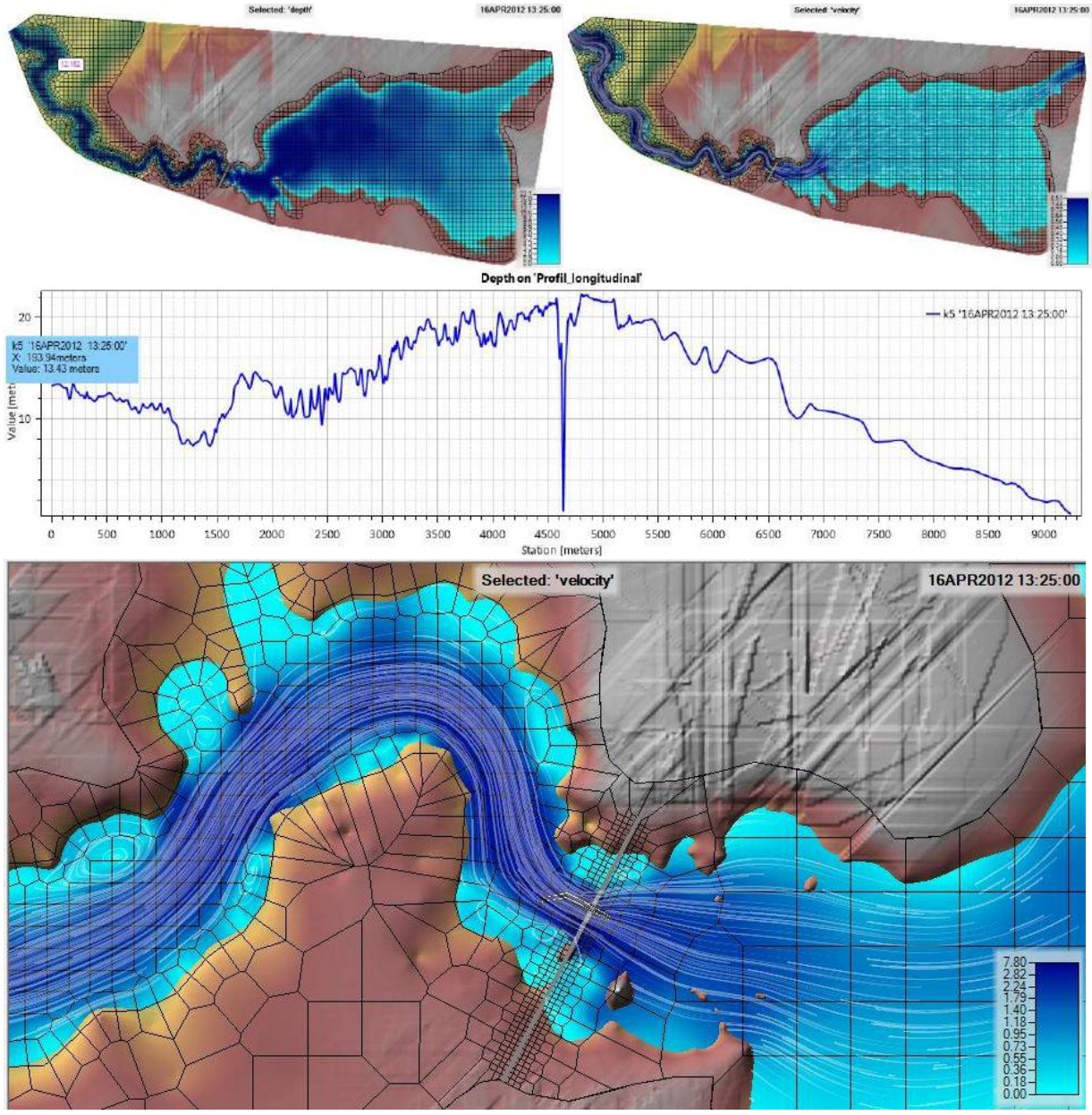

Fig. 14. Surface level distribution in 2D (in maSL), tracing the trajectories of overlapping particles over the speed distribution (in m/s), depth variation in the longitudinal outline (in m), respectively and a detail in the dam area at 13:25 on April 16, 2012, and flow through a gap of approx.3070m^3/s

5. Conclusions and recommendations

Flood wave assimilated with a synthetic allure and known period: April 15 - May 1, 2012, which transits the Gladna River, reaches the maximum recorded flow of 106.72 m^3 / s and corresponds to a probability of exceeding 0.1%. The water level in the accumulation lake recorded at the start time in numerical modeling was at the level of 196.11 maSL. At the appearance of the accidental flood wave that brings a significant volume of water, the level in the accumulation lake increases continuously from the elevation of 196.11 maSL and reaches on April 16, 2012 at 12:23 the elevation of 197.50 maSL (Fig.13a), and the flow through the two bottom emptying reaches the value of approx.36.13 m^3 / s.

It is found on the discrete numerical model that the beginning of the formation of the circular breach is on April 16, 2012 at 12:32, as a location in the reference area associated with the quota of 185.50 maSL, and the flow infiltrated through the breach reaches the value of 0.04 m^3/s. Further

the breach develops and at the current time 16 April 2012 at 12:45, the infiltrated flow reaches the value of 613.15 m^3/s (Fig.13b).

With the time, the breach develops and reaches its final shape on April 16, 2012 at 12:51 pm, when the flow through the breach reaches the maximum value of 4053.37 m^3/s (Fig.13c). The level in the accumulation lake decreases continuously which leads to the decrease of the flow through the breach and thus on April 16, 2012 at 12:58 it reaches the value 3806.11 m^3/s (Fig.13d).

In the graphic presentation from (Fig.13e) it is found that with time passing (April 16, 2012 at 13:25), the water level in the end area of the numerical model has increased and reaches the maximum value in the area of Surducu Mic of approx. 171.80 maSL, and the flow associated with the breach has the value of 3069.83 m^3/s. Similarly, in the graphic presentation from (Fig.13g and h) the situation of flow transit is observed when the level in the accumulation lake reaches the quota of 183.45 maSL, respectively, the quota of 180.58 maSL (quota representing the level in the lake, in the final situation at the expiration of the analysis time). In the graphical representations from (Fig.14) for the analysis time at 13:25 on April 16, 2012, it is observed that the wave height in the longitudinal outline, in the end area, in the trough (at a distance from the end → approx. X: 193.43 m), reaches the maximum value of 13.43 m, and compared to the land level of Surducu Mic, of approx. 7.43 m. It is also observed that the maximum speed selected on the entire discrete numerical model reaches the value of 8.51 m/s, respectively, a value of 7.80 m/s in the graphical presentation updated in detail.

References

[1] Nicoară, Ş.V., Gh.I. Lazăr, and A.T. Constantin. *Alternative study on 1D and 2D numerical model in HEC–RAS 5.05, on the river Timiș, at the confluence with the river Sebeș, in the municipality of Caransebeş, at the transit of an accidental flood wave* / *Studiu alternativ pe model numeric 1D și 2D în HEC–RAS 5.05, pe râul Timiș, la confluența cu râul Sebeș, în municipiul Caransebeş, la tranzitarea unei unde de viitură accidentală*. November 2018.

[2] ***. *HEC–GeoRAS GIS Tools for Support of HEC-RAS using ArcGIS User's Manual, Version 4.3.93*. US Army Corps of Engineers Institute for Water Resources Hydrologic Engineering Center, February 2011.

[3] Brunner, G.W. *HEC–RAS 5.07*. US Army Corps of Engineers, 2019.

[4] ***. *HEC-RAS River Analysis System, Supplemental to HEC- RAS Version 5.0 User's Manual Version 5.0.4.* US Army Corps of Engineers, 2018.

[5] Brunner, G.W. *HEC–RAS 4.1, River Analysis System Hydraulic Reference Manual*. US Army Corps of Engineers, November 2002.

[6] Brunner, G.W. *Combined 1D and 2D Modeling with HEC–RAS. October, vers.5*. US Army Corps of Engineers, 2016.

[7] Kiers, G. *Lifting Terrain in HEC-RAS 5.0*. VIZITERV Consult Kft., Hungary, Copyright © The RAS Solution and Gerrit Kiers 2015.

Biomass Processing from Agricultural Residual Production and Maintenance Operations when Cutting Trees and Vines

PhD Stud. Eng. **Ioan PAVEL**[1], PhD Eng. **Gabriela MATACHE**[1*],
PhD Stud. Eng. **Alexandru-Polifron CHIRIȚĂ**[1], Dipl. Eng. **Alina Iolanda POPESCU**[1],
Cristian DIACONU[2]

[1] Hydraulics and Pneumatics Research Institute INOE 2000-IHP

[2] S.C. TOP SB S.R.L.

* fluidas@fluidas.ro

Abstract: *The article presents aspects related to the processing of biomass from agricultural secondary production, from maintenance operations when cutting trees and vines, and also an original solution of branch chopper with pulling knife through which branch segments with longer length are obtained compared to the classic solutions of segmentation (chopping) of the branches.*

Keywords: *Biomass, agricultural secondary production, choppers, branch segmentation*

1. Introduction

In general, all aspects of human life require the consumption of significant amounts of energy. Thus, in order to ensure normal living conditions in the cold season, significant amounts of heat are needed in order to ensure acceptable temperatures in homes. Also, living in civilized conditions involves the daily preparation, regardless of the season, for each person, of a certain amount of domestic hot water and this is also done by consuming appropriate amounts of heat. In this sense, Romania has a high biomass potential, coming mainly from agricultural (60%) and forest (20%) wastes [1].
The environmental standards of the European Union, as well as the fulfilment of the commitments assumed by Romania in the negotiation process of Chapter 22 of the Community acquis, once our country enters the EU, imposed the alignment with the ecological requirements that require the complete disposal of wastes.
A significant amount of wood wastes results from forestry areas (forestry industry) and wood processing industry (about 3% in the forestry industry sector and 11% in the woodworking industry from processed wood). Wastes resulting in the wood industrialization process, based on the technological sequences that generate them, they are the following:
- Harvesting wood by cutting it (branches, stubs, chips, sawdust)
- Primary wood processing (wood scraps, shells, chips, sawdust)
- Superior wood processing (veneer scrap, sawdust, wood chips, wood powder, solid wood scraps, etc.)
- Finishing of wood products (wood preservatives, residues of reusable substances as solvent, glues, resins, adhesives, dust retained by air filter bags, etc.)
The most representative categories of combustible wood materials are: firewood, tree bark, branches resulted from the forest logging, branches resulted from the tree orchards maintenance, vine ropes, sawdust, wood chips, small pieces of timber and other residues resulted from processing wood. Typically, trees resulted from logging are a high-quality homogeneous biofuel. From an energy point of view, combustible wood materials have an average energy content of between 14 MJ/kg and 19 MJ/kg.
The cuttings in the orchards are made in the non-vegetative period and as a result the average humidity of the cut branches is 30-35%. If we take into account a humidity of 35% of a ton of cuttings, by drying up to an average humidity of 15%, it results in 765 kg of biomass usable for the production of thermal energy. It results that a ton of cuttings has an average energy potential of 11.856 MJ or 3.3 MWhth. From a hectare of intensive orchard annually, on average, about 3000 kg of biomass is cut which has an energy potential of 35.628 GJ/ha·year.

The biomass from the cuttings is transported to the row head where it is chopped with a specialized machine at 10 ... 50 mm and stored in containers with perforated walls for a good air circulation. On average, the bulk density of the wet cut is 250 kg/m^3, which leads to a need of about 12 containers per hectare of orchard. By natural drying or forced ventilation, the biomass reaches an average humidity of 15% and a bulk density of about 200 kg / m^3.
From the published data, for Europe, results an average cost of gathering, chopping and transport for a ton of cuts of about 40 € /t. Taking into account a profit of 20% and VAT it results that a ton of biomass usable for thermal energy production can be sold for about 80 € /t. The specific price for the primary energy of biomass is in the case studied of 5.2 € /GJ or 18.6 € /MWhth, values much lower than those for diesel of 33.22 € /GJ or for LPG of 21.52 € /GJ [2].
In the combustion process, thermal power plants generally generate pollution. The size of the pollution depends on the fuel used to generate the thermal energy on the one hand, as well as on the ways of burning the fuels, on the other hand. Solid fuel in the form of pellets and briquettes that are produced from agricultural residues (straw, corn cobs, corn stalks, residues of soya, rape and tobacco, vine ropes, technological residues from orchards maintenance, etc.), is an ecological fuel and is an efficient alternative to conventional fuels for thermal boilers (natural gas, liquid fuel, coal, firewood, etc.). The major difference from the classic ones is the small size and regular shape of the pellets, which allows their use as fuel for automated heating plants.
The chemical composition of biomass differs greatly depending on the species, but it can be said that plants contain (15-30% in the dry state) lignin ($C_{40}H_{44}O_6$) and carbohydrates (sugars or glucides). The carbohydrate fraction consists of several glucides molecules bound together in long chains or polymers. The two representative categories of carbohydrates are (40-45%) cellulose ($C_6H_{10}O_5$) and (20-35%) hemi-cellulose [3].
The physical characteristics of solid fuels obtained from biomass are the following [4]:
▪ dimensions and shape - influences the handling and combustion technology;
▪ moisture content - influences the storage time, the design of the installation and the power calorific;
▪ calorific value - is the most important property of a fuel that influences the method of obtaining thermal energy and the design of the combustion plant;
▪ bulk density - influences the transport, handling and storage of fuel;
▪ ash content - also an important feature that influences technology combustion, emission of solid particles, handling and use of ash;
▪ granulation - influences the drying and formation of dust;
▪ abrasion resistance - influences segregation and quality change;
▪ ash melting temperature - influences the combustion technology, the safety in operation and the control system of the combustion installation.
The chemical characteristics of solid fuels obtained from biomass are as follows [4]:
▪ C content - important characteristic that influences the calorific value, which must be as high as possible;
▪ O content - important characteristic that influences the calorific value, which must be as high as possible;
▪ H content - important characteristic that influences the calorific value, which must be as high as possible;
▪ N content - influences NOx emissions (toxic);
▪ S content - influences SOx emissions (toxic) and corrosion;
▪ Cl content - influences HCl (toxic) emissions and corrosion;
▪ K content - influences the use of ash, the formation of aerosols, the corrosion of the combustion plant and reduces the melting temperature of the ash;
▪ Na content - influences the formation of aerosols, corrosion of the combustion plant and reduces the melting temperature of the ash;
▪ Mg content - influences the use of ash and the melting temperature of ash;
▪ Ca content - influences the use of ash, the formation of aerosols and increases the melting temperature of ash;
▪ volatile substances content - influences the design of the combustion plant in order to increase its efficiency;

▪ heavy metal content - increases pollutant emissions and reduces the possibilities of using ash

The use of biomass from agricultural secondary production and from periodic pruning of vines and orchards or from the technological process of wood processing has several advantages such as:
• Solves the problem of environmental pollution with sawdust and wood wastes or by burning stubble and plant debris;
• Dry agricultural biomass and energy plants are an inexhaustible resource of raw material;
• The production of pellets and briquettes (ecological, non-polluting products) is undertaken with the application of a technology with a high degree of mechanization, low manufacturing costs and allows obtaining thermal energy with advantageous costs.
• The natural chopping and drying of the branches are a resource of combustible material for heating.
The main potential beneficiaries are small and medium farmers, associations of agricultural landowners, economic agents who carry out activities in the agricultural field and who want to provide part or all of their thermal energy by using their own renewable energy sources, marketing pellets and briquettes in order to ensuring energy independence [5].

2. Branch chopper with pulling knife

Wood is the most widely used solid biofuel. The raw material can have the following shapes: logs, stumps, stems, leaves and needles from the forest, bark, sawdust, firewood and wood chips from the wood industry and wood recovered from construction. They can be used chopped when is possible directly as a fuel, or they can be processed into forms that are easier to transport, store and burn, such as: pellets, briquettes and wood dust.
In most cases of energy conversion of biomass, the potential chemical energy from biomass is converted - directly or after some preparatory biological and / or chemical processes - into heat obtained by combustion. We can say that the main form of energy conversion of biomass is its "generic combustion" and the main primary form of usable energy obtained in this way is heat.
The first operation for the use as an energy source of branches resulting from periodic cuttings in orchards and vineyards is their segmentation (chopping).

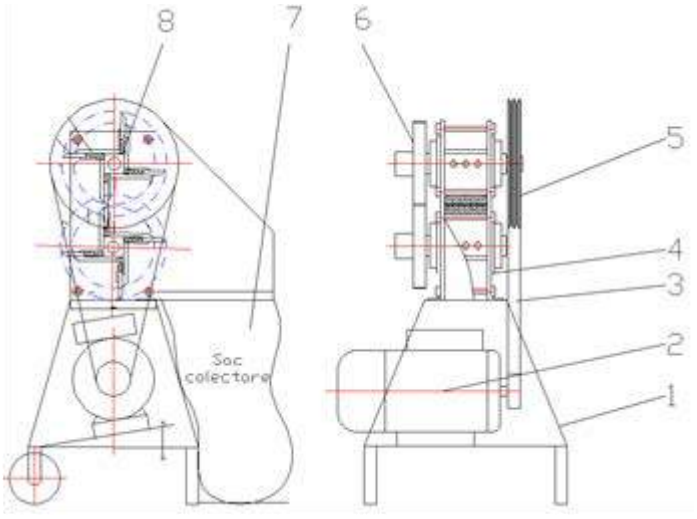

1. Mobile frame
2. Electric engine
3. Transmission belt
4. Frame with bearings
5. Belt wheel
6. Gears
7. Beg collection system
8. Chopping assembly

Fig. 1. Branch chopper with pulling knife

The forest wastes chopper has the role of crushing the forest residues from the field (branches, twigs, etc.), obtaining a roughly segmented wood mass, which will be used either for direct burning in stoves or for crushing to specific granulation for briquetting or pelletizing.
Below is an original solution of chopper with pulling knife [6] used in the industrial or domestic field for branch chopping, vine ropes or other wood materials from agricultural secondary production in order to use them for burning in stoves.

The chopper with pulling knife, fig. 1, consists of a mobile frame with two wheels (1), an electric engine (2) a transmission belt (3) a frame with bearings (4) a belt wheel (5) two gears (6) a bag collection system (7) and two axes (8) with four cutting knives on which are mounted pulling arms that ensure the advance of the chopping material between the cutting sequences resulting in a longer length of the cut segments.

The chopping assembly according to fig. 2 consists of two axles, one drive axle, actuated by the belt wheel and one drive axle led by a gearing with gears with transmission ratio 1. The shaft (5) is bearing at the ends and the central part is square in shape. The cutting knives (4) are screwed to each side of the square. On each cutting knife is mounted with screws a housing (2) in which the pulling arm (1) is seized which slides in the housing against a spring (3). When the chopping material is touched, the pulling arm (1) takes it and pushes it forward until the two cutting knives (4) positioned in the mirror cut the chopping material, with length L2, larger by L3 compared to the version without pulling arm L1 [6].

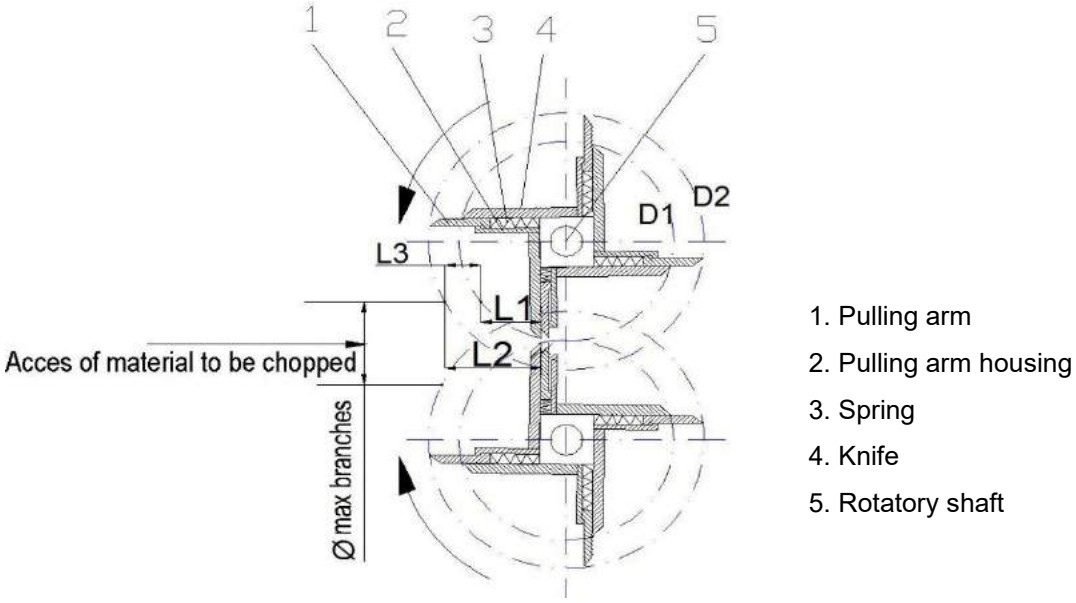

Fig. 2. Chopping assembly

The cutting force varies in very large limits depending on the wood structure, its length and diameter, knots, species, fiber distribution, etc.
To calculate the sizing of the chopping equipment, start from the force required for the cutting process.

$$F = K \cdot p \cdot L \cdot d \quad (1)$$

where:
k - a coefficient that takes into account the angle of the knife and the state of sharpening, the species and the humidity of the wood; indicative values between 0.003 and 0.009;
p - specific resistance to cutting;
The resistance to compression parallel to the fibers has values between 30 - 90 N/mm^2, depending on the essence of the wood.
L, d - length and diameter of the wood to be cut.
For the calculation, values will be chosen slightly above average.

$$F = 0.009 \cdot 70 \cdot 40 \cdot 40$$

$$F = 1008\text{N} = 100.8\ \text{kgf}$$

It is taken into account $F_{max} = 100$ kgf. [7]

3. Conclusions

The need to provide heat in the cold season but also for food preparation has been and remains a very important factor in people's lives. Also, the accessibility of the population to the fuels necessary to ensure the current energy, is becoming more and more important both from a logistical and financial point of view. That is why a first conclusion is that wood biomass in its various forms, which is a cheap source of heating and is found in abundance, can provide the energy needed for a part of the population.
The chopping operation contributes both to the easier handling of biomass and to the creation of a compact finished product for final consumers. In order for the chopping of the branches to be carried out with optimal energy consumption in the specialized literature, there are studies and researches aimed at improving the chopping and shredding equipment, both in terms of design and in terms of fulfilment the requirements of processing of the shredded material after this stage.
The advantages of chopped biomass obtained with the chopper with pulling knife are the following;

• Larger firewood segments are obtained that behave better when burning in stoves;

• Can be handled more easily;

• They can be stored easier and with smaller volumes;

• Wood materials from agricultural secondary production are used;

• It creates a source of ecological energy from renewable sources;

The presented solution of chopper with pulling knife can contribute to the modernization of the equipment in the biomass processing technology chain resulting from periodic cuttings of vines and orchards.

Acknowledgments

This paper has been developed in INOE 2000-IHP, as part of a project co-financed by the European Union through the European Regional Development Fund, under Competitiveness Operational Programme 2014-2020, Priority Axis 1: Research, technological development and innovation (RD&I) to support economic competitiveness and business development, Action 1.2.3 – Partnerships for knowledge transfer, project title: Eco-innovative technologies for recovery of biomass wastes, project acronym: ECOVALDES, SMIS code: 105693-594, Financial agreement no. 129/23.09.2016.

References

[1] Ministry of Economy, Trade and Business Environment - Romania; NL Agency - Netherlands; ENERO – Romania, 2010 – "Master Plan Biomass for Romania / Master Plan Biomasă pentru România", version 2, www.minind.ro/biomasa/ Plan_de_Actiune_pentru_Biomasa.pdf.
[2] Murad, Erol, M. Seiculescu, C. Sima, and G. Haraga. "The use of the energetic potential of the vine ropes / Utilizarea potenţialului energetic al corzilor de viţă." Paper presented at Scientific Communications Conference, INCVV Valea Călugărească, Romania, June 10, 2010.
[3] Ion, V.I., and D.I. Ion. "*Biomass Energy, Theoretical Considerations."/* „Energie din Biomasa, Consideraţii teoretice." *Energie* 7, no. 38 (2006): 14-30.
[4] Danciu, A., et al. *Technology for the recovery of solid agricultural and forestry biomass in order to obtain clean energy and reduce greenhouse gas emissions / Tehnologie pentru valorificarea biomasei solide agricole şi forestiere în vederea obţinerii de energie curată şi a reducerii emisiilor de gaze cu efect de seră*. Research Report, contract no. 21-008 (2008).
[5] Murad, Erol, Gh. Achim, C. Rusănescu. "Energy and ecological recovery of biomass from orchards cuttings / Valorificarea energetică şi ecologică a biomasei tăierilor din livezi." Paper presented at Scientific communications session - ICDIMPH-HORTING, Bucharest, Romania, September 20, 2012.
[6] Patent application no. A / 00408 of 15.07.2020.
[7] "Biodegradable wastes management / Managementul deseurilor biodegradabile" (http://55951_md_2013_06_03_manual.pdf).

Noise and Vibration Sources in Engines (Part I)

Dr. **Sunny NARAYAN**[1*], Dr. **Vipul GUPTA**[2]

[1] Mechanical Engineering Department, Qassim University, Saudi Arabia

[2] Mechanical Engineering Department, Indus University, India

* rarekv@qec.edu.sa

Abstract: *Noise and vibrations from automotive systems form important benchmarks for customers' choice. These have determinant effect on shelf life of engines. Hence it is important to study sources and properties of these noise and vibration sources. The presented work discusses various noise and vibration sources found in an automotive system.*

Keywords: *Acoustics, Noise, Vibration, Automotive*

1. Introduction

Combustion engines are major sources of power for various automotive as well as machinery. About one fifth of the total energy consumption in U.S.A. goes towards operating these engines [1-5]. Figure 1 summarizes Sales of diesel engines-based vehicles.

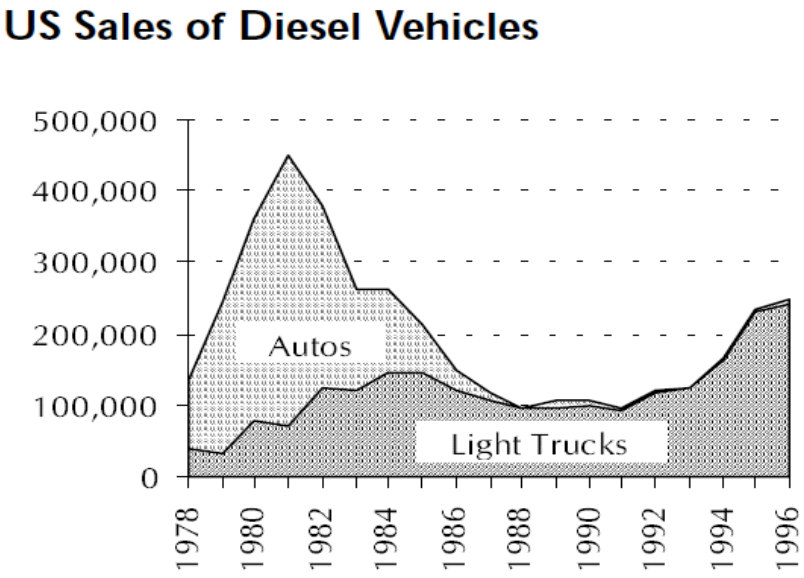

Fig. 1. Sales of various diesel engine-based automobiles

Gasoline engines use spark ignition system for fuel combustion as compared to with diesel engines (that use compression ignition. Diesel engines have higher compression ratios, thus allowing Combustion to take place away from chamber walls. In addition, there are various losses in petrol engines. Hence efficiency of gasoline engines is lesser when compared with diesel engines [6-10]. These factors have led to growing interest of automotive makers in diesel engines. Table no 1 shows the market share of diesel engines based automotive in U.S.A.

Table 1: Major Diesel engine car makers

Automotive Make	Engine Make	Market Share
Hino	Hino	100%
Freightliner	Cummins	62.3%
	Detroit Diesel	37.0%
	Mercedes Benz	0.7%
International	Cummins	7.2%
	Navistar	92.8%
Volvo	Cummins	13.6%
	Volvo	86.4%
Western Star	Cummins	21.2%
	Detroit Diesel	78.8%
Mack	Cummins	6.0%
	Mack	94.0%
Peterbilt	Cummins	65.2%
	PACCAR	34.8%

2. Summary of various sources of noise

Vehicle noise and vibrations can have a bad effect on overall performance of automobiles. These aspects also form important benchmarks for perception of customers while choosing a vehicle as parameters of comfort levels and vehicle reliability. A layout of vehicle consists of several units like power train, chassis, heating, ventilation and air conditioning systems (HVAC) as well as various electronics systems as shown in figure 2,3 [11-20].

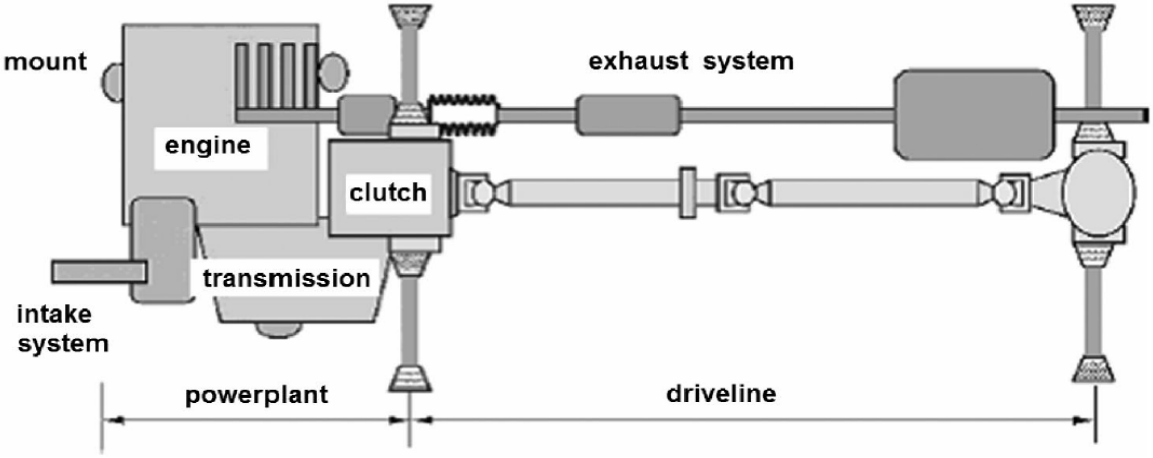

Fig. 2. Powertrain

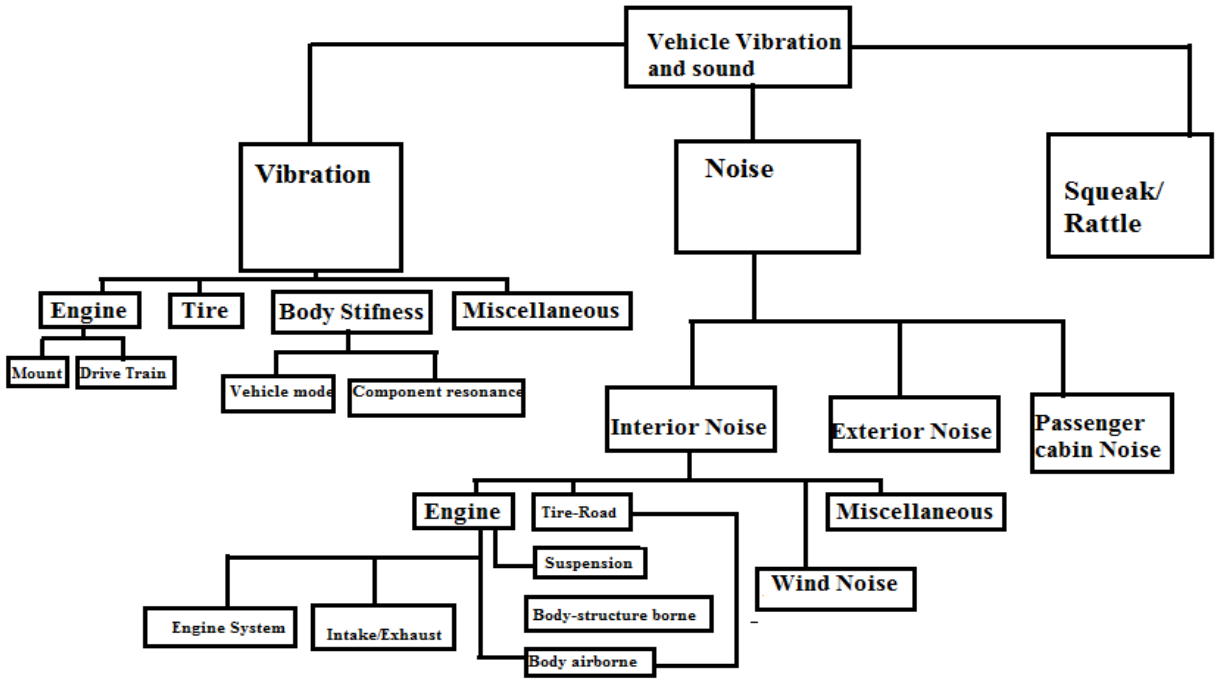

Fig. 3. Noise and vibration sources

Combustion noise is generated as an impulsive pressure wave [20]. The intensity of this noise depends on square of in cylinder pressure developed. Mechanical based noise includes piston motion, bearing misalignment noise, cam and oil pump noise [20]. Flow based noise includes aerodynamic noise due to motion of fan. Table 2 summarizes various sources with their frequency ranges [20].

Table 2: Frequency ranges of various noise sources

Source	Frequency range	Effecting factor
Combustion based Noise	500-8000Hz	In cylinder pressure
Piston Noise	2000-8000Hz	Speed, design
Valve Noise	500-2000Hz	Valve ,Engine
Fan Noise	200-2000Hz	Speed, Blades
Intake Noise	50-5000Hz	Flow
Exhaust Noise	50-5000Hz	Flow
Injection Pump Noise	2000Hz	Pump design
Gear operation noise	4000Hz	Speed, Teeth

3. Quantification

Various methods used include:

a) **lead covering method**- This method includes measurement of noise emissions from engine using selective covering of engine parts with lead.
b) **vibration method**-The sound power level of engine (L_w[A]) can be expressed in terms of acoustic impedance (ρc), surface velocity (u), radiation efficiency (σ) and surface area (S) by following relationship:

$$L_w[A]= 10*\log(\rho c)+10*\log(S)+10*\log(\sigma)+10*\log(u) \quad (1)$$

c) Spectro- filters

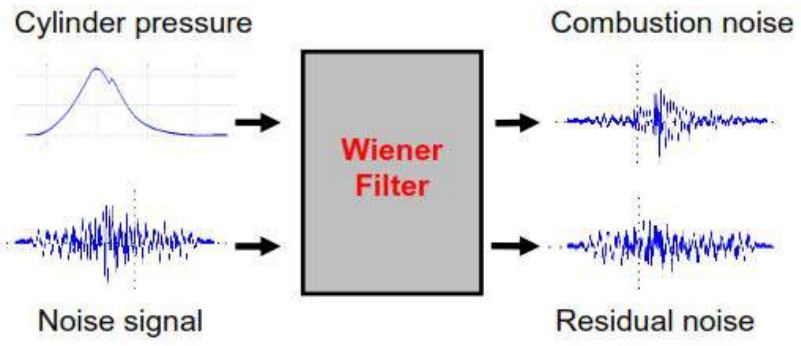

Fig. 4. Application of Wiener filter

Input response P(t) giving a single output response C(t) as seen from figure 4. The impulse response function has been denoted by H(t). The system is corrupted by external component M(t).

$$C(t)=C_1(t)+C_2(t) \quad (2)$$

4. Summary

Car industry had turnover of about 1 Trillion U.S.$ [20]. Attributes such as durability and serviceability require a vehicle to be in service for certain period of time. In the present work summarizes sources, properties and methods of quantification of various sources of noise and vibrations in combustion engines. The discussed methodology can be useful for early fault detection and hence help in effective condition monitoring of an engine.

References

[1] Kaisan, Muhammad Usman, Latifat Ovaiyoza Yusuf, Ibrahim Umar Ibrahim, and Sunny Narayan. "Effects of Propanol and Camphor Blended with Gasoline Fuel on the Performance and Emissions of a Spark Ignition Engine." *ACS Omega* 5, no. 41 (2020): 26454-26462.

[2] Mahroogi, Faisal O., and Sunny Narayan. "A recent review of hybrid automotive systems in Gulf Corporation Council region." *Proceedings of the Institution of Mechanical Engineers, Part D: Journal of Automobile Engineering* 233, no.14 (2019): 3579-3587.

[3] Narayan, S., S. Milojevic, and V. Gupta. "Combustion monitoring in engines using accelerometer signals." *Journal of Vibroengineering* 21, no. 6 (2019): 1552-1563.

[4] Narayan, Sunny, Ali Sulaiman Alsagri, and Vipul Gupta. "The design and analysis of hybrid automotive suspension system." *International Journal of Mechanical and Production Engineering Research and Development* 9, no. 4 (2019): 637-642.

[5] Kaisan, M.U., S. Abubakar, B. Ashok, Dhinesh Balasubramanian, S. Narayan, Ivan Grujic, Nadica Stojanovic. "Comparative analyses of biodiesel produced from jatropha and neem seed oil using a gas chromatography–mass spectroscopy technique." *Biofuels* (2018).

[6] Narayan, Sunny, and Vipul Gupta. "Numerical Analysis of Secondary Motion of Piston Skirt in Engines." *International Journal of Acoustics and Vibration* 23, no. 4 (2018): 1-10.

[7] Mahroogi, Faisal O., S. Narayan, and Vipul Gupta. "Acoustic transfer function in gasoline engines." *International Journal of Vehicle Noise and Vibration* 14, no.3 (2018): 270-280.

[8] Narayan, S. "Analysis of piston slap motion." *International Journal of Applied Mechanics and Engineering* 20, no.2 (2015):445-450.

[9] Narayan, Sunny. "Modeling of Noise Radiated from Engines." SAE Tech paper 2015-01-0107, 2015. Paper presented at The 11th International Conference on Automotive Engineering (ICAE 11), Bangkok, Thailand, March 30 - April 1, 2015.

[10] Narayan, Sunny. "Effects of various parameters on piston secondary motion." SAE Tech paper 2015-01-0079, 2015. Paper presented at 18th Asia Pacific Automotive Engineering Conference (APAC 18), Melbourne, Victoria, Australia, March 10-11, 2015.

[11] Narayan, S. "A review of diesel engine acoustics." *FME Transactions* 42, no.2 (2014): 150-154.

[12] Narayan, S. "Piston Slap Noise in Engines." *International Journal of Applied Engineering Research* 8, no.14 (2013): 1695-1700.
[13] Narayan, S. "Effect of Dwell Time on Noise Radiated from Diesel Engines." *International Journal of applied engineering research* 8, no.11 (2013): 1339-1347.
[14] Narayan, S. "Wavelet analysis of diesel engine noise." *Journal of Engineering and Applied Sciences* 8, no. 8 (2013): 255-259.
[15] Narayan, Sunny, Ali Sulaiman Alsagri, and Vipul Gupta. "The design and analysis of hybrid automotive suspension system." *International Journal of Mechanical and Production Engineering Research and Development* 9, no. 4 (2019): 637-642.
[16] Gupta, Aman, Shubham Sharma, and Sunny Narayan. "Gasoline Engine Technology." Chapter in *Combustion Engines: An Introduction to Their Design, Performance, and Selection*. Hoboken, New Jersey, John Wiley & Sons; Salem, Massachusetts, Scrivener Publishing, 2016: 27-47.
[17] Gupta, Aman, Shubham Sharma, and Sunny Narayan. "Turbocharging." Chapter in *Combustion Engines: An Introduction to Their Design, Performance, and Selection*. Hoboken, New Jersey, John Wiley & Sons; Salem, Massachusetts, Scrivener Publishing, 2016: 69-76.
[18] Gupta, Aman, Shubham Sharma, and Sunny Narayan. "Lubrication Dynamics." Chapter in *Liquid Piston Engines*. Hoboken, New Jersey, John Wiley & Sons; Salem, Massachusetts, Scrivener Publishing, 2017: 91-144.
[19] Gupta, Aman, Shubham Sharma, and Sunny Narayan. "Power Train NVH." Chapter in *Combustion Engines: An Introduction to Their Design, Performance, and Selection*. Hoboken, New Jersey, John Wiley & Sons; Salem, Massachusetts, Scrivener Publishing, 2016: 121-209.
[20] Gupta, Aman, Shubham Sharma, and Sunny Narayan. "Emissions Control by Turbo Charged SI Engines." Chapter in *Liquid Piston Engines*. Hoboken, New Jersey, John Wiley & Sons; Salem, Massachusetts, Scrivener Publishing, 2017: 231-232.

Noise and Vibration Sources in Engines (Part II)

Dr. **Sunny NARAYAN**[1*], Dr. **Vipul GUPTA**[2]

[1] Mechanical engineering department, Qassim University, Saudi Arabia

[2] Mechanical engineering department, Indus University, India

* rarekv@gmail.com

Abstract: *There are several sources of Noise and vibrations in automotive engines which must be controlled for proper working of engines. Combustion and motion-based noise are two important sources of noise. This work focuses on these two aspects of NVH resources. The presented work may provide important aspect of diagnosis methodology of engines.*

Keywords: *Acoustics, Noise, Vibration, Automotive*

1. Introduction

Noise and vibration testing of combustion engine is key in planning of design of automotive systems [1, 2, 3]. Noise emissions from vehicle is of structure borne noise and air borne type. Air based noise due to acoustic path is called air borne noise, whereas structural path based with vibrational energy is structure borne noise. The structural noise has low frequency ranges, whereas the air borne has higher ranges. Various investigations take into account the following aspects:

A. Overall sound pressure levels.
B. Identification of various sources.
C. Analysis of transfer paths and mechanisms.
D. Subjective and objective investigations.

2. Combustion based noise

Combustion based is transferred to surroundings from top surface of cylinder, walls and connecting rod. This depends on the rate of gas pressure rise. Structural attenuation plays a crucial role. Higher stiffness of parts leads to higher values of resonant frequencies.

Knocking is also an important source of noise. Reduction in the ignition delay period may lead to lower values of combustion noise. Higher compression ratios, intake air pressure and exhaust gas recirculation can also prove beneficial to reduce noise [4-10]. AVL noise meter, wavelet-based noise meters and, decomposition of cylinder pressure has proved to be effective techniques to analyze noise [11-13].

3. Piston skirt assembly noise

Tickling noise, piston slapping and rattle noise are three major sources in piston skirt. Piston slapping noise or piston secondary motion noise has a major contribution in diesel engines as shown in figure no 1 [14-18].
Major factors that influence this motion include:
A) Side thrust force-lower speeds, low piston masses and higher crank radius to connecting rod length ratio can reduce this force and hence resulting slapping noise [19].
B) Moments of forces - lower inertia, piston pin and crankshaft offsets, supply of the lubrication may help to reduce piston motion [20].
C)Distance of travel of skirt before striking liner wall- smaller lateral gap between piston skirt-to-bore can help to reduce the lateral motion.
D)Oil damping force -sufficient oil in skirt can help to reduce slapping noise significantly [20].
E) Damping and stiffness of parts–impacts of soft piston skirt causes lesser noise emissions due to

larger deformations.

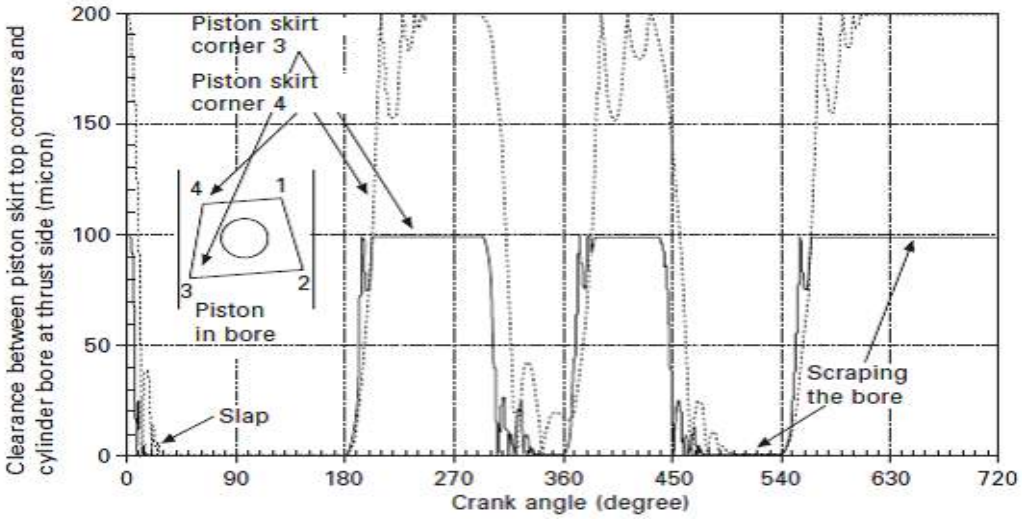

Fig. 1. Piston slapping motion [18]

4. Valve train noise

This type of high frequency noise includes following three major excitation sources:
A) Acceleration of cam- opening and closure of cam causes higher frequency vibrations.
B) Valve impacts - impulsive impacts during operation of valve as well as bouncing noise at higher speeds.
C) Frictional vibrations-This noise is observed at lower speed ranges.

5. Gear train noise

The rattling noise during transmissions is major cause of concern that is caused by non-uniform torque from crank train to drive train causes rattle noise in gears. Clearances, thermal expansions, tooth deflection and tolerances cause whining noise. This noise depends on the number of teeth, size of teeth and magnitude of torsional inputs.

6. Crank train and engine block vibrations

Torsional vibrations in the crank shaft and thin sections of engine block are important sources of noise and vibrations.

7. Flow noise

Lower frequency range intake flow noise is due to fluctuations in flow of charge at ducts and is dependent on valve area and engine speed. Turbocharging noise also forms an important part of aerodynamic noise.

8. Bearing noise

Bearings present in the crankshaft and connecting rod have clearances which are likely to generate as seen in figure no 2 [1-13].

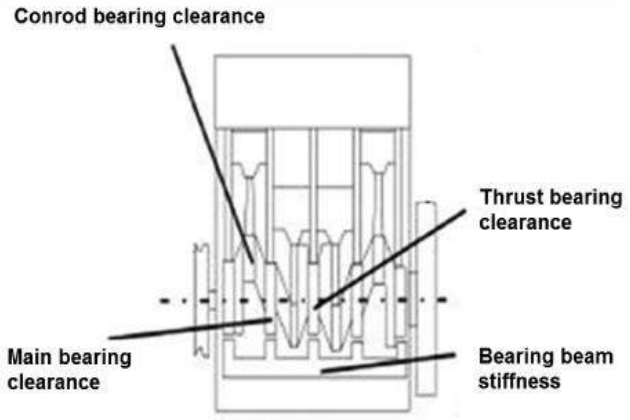

Fig. 2. Sources of Bearing noise [3]

Optimization of clearances, crank shaft damper and flexible flywheel design are effective ways to control this noise.

9. Belt and chain noise

Meshing impact and polygon effect depends on speed and number of meshing teeth as shown in figure no 3 [13-20].

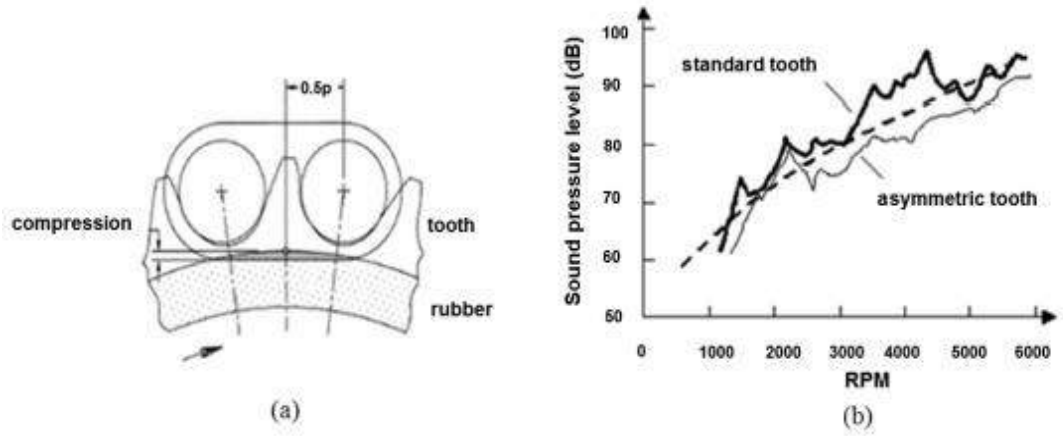

Fig. 3. Timing belt and its noise spectrum [3]

Use of rubber ring sprocket in chain sprocket can help to reduce this noise. Combustion engines also have transmission belts systems that have several modes of vibrations as seen from figure no 4,5.

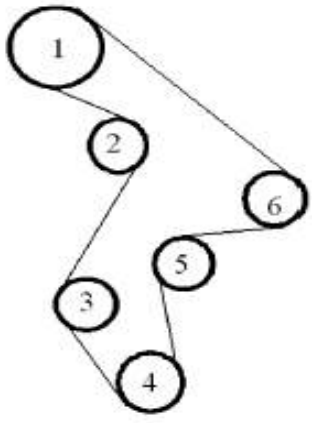

Fig. 4. Timing belt system [3]

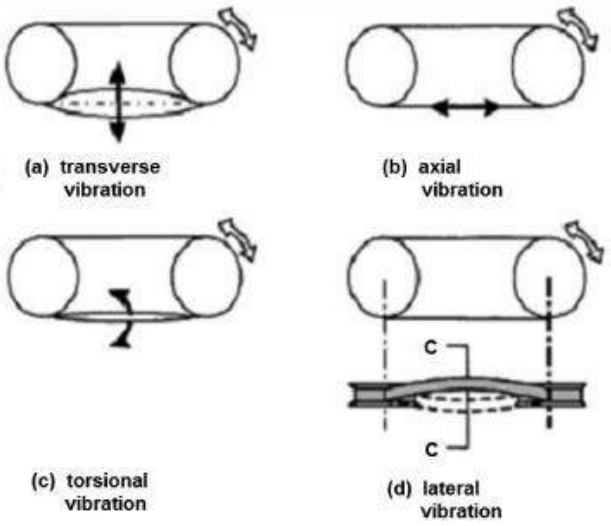

Fig. 5. Timing belt distortions [3]

10. Conclusion

Figure no 6 shows mechanism for generation and transmission of noise sources in an engine.

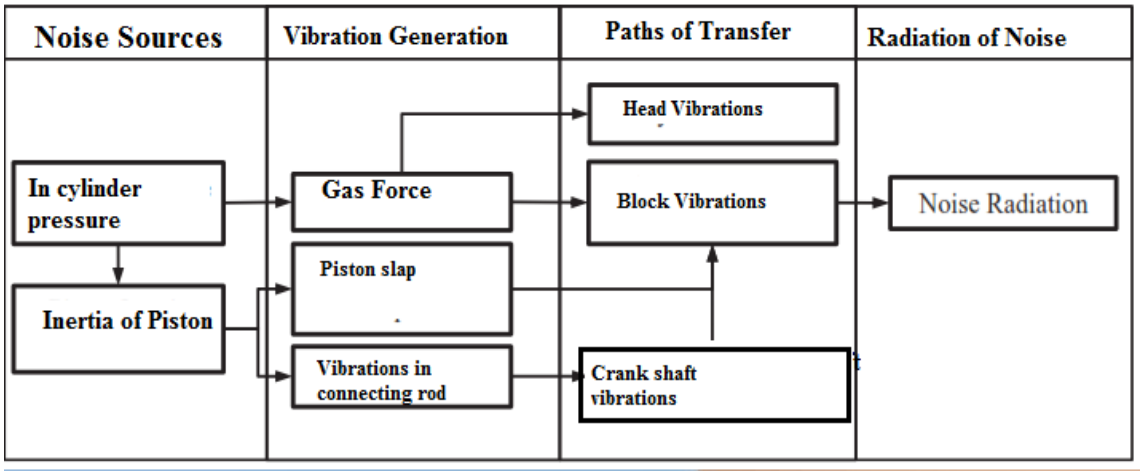

Fig. 6. Mechanism of noise generation [3]

As obvious from the above figures, the combustion-based noise and motion-based noise have major contributions, hence it is necessary to focus on these aspects of engine acoustics.

References

[1] Abubakar, S., F.O. Anafi, M.U. Kaisan, S. Narayan, S. Umar, and U.A. Umar. "Comparative analyses of experimental and simulated performance of a mixed-mode solar dryer." *Proceedings of the Institution of Mechanical Engineers, Part C: Journal of Mechanical Engineering Science* 234, no. 7 (2020): 1393 - 1402.

[2] Kaisan, Muhammad Usman, Latifat Ovaiyoza Yusuf, Ibrahim Umar Ibrahim, Shitu Abubakar, and Sunny Narayan. "Effects of Propanol and Camphor Blended with Gasoline Fuel on the Performance and Emissions of a Spark Ignition Engine." *ACS Omega* 5, no. 41 (2020): 26454-26462.

[3] Sheng, G. *Vehicle Noise, Vibration, and Sound Quality*. Warrendale, Pennsylvania, USA, SAE International, 2012.

[4] Mahroogi, Faisal O., and Sunny Narayan. "A recent review of hybrid automotive systems in Gulf Corporation Council region." *Proceedings of the Institution of Mechanical Engineers, Part D: Journal of Automobile Engineering* 233, no. 14 (2019): 3579 -3587.

[5] Narayan, S., S. Milojevic, and V. Gupta. "Combustion monitoring in engines using accelerometer signals." *Journal of Vibroengineering* 21, no. 6 (2019): 1552 -1563.

[6] Narayan, Sunny, Ali Sulaiman Alsagri, and Vipul Gupta. "The design and analysis of hybrid automotive suspension system." *International Journal of Mechanical and Production Engineering Research and Development* 9, no. 4 (2019): 637-642.
[7] Kaisan, M.U., S. Abubakar, B. Ashok, Dhinesh Balasubramanian, S. Narayan, Ivan Grujic, and Nadica Stojanovic. "Comparative analyses of biodiesel produced from jatropha and neem seed oil using a gas chromatography–mass spectroscopy technique." *Biofuel*s (2018).
[8] Narayan, Sunny, and Vipul Gupta. "Numerical Analysis of Secondary Motion of Piston Skirt in Engines." *International Journal of Acoustics and Vibration* 23, no. 4 (2018): 1-10.
[9] Mahroogi, Faisal O., S. Narayan, and Vipul Gupta. "Acoustic transfer function in gasoline engines." *International Journal of Vehicle Noise and Vibration* 14, no. 3 (2018): 270 - 280.
[10] Narayan, S., Ivan Grujic, and Nadica Stojanovic. "Engine Load Impact on Maximum Value of Normal Force in piston mechanism." *Tractors and power machines* 23, no. 1-2 (2018): 10 -16.
[11] Singh, A., S. Bharadwaj, and S. Narayan. "Analiza različitih NVH izvora motora s unutarnjim izgaranjem." *Tehnički glasnik* 10, no. 1-2 (2016): 29 - 37.
[12] Gupta, Aman, and Sunny Narayan. "An Introduction to Combustion Engines." *Hidraulica Magazine*, no. 4 (December 2016): 69 -77.
[13] Gupta, Aman, Sunny Narayan, and Shubham Bharadwaj. "A Review of Various NVH Sources of Combustion Engines." *International Journal of Mechanical Engineering and Automation* 3, no. 6 (2016): 249 - 261.
[14] Gupta, Aman, and Sunny Narayan. "Analysis of Liquid Piston Fluidyne Systems." *International Journal of Mechanical Engineering and Automation* 3, no. 1 (2016): 21– 26.
[15] Gupta, Aman, Sunny Narayan, and Shubham Bharadwaj. "Effects of Turbocharging in a S.I. Engine." *International Journal of Mechanical Engineering and Automation* 3, no. 3 (2016): 107 - 113.
[16] Gupta, Vipul, Ranjeet Singh, and Sunny Narayan. "Motion analysis of fluidyne engines.” *Tehnički glasnik* 9, no. 3 (2015): 242 - 244.
[17] Narayan, S. "Analysis of piston slap motion." *International Journal of Applied Mechanics and Engineering* 20, no. 2 (2015): 445- 450.
[18] Narayan, Sunny. "Modeling of Noise Radiated from Engines." SAE Tech paper 2015-01-0107, 2015. Paper presented at The 11th International Conference on Automotive Engineering (ICAE 11), Bangkok, Thailand, March 30 - April 1, 2015.
[19] Narayan, Sunny. "Effects of various parameters on piston secondary motion." SAE Tech paper 2015-01-0079, 2015. Paper presented at 18th Asia Pacific Automotive Engineering Conference (APAC 18), Melbourne, Victoria, Australia, March 10-11, 2015.
[20] Narayan, Sunny. "Analysis of Combustion Noise in Diesel Engines." *Acta Mechanica Slovaca* 18, no. 3-4 (2015): 28- 35.

FLUIDAS

NATIONAL PROFESSIONAL ASSOCIATION OF HYDRAULICS AND PNEUMATICS IN ROMANIA

fluidas@fluidas.ro